



## THESIS APPROVAL

### GRADUATE SCHOOL, KASETSART UNIVERSITY

Master of Science (Earth Science and Technology)

#### DEGREE

Earth Science and Technology

Earth Sciences

#### FIELD

#### DEPARTMENT

**TITLE:** Atomic Force Microscopy of Synthetic Corundum before and after  
Annealing

**NAME:** Mr. Thanapong Lhuaamporn

**THIS THESIS HAS BEEN ACCEPTED BY**

#### THESIS ADVISOR

( Assistant Professor Pornsawat Wathanakul, Dr.rer.nat. )

#### THESIS CO-ADVISOR

( Mrs. Somruedee Satitkune, Dr.rer.nat. )

#### THESIS CO-ADVISOR

( Mr. Wiwat Wongkokua, Ph.D. )

#### DEPARTMENT HEAD

( Mr. Passakorn Pananont, Ph.D. )

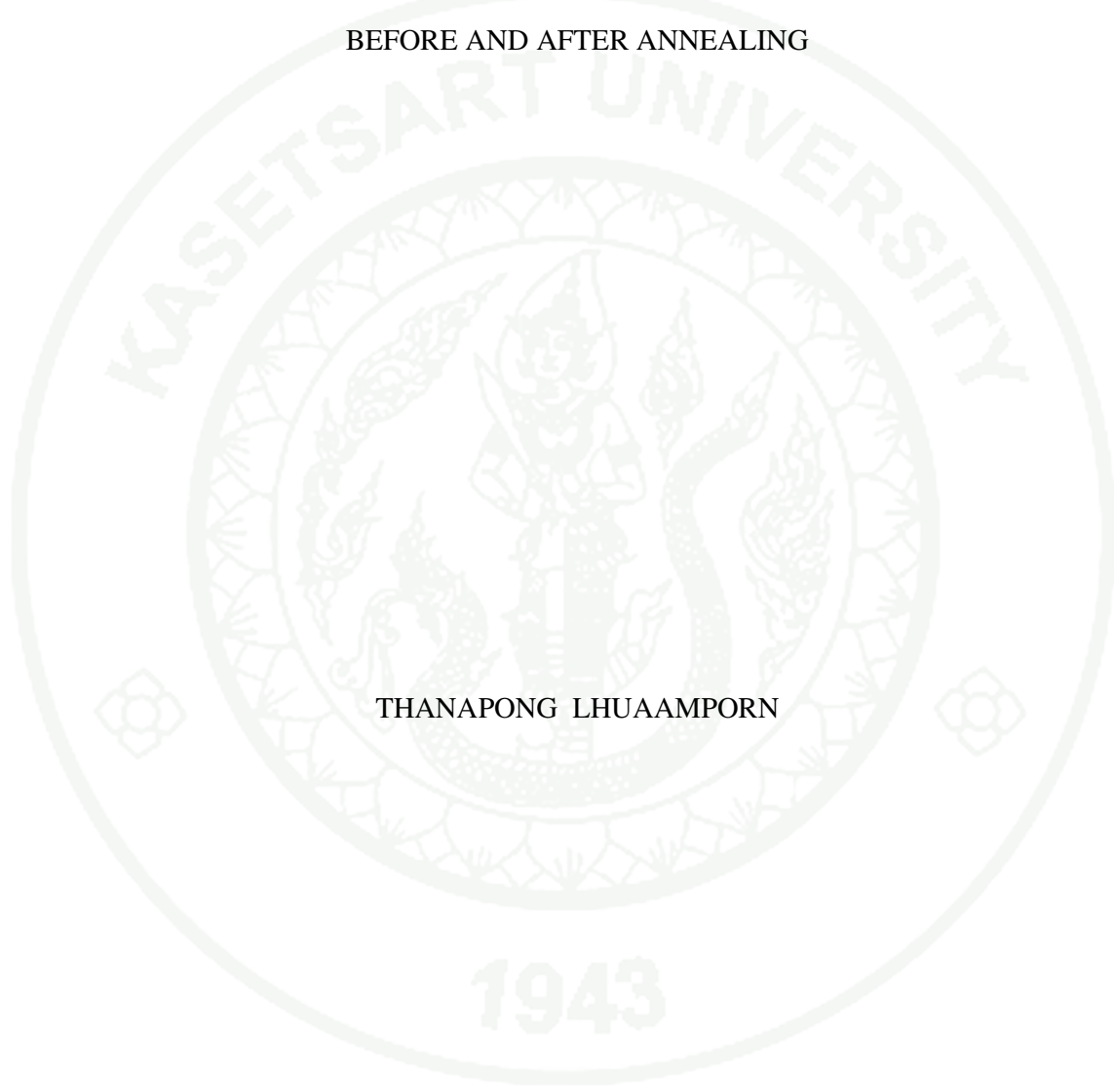
**APPROVED BY THE GRADUATE SCHOOL ON**

#### DEAN

( Associate Professor Gunjana Theeragool, D.Agr. )

THESIS

ATOMIC FORCE MICROSCOPY OF SYNTHETIC CORUNDUM  
BEFORE AND AFTER ANNEALING



THANAPONG LHUAAMPORN

A Thesis Submitted in Partial Fulfillment of  
the Requirements for the Degree of  
Master of Science (Earth Science and Technology)  
Graduate School, Kasetsart University

2012

Thanapong Lhuaamporn 2012: Atomic Force Microscopy of Synthetic Corundum before and after Annealing. Master of Science (Earth Science and Technology), Major Field: Earth Science and Technology, Department of Earth Sciences. Thesis Advisor: Assistant Professor Pornsawat Wathanakul, Dr.rer.nat. 168 pages.

Samples of Verneuil synthetic pink sapphire and ruby were cut into different faces, i.e., [0001], [1 $\bar{1}$ 00], [0 $\bar{1}$ 10], [1 $\bar{2}$ 10], [ $\bar{1}$  $\bar{1}$ 20], in order to investigate for their surface features in micro-nanometer scale before and after annealing at 1650 °C. The Atomic Force Microscope (AFM) was employed in cooperated with FTIR and UV-Vis-NIR spectroscopy to identify the annealing experienced by the samples.

The AFM images of the annealed samples exhibit multiple atomic steps with sharper edges and clearer step patterns than those of the unheated ones. The average step heights of most samples tend to increase after annealing. The untreated samples often showed the mono atomic steps (~0.22 nm) particularly on [0001] or c-planes. Multiple atomic steps usually formed after annealing with increasing step heights for about 10-100 times, i.e., ~2-20 nm. However, the average atomic step height on the annealed prism faces is usually less than that of the c-surfaces. FTIR spectra of unheated samples showed structural Ti-OH and possibly V-OH stretchings at 3309 and 3237 cm<sup>-1</sup>, respectively. UV-Vis-NIR spectra showed Cr<sup>3+</sup> absorptions at 405, 555 nm for both sample types, but the 695 nm presents only in the synthetic ruby.

The study can be further applied for possible investigations of heating evidences in natural corundum, and other gemstones.

\_\_\_\_\_  
Student's signature

\_\_\_\_\_  
Thesis Advisor's signature

\_\_\_/\_\_\_/\_\_\_

## ACKNOWLEDGEMENTS

I would like to express my sincere gratitude to my advisor, Assistant Professor Dr. Pornsawat Wathanakul, and both co-advisors, Dr. Wiwat Wongkokua and Dr. Somruedee Satitkune for their supervisions and suggestions throughout the completion of this thesis.

I also would like to thank Associate Professor Dr. Mingkwan Mingmuang and Mrs. Wilawan Atichat, the director of the Gem and Jewelry Institute of Thailand (Public Organization) for accepting to be my thesis committee members.

Sincere appreciations are due to the Gem and Mineral Sciences Special Research Unit, Department of Earth Sciences, Faculty of Science, Kasetsart University for laboratory facilities including FTIR and UV-Vis-NIR spectrophotometers; the Scientific Equipment Center, Faculty of Science, Kasetsart University for Atomic Force Microscope (AFM) facility; the Gem and Jewelry Institute of Thailand (Public Organization) or GIT for granting the Micro-nano'53 research project.

Finally, my heartfelt thanks are extended to my family, friends at KU, and staff at the GIT for their kind supports and encouragements.

Thanapong Lhuaamporn  
March 2012

**TABLE OF CONTENTS**

	<b>Page</b>
TABLE OF CONTENTS	i
LIST OF TABLES	ii
LIST OF FIGURES	v
LIST OF ABBREVIATIONS	xx
INTRODUCTION	1
OBJECTIVE	2
LITERATURE REVIEW	3
MATERIALS AND METHODS	15
Materials	15
Methods	21
RESULTS AND DISCUSSION	32
Results	32
Discussion	131
CONCLUSION AND RECOMMENDATION	141
Conclusion	141
Recommendation	143
LITERATURE CITED	144
APPENDIX	148
CURRICULUM VITAE	168

## LIST OF TABLES

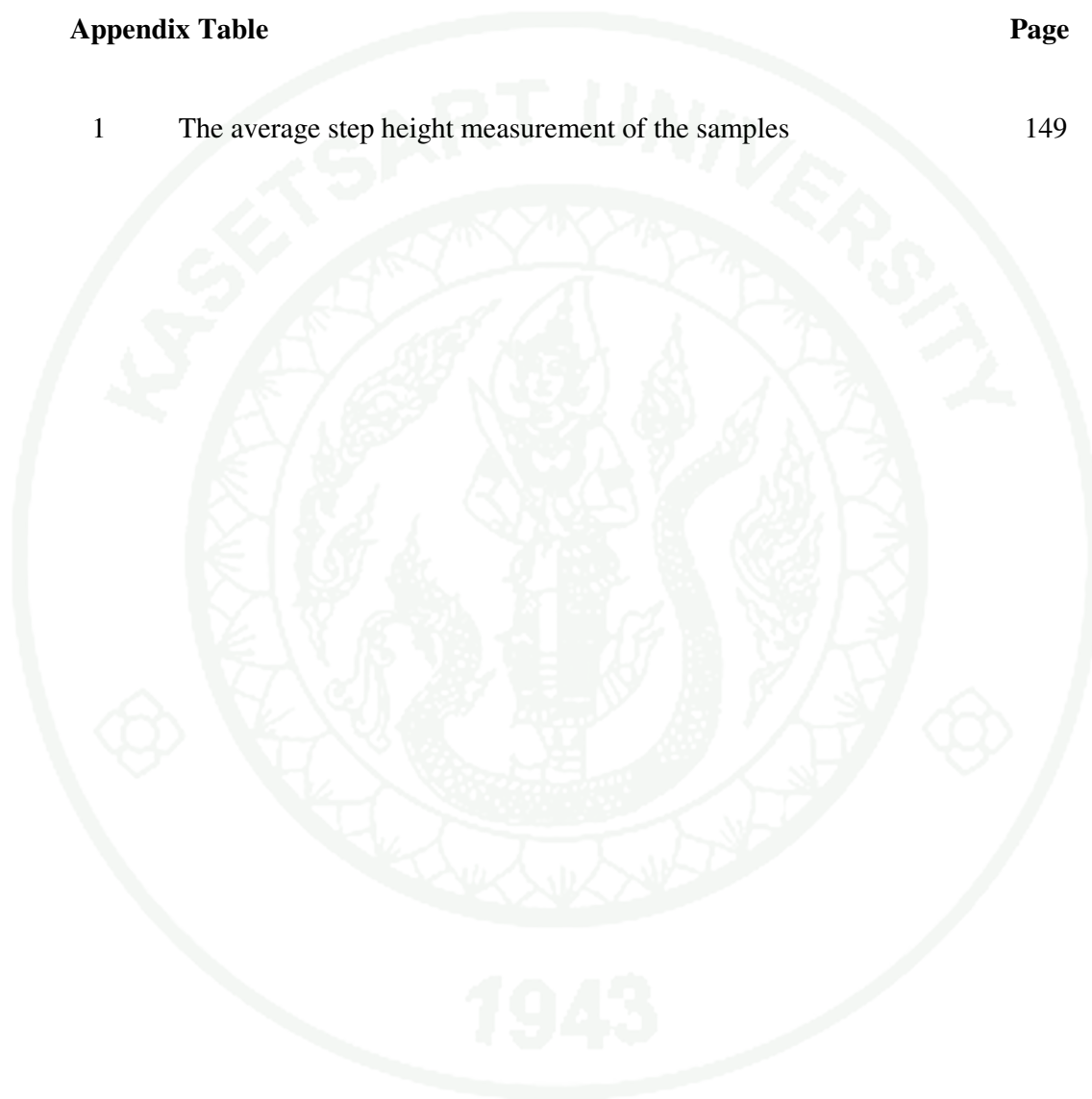
<b>Table</b>		<b>Page</b>
1	Sample registration of set 1 (pink sapphire) after cutting and polishing	17
2	Sample registration of set 2 (ruby) after cutting and polishing	18
3	Physical properties of synthetic pink sapphires (set 1) at different surface orientations	32
4	Physical properties of synthetic ruby samples (set 2) at different surface orientations	34
5	The UV-Vis-NIR result conclusions of the synthetic pink sapphire and ruby samples	48
6	The infrared absorbance characteristic of the samples	50
7	The concentration in ppm of the chemical substance in pink sapphire boule which were detected by LA-ICPMS.	50
8	The average step height from the A-C line on figure 52	52
9	The average step height from the A-E line on figure 54	55
10	The average step height from the A-C line on figure 56	57
11	The average step height from the A-D lines on figure 58	59
12	The average step height from the A-C lines on figure 60	60
13	The average step height from the A-D lines on figure 62	63
14	The average step height from the A-C lines on figure 64	64
15	The average step height from the A-D lines on figure 66	67
16	The average step height from the A-C lines on figure 68	68
17	The average step height from the A-C lines on figure 70	70
18	The average step height from the A-D lines on figure 72	73
19	The average step height from the A-D lines on figure 74	74
20	The average step height from the A-C lines on figure 76	76
21	The average step height from the A-D lines on figure 78	78
22	The average step height from the A-B lines on figure 80	80
23	The average step height from the A line on figure 82	82

**LIST OF TABLES (Continued)**

<b>Table</b>		<b>Page</b>
24	The average step height from the A-D lines on figure 84	85
25	The average step height from the A-C lines on figure 86	86
26	The average step height from the A-D lines on figure 88	89
27	The average step height from the A-C lines on figure 90	91
28	The average step height from the A-C lines on figure 92	92
29	The average step height from the A-E lines on figure 94	95
30	The average step height from the A-C lines on figure 96	96
31	The average step height from the A-F lines on figure 98	99
32	The average step height from the A-C lines on figure 100	100
33	The average step height from the A-D lines on figure 102	103
34	The average step height from the A-C lines on figure 104	104
35	The average step height from the A-D lines on figure 106	107
36	The average step height from the A-E lines on figure 108	109
37	The average step height from the A-E lines on figure 110	111
38	The average step height from the A-D lines on figure 112	113
39	The average step height from the A-E lines on figure 114	115
40	The average step height from the A-E lines on figure 116	117
41	The average step height from the A-C lines on figure 118	118
42	The average step height from the A-C lines on figure 120	121
43	The average step height from the A-D lines on figure 122	123
44	The average step height from the A-D lines on figure 124	124
45	The average step height from the A-E lines on figure 126	126
46	The average step height from the A-C lines on figure 128	128
47	The average step height from the A-D lines on figure 130	130
48	The average steps height of the samples on five orientation	139

**LIST OF TABLES (Continued)**

<b>Appendix Table</b>		<b>Page</b>
1	The average step height measurement of the samples	149



## LIST OF FIGURES

Figure		Page
1	The screw dislocation is the site that grows up to a new layer.	4
2	The spiral growth starts from the screw dislocation.	4
3	The spiral growth on a crystal face	5
4	The Verneuil process	7
5	The diagram of energy levels, transitions, and colour absorptions in ruby	8
6	The direction of intense colour in Verneuil synthetic corundum of the natural one, showing traditionally cut profile direction.	9
7	The AFM images of [0001] sapphire: (a) unheated ( $1 \times 1 \mu\text{m}^2$ ), (b) heated at $1000^\circ\text{C}$ for 1 hour ( $1 \times 1 \mu\text{m}^2$ ), (c) heated at $1400^\circ\text{C}$ for 1 hour ( $3 \times 3 \mu\text{m}^2$ ) showing the image after heating at $1400^\circ\text{C}$ ; the smooth step appear, and the step height increase.	11
8	The $c/6$ step height of 0.22 nm with the multiple steps on the miscut [0001].	12
9	The comparison of step height at 1100 and $1400^\circ\text{C}$ respectively	13
10	Showing the merging step of two steps (b) become the higher step (c).	14
11	A synthetic pink sapphire boule (a) and a synthetic ruby boule (b) before cutting and polishing	15
12	a) Perspective sketches showing sample orientations for cutting through $a_1$ -, $a_2$ - and $a_3$ -axes. b) Sketches showing, how the first piece from figure 11a) was further cut to obtain samples with different orientations, for examples, the miscut of $[0\bar{1}10]$ (RR01b) and the miscut of $[1\bar{1}00]$ (RR01a). c) The miscut of $[1\bar{2}10]$ from the second piece in the figure 11a). d) The miscut orientations of $[\bar{1}\bar{1}20]$ and $[0001]$ from the third piece in the figure 11a).	15
13	Flow chart of research methodology	22

## LIST OF FIGURES (Continued)

Figure		Page
14	An electronic balance for measuring S.G. at Department of Earth Sciences, Faculty of Science, Kasetsart University	23
15	Refractometer, Rayner, and R.I. liquid at Department of Earth Sciences, Faculty of Science, Kasetsart University	24
16	Light beams reflected (R) and transmitted or refracted (T) at the interface between two refractive indexes, $n_1$ and $n_2$ , the second being greater than the first.	24
17	Polariscope at Department of Earth Sciences, Faculty of Science, Kasetsart University.	25
18	Thai sawing and grinding machines for gem cutting at Department of Earth Sciences, Faculty of Science, Kasetsart University	26
19	Sticking sample with bar (left) then truncate by thai grinding machine (right) at Department of Earth Sciences, Faculty of Science, Kasetsart University.	27
20	Thai local made faceting machine at Department of Earth Sciences, Faculty of Science, Kasetsart University	27
21	The electric furnace; Lenton, model UAF18/5 at Earth Sciences Department, Kasetsart University, Bangkok	28
22	NEXUS 470 FTIR Spectrophotometer at Department of Earth Sciences, Faculty of Science, Kasetsart University	29
23	UV-Vis-NIR Spectroscopy model of Perkin Elmer LAMDA 900 placed at the Department of Earth Sciences, Faculty of Science, Kasetsart University	29
24	Atomic Force Microscope model MFP-3D-BIO AFM from Asylum Research based at the Scientific Equipment Center, Faculty of Sciences, Kasetsart University, Bangkok.	31

## LIST OF FIGURES (Continued)

Figure		Page
25	The working principle of AFM tip to present the image on the monitor	31
26	UV-Vis-NIR absorption spectrum of the unheated synthetic pink sapphire sample set 1, the beam was perpendicular to the miscus prism $[1\bar{1}00]$ face (RR01a).	36
27	UV-Vis-NIR absorption spectrum of the unheated synthetic pink sapphire sample set 1, the beam was perpendicular to the miscus prism $[0\bar{1}10]$ face (RR01b).	36
28	UV-Vis-NIR absorption spectrum of the heated synthetic pink sapphire sample set 1, the beam was perpendicular to the miscus prism $[0\bar{1}10]$ face (RR01c).	37
29	UV-Vis-NIR absorption spectrum of the heated synthetic pink sapphire sample set 1, the beam was perpendicular to the miscus prism $[1\bar{1}00]$ face (RR01d).	37
30	UV-Vis-NIR absorption spectrum of the unheated synthetic pink sapphire sample set 1, the beam was perpendicular to the miscus prism $[1\bar{2}10]$ face (RR02a).	38
31	UV-Vis-NIR absorption spectrum of the heated synthetic pink sapphire sample set 1, the beam was perpendicular to the miscus prism $[1\bar{2}10]$ face (RR02c)	38
32	UV-Vis-NIR absorption spectrum of the unheated synthetic pink sapphire sample set 1, the beam was perpendicular to the miscus prism $[\bar{1}\bar{1}00]$ face (RR04a)	39
33	UV-Vis-NIR absorption spectrum of the heated synthetic pink sapphire sample set 1, the beam was perpendicular to the miscus prism $[\bar{1}\bar{1}00]$ face (RR04c)	39

## LIST OF FIGURES (Continued)

Figure		Page
34	UV-Vis-NIR absorption spectrum of the unheated synthetic pink sapphire sample set 1, the beam was perpendicular to the miscus pinacoid [0001] face (RR05a).	40
35	UV-Vis-NIR absorption spectrum of the heated synthetic pink sapphire sample set 1, the beam was perpendicular to the miscus pinacoid [0001] face (RR05e).	40
36	UV-Vis-NIR absorption spectrum of the unheated synthetic ruby sample set 2, the beam was perpendicular to the miscus prism $[1\bar{1}00]$ face (RRb01a).	41
37	UV-Vis-NIR absorption spectrum of the unheated synthetic ruby sample set 2, the beam was perpendicular to the miscus prism $[0\bar{1}10]$ face (RRb01b).	41
38	UV-Vis-NIR absorption spectrum of the heated synthetic ruby sample set 2, the beam was perpendicular to the miscus prism $[0\bar{1}10]$ face (RRb01c).	42
39	UV-Vis-NIR absorption spectrum of the heated synthetic ruby sample set 2, the beam was perpendicular to the miscus prism $[1\bar{1}00]$ face (RRb01d).	42
40	UV-Vis-NIR absorption spectrum of the unheated synthetic ruby sample set 2, the beam was perpendicular to the miscus prism $[1\bar{2}10]$ face (RRb02a).	43
41	UV-Vis-NIR absorption spectrum of the heated synthetic ruby sample set 2, the beam was perpendicular to the miscus prism $[1\bar{2}10]$ face (RRb02c).	43
42	UV-Vis-NIR absorption spectrum of the unheated synthetic ruby sample set 2, the beam was perpendicular to the miscus prism $[\bar{1}\bar{1}00]$ face (RRb04a).	44

## LIST OF FIGURES (Continued)

Figure		Page
43	UV-Vis-NIR absorption spectrum of the heated synthetic ruby sample set 2, the beam was perpendicular to the miscus prism $[\bar{1}\bar{1}00]$ face (RRb04c).	44
44	UV-Vis-NIR absorption spectrum of the unheated synthetic ruby sample set 2, the beam was perpendicular to the miscus pinacoid $[0001]$ face (RRb05a).	45
45	UV-Vis-NIR absorption spectrum of the heated synthetic ruby sample set 2, the beam was perpendicular to the miscus pinacoid $[0001]$ face (RRb05e).	45
46	UV-Vis-NIR absorption spectrum at the miscut pinacoid $[0001]$ face of heated sample (RR05e) has higher absorption than the unheated one (RR05a).	46
47	UV-Vis-NIR absorption spectrum at the miscut prism $[1\bar{2}10]$ face of heated sample (RR02c) has lower absorption than the unheated one (RR02a).	47
48	UV-Vis-NIR absorption spectrums of unheated synthetic samples before calculate the absorption with path length.	47
49	UV-Vis-NIR absorption spectrums of unheated synthetic samples after calculate the absorption with path length.	48
50	FTIR result of synthetic pink sapphire samples set 1, the laser was perpendicular to the miscus prism $[1\bar{1}00]$ face (RR01a, RR01d).	49
51	3D-Image of unheated synthetic pink sapphire (set 1) on the miscut of prism $[1\bar{1}00]$ face (RR01a)	51
52	Measurement of average step height of unheated synthetic pink sapphire (set 1) on the miscut of prism $[1\bar{1}00]$ face (RR01a)	52
53	3D-Image of unheated synthetic pink sapphire (set 1) on the miscut of prism $[1\bar{1}00]$ face (RR01a)	53

## LIST OF FIGURES (Continued)

Figure		Page
54	Measurement of average step height of unheated synthetic pink sapphire (set 1) on the miscut of prism $[1\bar{1}00]$ face (RR01a) and the scratch lines	54
55	3D-Image of heated synthetic pink sapphire (set 1) on the miscut of prism $[1\bar{1}00]$ face (RR01d)	55
56	Measurement of average step height of heated synthetic pink sapphire (set 1) on the miscut of prism $[1\bar{1}00]$ face (RR01d)	56
57	3D-Image of heated synthetic pink sapphire (set 1) on the miscut of prism $[1\bar{1}00]$ face (RR01d)	57
58	Measurement of average step height of heated synthetic pink sapphire (set 1) on the miscut of prism $[1\bar{1}00]$ face (RR01d)	58
59	3D-Image of unheated synthetic pink sapphire (set 1) on the miscut of prism $[0\bar{1}10]$ face (RR01b)	59
60	Measurement of average step height of unheated synthetic pink sapphire (set 1) on the miscut of prism $[0\bar{1}10]$ face (RR01b) and the scratch lines	60
61	3D-Image of unheated synthetic pink sapphire (set 1) on the miscut of prism $[0\bar{1}10]$ face (RR01b)	61
62	Measurement of average step height of unheated synthetic pink sapphire (set 1) on the miscut of prism $[0\bar{1}10]$ face (RR01b) and the scratch lines	62
63	3D-Image of heated synthetic pink sapphire (set 1) on the miscut of prism $[0\bar{1}10]$ face (RR01c)	63
64	Measurement of average step height of heated synthetic pink sapphire (set 1) on the miscut of prism $[0\bar{1}10]$ face (RR01c)	64
65	3D-Image of heated synthetic pink sapphire (set 1) on the miscut of prism $[0\bar{1}10]$ face (RR01c)	65

## LIST OF FIGURES (Continued)

Figure		Page
66	Measurement of average step height of heated synthetic pink sapphire (set 1) on the miscut of prism $[0\bar{1}10]$ (RR01c)	66
67	3D-Image of unheated synthetic pink sapphire (set 1) on the miscut of prism $[1\bar{2}10]$ prism (RR02a)	67
68	Measurement of average step height of unheated synthetic pink sapphire (set 1) on the miscut of prism $[1\bar{2}10]$ face (RR02a) and the scratch lines	68
69	3D-Image of unheated synthetic pink sapphire (set 1) on the miscut of prism $[1\bar{2}10]$ face (RR02a)	69
70	Measurement of average step height of unheated synthetic pink sapphire (set 1) on the miscut of prism $[1\bar{2}10]$ face (RR02a) and the scratch lines	70
71	3D-Image of heated synthetic pink sapphire (set 1) on the miscut of prism $[1\bar{2}10]$ face (RR02c)	71
72	Measurement of average step height of heated synthetic pink sapphire (set 1) on the miscut of prism $[1\bar{2}10]$ face (RR02c)	72
73	3D-Image of heated synthetic pink sapphire (set 1) on the miscut of prism $[1\bar{2}10]$ face (RR02c)	73
74	Measurement of average step height of heated synthetic pink sapphire (set 1) on the miscut of prism $[1\bar{2}10]$ face (RR02c) and the artifact	74
75	3D-Image of unheated synthetic pink sapphire (set 1) on the miscut of prism $[\bar{1}\bar{1}20]$ face (RR04a)	75
76	Measurement of average step height of unheated synthetic pink sapphire (set 1) on the miscut of prism $[\bar{1}\bar{1}20]$ face (RR04a)	76

## LIST OF FIGURES (Continued)

Figure		Page
77	3D-Image of unheated synthetic pink sapphire (set 1) on the miscut of prism $[\bar{1}\bar{1}20]$ face (RR04a)	77
78	Measurement of average step height of unheated synthetic pink sapphire (set 1) on the miscut of prism $[\bar{1}\bar{1}20]$ face (RR04a)	78
79	3D-Image of heated synthetic pink sapphire (set 1) on the miscut of prism $[\bar{1}\bar{1}20]$ face (RR04c)	79
80	Measurement of average step height of heated synthetic pink sapphire (set 1) on the miscut of prism $[\bar{1}\bar{1}20]$ face (RR04c)	80
81	3D-Image of heated synthetic pink sapphire (set 1) on the miscut of prism $[\bar{1}\bar{1}20]$ face (RR04c)	81
82	Measurement of average step height of heated synthetic pink sapphire (set 1) on the miscut of prism $[\bar{1}\bar{1}20]$ face (RR04c)	82
83	3D-Image of unheated synthetic pink sapphire (set 1) on the miscut of pinacoid $[0001]$ face (RR05a)	83
84	Measurement of average step height of unheated synthetic pink sapphire (set 1) on the miscut of $[0001]$ (RR05a) and the scratch line	84
85	3D-Image of unheated synthetic pink sapphire (set 1) on the miscut of pinacoid $[0001]$ face (RR05a)	85
86	Measurement of average step height of unheated synthetic pink sapphire (set 1) on the miscut of pinacoid $[0001]$ face (RR05a) and the scratch line	86
87	3D-Image of heated synthetic pink sapphire (set 1) on the miscut of pinacoid $[0001]$ face (RR05e)	87
88	Measurement of average step height of heated synthetic pink sapphire (set 1) on the miscut of pinacoid $[0001]$ face (RR05e)	88
89	3D-Image of heated synthetic pink sapphire (set 1) on the miscut of pinacoid $[0001]$ face (RR05e)	89

## LIST OF FIGURES (Continued)

Figure		Page
90	Measurement of average step height of heated synthetic pink sapphire (set 1) on the miscut of pinacoid [0001] face (RR05e)	90
91	3D-Image of unheated synthetic ruby (set 2) on the miscut of prism $[1\bar{1}00]$ face (RRb01a)	91
92	Measurement of average step height of unheated synthetic ruby (set 2) on the miscut of prism $[1\bar{1}00]$ face (RRb01a)	92
93	3D-Image of unheated synthetic ruby (set 2) on the miscut of prism $[1\bar{1}00]$ face (RRb01a)	93
94	Measurement of average step height of unheated synthetic ruby (set 2) on the miscut of prism $[1\bar{1}00]$ face (RRb01a)	94
95	3D-Image of heated synthetic ruby (set 2) on the miscut of prism $[1\bar{1}00]$ face (RRb01d)	95
96	Measurement of average step height of heated synthetic ruby (set 2) on the miscut of prism $[1\bar{1}00]$ face (RRb01d)	96
97	3D-Image of heated synthetic ruby (set 2) on the miscut of prism $[1\bar{1}00]$ face (RRb01d)	97
98	Measurement of average step height of heated synthetic ruby (set 2) on the miscut of prism $[1\bar{1}00]$ face (RRb01d)	98
99	3D-Image of unheated synthetic ruby (set 2) on the miscut of prism $[0\bar{1}10]$ face (RRb01b)	99
100	Measurement of average step height of unheated synthetic ruby (set 2) on the miscut of prism $[0\bar{1}10]$ face (RRb01b)	100
101	3D-Image of unheated synthetic ruby (set 2) on the miscut of prism $[0\bar{1}10]$ face (RRb01b)	101
102	Measurement of average step height of unheated synthetic ruby (set 2) on the miscut of $[0\bar{1}10]$ (RRb01b)	102

## LIST OF FIGURES (Continued)

Figure		Page
103	3D-Image of heated synthetic ruby (set 2) on the miscut of prism [0 $\bar{1}$ 10] face (RRb01c)	103
104	Measurement of average step height of heated synthetic ruby (set 2) on the miscut of prism [0 $\bar{1}$ 10] face (RRb01c)	104
105	3D-Image of heated synthetic ruby (set 2) on the miscut of prism [0 $\bar{1}$ 10] face (RRb01c)	105
106	Measurement of average step height of heated synthetic ruby (set 2) on the miscut of prism [0 $\bar{1}$ 10] face (RRb01c)	106
107	3D-Image of unheated synthetic ruby (set 2) on the miscut of prism [1 $\bar{2}$ 10] face (RRb02a)	107
108	Measurement of average step height of unheated synthetic ruby (set 2) on the miscut of prism [1 $\bar{2}$ 10] face (RRb02a) and the scratch line	108
109	3D-Image of unheated synthetic ruby (set 2) on the miscut of prism [1 $\bar{2}$ 10] face (RRb02a)	109
110	Measurement of average step height of unheated synthetic ruby (set 2) on the miscut of [1 $\bar{2}$ 10] (RRb02a) and the scratch lines	110
111	3D-Image of heated synthetic ruby (set 2) on the miscut of prism [1 $\bar{2}$ 10] face (RRb02c)	111
112	Measurement of average step height of heated synthetic ruby (set 2) on the miscut of prism [1 $\bar{2}$ 10] face (RRb02c)	112
113	3D-Image of heated synthetic ruby (set 2) on the miscut of prism [1 $\bar{2}$ 10] face (RRb02c)	113
114	Measurement of average step height of heated synthetic ruby (set 2) on the miscut of prism [1 $\bar{2}$ 10] face (RRb02c)	114

## LIST OF FIGURES (Continued)

Figure		Page
115	3D-Image of unheated synthetic ruby (set 2) on the miscut of prism [ $\bar{1}\bar{1}20$ ] face (RRb04a)	115
116	Measurement of average step height of unheated synthetic ruby (set 2) on the miscut of prism [ $\bar{1}\bar{1}20$ ] face (RRb04a)	116
117	3D-Image of unheated synthetic ruby (set 2) on the miscut of prism [ $\bar{1}\bar{1}20$ ] face (RRb04a)	117
118	Measurement of average step height of unheated synthetic ruby (set 2) on the miscut of prism [ $\bar{1}\bar{1}20$ ] face (RRb04a)	118
119	3D-Image of heated synthetic ruby (set 2) on the miscut of prism [ $\bar{1}\bar{1}20$ ] face (RRb04c)	119
120	Measurement of average step height of heated synthetic ruby (set 2) on the miscut of prism [ $\bar{1}\bar{1}20$ ] face (RRb04c)	120
121	3D-Image of heated synthetic ruby (set 2) on the miscut of prism [ $\bar{1}\bar{1}20$ ] face (RRb04c)	121
122	Measurement of average step height of heated synthetic ruby (set 2) on the miscut of prism [ $\bar{1}\bar{1}20$ ] face (RRb04c)	122
123	3D-Image of unheated synthetic ruby (set 2) on the miscut of pinacoid [0001] face (RRb05a)	123
124	Measurement of average step height of unheated synthetic ruby (set 2) on the miscut of pinacoid [0001] face (RRb05a)	124
125	3D-Image of unheated synthetic ruby (set 2) on the miscut of pinacoid [0001] face (RRb05a)	125
126	Measurement of average step height of unheated synthetic ruby (set 2) on the miscut of pinacoid [0001] face (RRb05a)	126
127	3D-Image of heated synthetic ruby (set 2) on the miscut of pinacoid [0001] face (RRb05e)	127

## LIST OF FIGURES (Continued)

Figure		Page
128	Measurement of average step height of heated synthetic ruby (set 2) on the miscut of pinacoid [0001] face (RRb05e)	128
129	3D-Image of heated synthetic ruby (set 2) on the miscut of pinacoid [0001] face (RRb05e)	129
130	Measurement of average step height of heated synthetic ruby (set 2) on the miscut of pinacoid [0001] face (RRb05e)	130
131	(a) The c-plane in nano-scale from Cucureddu <i>et al.</i> , 2010, (b) the c-plane of synthetic pink sapphire sample in this study and (c) the c-plane of synthetic ruby sample in this study	135
132	(a) The prism face in nano-scale from Curiotto <i>et al.</i> , 2009, (b) the prism face of synthetic pink sapphire sample and (c) the prism face of synthetic ruby sample	135
133	The oxygen height at side view of [0001] is about 0.21 nm	136
134	The oxygen height at side view of $[1\bar{1}00]$ is about 0.13 nm	137
135	The oxygen height at a side view of $[0\bar{1}10]$ is about 0.15 nm.	137
136	Three different views of the structure of corundum; the top shows the structure looking down the c axis, below is a view perpendicular to the c axis and right is a perspective view.	139

### Appendix Figure

1	UV-Vis-NIR absorption spectrum at the miscut prism $[1\bar{1}00]$ face of heated sample (RR01d) has lower absorption than the unheated one (RR01a).	159
2	UV-Vis-NIR absorption spectrum at the miscut prism $[0\bar{1}10]$ face of heated sample (RR01c) has lower absorption than the unheated one (RR01b).	159

## LIST OF FIGURES (Continued)

Appendix Figure		Page
3	UV-Vis-NIR absorption spectrum at the miscut prism [ $\bar{1}\bar{1}00$ ] face of heated sample (RR04c) has lower absorption than the unheated one (RR04a).	160
4	UV-Vis-NIR absorption spectrum at the miscut prism [ $1\bar{1}00$ ] face of heated sample (RRb01d) has lower absorption than the unheated one (RRb01a).	160
5	UV-Vis-NIR absorption spectrum at the miscut prism [ $1\bar{1}00$ ] face of heated sample (RRb01c) has lower absorption than the unheated one (RRb01b).	161
6	UV-Vis-NIR absorption spectrum at the miscut prism [ $1\bar{2}10$ ] face of heated sample (RRb02c) has lower absorption than the unheated one (RRb02a).	161
7	UV-Vis-NIR absorption spectrum at the miscut prism [ $\bar{1}\bar{1}00$ ] face of heated sample (RRb04c) has lower absorption than the unheated one (RRb04a).	162
8	UV-Vis-NIR absorption spectrum at the miscut prism [ $\bar{1}\bar{1}00$ ] face of heated sample (RRb05e) has higher absorption than the unheated one (RRb05a).	162
9	FTIR spectra of synthetic pink sapphire samples set 1, through the miscus prism [ $0\bar{1}10$ ] face of the samples (RR01b, RR01c).	163
10	FTIR spectra of synthetic pink sapphire samples set 1, through the miscus prism [ $1\bar{2}10$ ] face of the samples (RR02a, RR02c).	163
11	FTIR spectra of synthetic pink sapphire samples set 1, through the miscus prism [ $\bar{1}\bar{1}20$ ] face of the samples (RR04a, RR04c).	164
12	FTIR spectra of synthetic pink sapphire samples set 1, through the miscus pinacoid [ $0\bar{1}10$ ] face of the samples (RR05a, RR05e).	164

**LIST OF FIGURES (Continued)**

<b>Appendix Figure</b>		<b>Page</b>
13	FTIR spectra of synthetic ruby samples set 2, through the miscus prism $[1\bar{1}00]$ face of the samples (RRb01a, RRb01d).	165
14	FTIR spectra of synthetic ruby samples set 2, through the miscus prism $[0\bar{1}10]$ face of the samples (RRb01b, RRb01c).	165
15	FTIR spectra of synthetic ruby samples set 2, through the miscus prism $[1\bar{2}10]$ face of the samples (RRb02a, RRb02c).	166
16	FTIR spectra of synthetic ruby samples set 2, through the miscus prism $[\bar{1}\bar{1}20]$ face of the samples (RRb04a, RRb04c).	166
17	FTIR spectra of synthetic ruby samples set 2, through the miscus pinacoid $[0001]$ face of the samples (RRb05a, RRb05e).	167

## LIST OF ABBREVIATIONS

$\theta_1$	=	incident angle
$\theta_2$	=	refraction angle
<	=	less
$\Delta$	=	heated sample
$\nabla$	=	unheated sample
$^{\circ}\text{C}$	=	degree celcius
c	=	molar concentration
$\mu\text{m}$	=	micrometer
$\mu\text{m}^2$	=	square micrometer
AFM	=	Atomic Force Microscope
c/6	=	monostep
cm	=	centimeter
$\text{cm}^{-1}$	=	per centimeter
ct	=	carat, the unit of weight for gemstone
FTIR	=	Fourier Transform Infrared
GIT	=	The Gem and Jewelry Institute of Thailand
GMS	=	Gem and Mineral Science special research unit
L	=	path length
mm	=	millimeter
$n_1$	=	refractive index in air
$n_2$	=	refractive index in water
nm	=	nanometer
R.I	=	Refractive index
S.G.	=	specific gravity
T	=	transmission
UV-Vis-NIR	=	Ultraviolet-Visible- Near-Infrared
Wa	=	sample weight in air
Ww	=	sample weight in water

# **ATOMIC FORCE MICROSCOPY OF SYNTHETIC CORUNDUM BEFORE AND AFTER ANNEALING**

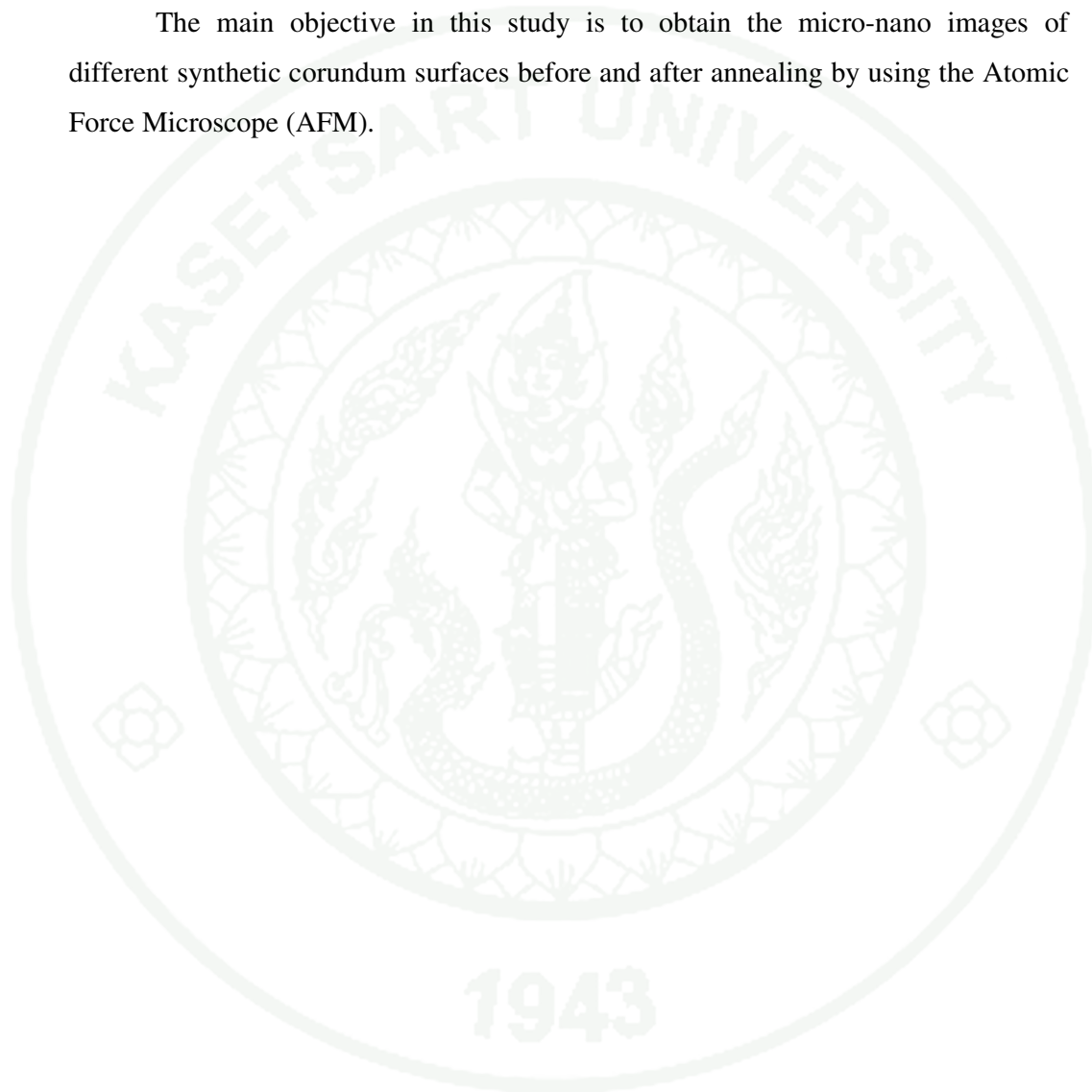
## **INTRODUCTION**

Corundum is a crystalline form of aluminium oxide ( $\text{Al}_2\text{O}_3$ ), which is called alumina. Alpha alumina is the hexagonal crystals with specific gravity about 4. Gamma alumina is composed of cubic crystals with specific gravity about 3.6. Ruby and sapphire is the gemstone in alpha alumina type. Sapphire is the corundum with the color e.g. pink sapphire, orange sapphire, but if the corundum is red, the gemstone is called ruby.

In electronic industry, the basal pinacoid or c plane of synthetic sapphire is normally used as a substrate for thin film growing; it has thus been widely studied by using atomic force microscope (AFM), yet in contrast to the AFM applications in gemology. Hence, various surface feature images at the atomic level on corundum facets could be observed under the AFM. In practice, each facet of a cut gemstone may pass through different crystal faces, i.e., miscuts on prism, basal pinacoid, etc. This study will focus on the micro-nano scaled surfaces of different atomic orientations of synthetic corundum samples in order to reveal their surface features before and after annealing at  $1650^\circ\text{C}$ .

## OBJECTIVE

The main objective in this study is to obtain the micro-nano images of different synthetic corundum surfaces before and after annealing by using the Atomic Force Microscope (AFM).



## LITERATURE REVIEW

### 1. Crystal growth of corundum

Corundum is a single-crystal of  $\text{Al}_2\text{O}_3$ , or  $\alpha$ -alumina, which is normally colorless when free of color-producing transition elements and/or color centers (Nassau, 1994). Corundum can be classified, based on their colors, into two main varieties: ruby and sapphire; blue colour is caused by intervalence charge transfer between  $\text{Ti}^{4+}$  and  $\text{Fe}^{2+}$  whereas  $\text{Cr}^{3+}$  is responsible for red color in ruby based on the crystal field theory. On the other hand, sapphire usually refers to corundum of various colors except red. Sapphires, therefore, may come in blue, yellow, green, pink, etc (Nassau, 2001).

Ideally, a crystal could be defined as a solid which the atoms are arranged in a perfectly ordered way throughout the whole solid. Reality, although the most crystals grown perfectly, it must contain point defects. The example of a point defect is a vacancy, which is one atom missing from its expected position. The impurity atoms or ions can be replaced a regular atom or ion, for example,  $\text{Cr}^{3+}$  substitute for  $\text{Al}^{3+}$  to form the red colour in ruby.

The crystal growth of corundum commonly is the spiral growth which is caused by the dislocation. The dislocation occurs when the defect places on the vacant site. The screw dislocation is the site that grows up to a new layer (Bard, 1986). The screw dislocation and the spiral growth are shown in Figure 1 and 2 respectively.

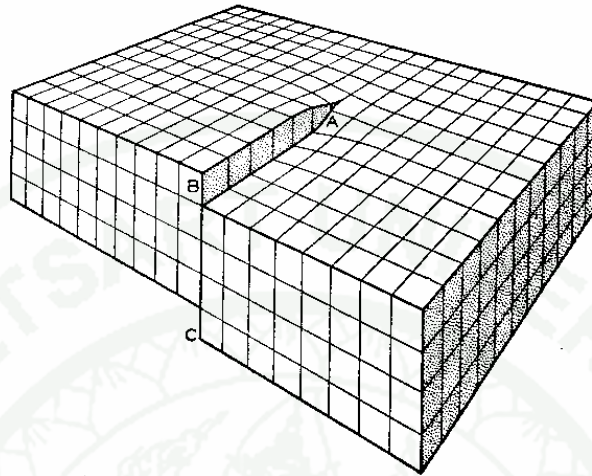


**Figure 1** The screw dislocation is the site that grows up to a new layer.

**Source:** Lourduoss (2010)

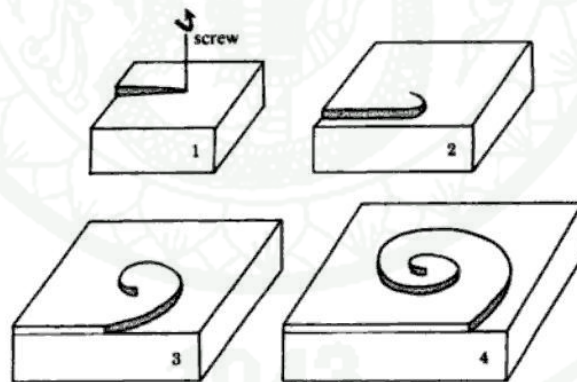


**Figure 2** The spiral growth starts from the screw dislocation.

**Source:** Bard (1986)

The screw dislocation from figure 1, that the units are added to the step or edge at B, and the spiral growth mechanism begin from figure 2 at A. The result is a growth spiral, as seen in Figure 3 (Nassau, 1980).



**Figure 3** The spiral growth on a crystal face

**Source:** Nassau (1980)

## **2. Synthesis of ruby**

Auguste Victor Louis Verneuil, doctor of science and professor of applied chemistry at the Museum of Natural History in Paris proudly did the first man-made gemstone that was the synthetic ruby until 1902. The synthetic rubies were produced already by several manufacturers at a total rate of some five million carats per year in 1907 (Nassau 1980).

The synthetic corundum is produced in many technique i.e., Verneuil process, Czochralski process, Floating zone process, Combination melt techniques, Solution growth process (Hughes, 1997). The Verneuil process is the popular technique, therefore; this study uses the Verneuil samples which were gotten from RusGems Co., Ltd.

In Verneuil's basic form, the flame-fusion process involves melting a mixture of alumina powder and the colouring agents such as  $\text{Cr}_2\text{O}_3$  for ruby,  $\text{Fe}_2\text{O}_3$  and  $\text{TiO}_2$  powder for blue sapphire in such a way that a single crystal forms.

The first step in Verneuil's ruby synthesis was the preparation of a suitable feed powder. Ruby is a single crystal corundum, aluminum oxide ( $\text{Al}_2\text{O}_3$ ) containing a small amount of chromium oxide ( $\text{Cr}_2\text{O}_3$ ) to provide the colour. The aluminum oxide is obtained from ammonium alum. The alum is dissolved when heated and the solution brought to the boiling point. After being filtered and cooled; the wet crystals are dried and roasted in furnaces at  $1200^\circ\text{C}$ , producing alumina. The synthetic colourless corundum was the product without any colouring additive. The chromium oxide affects ruby colour. If there is more chromium, the colour becomes deeper (Hughes, 1997).

The Verneuil process is shown in Figure 4; the container in a Verneuil furnace is the vessel for placing the finely powdered  $\text{Al}_2\text{O}_3$ . The furnace opening at the bottom is used to escape of the powder when the container is vibrated. The oxygen is supplied into the furnace while the powder is released then fall downward into a narrow tube which located within a larger tube that the hydrogen is supplied. At the point where narrow tube opens, the combustion occurs with a flame's core at least  $2000^\circ\text{C}$ . The powder passes through the flame then melts into small droplets. The rod is placed by the sinter cone which the droplets gradually form. The crystal, which forms on the rod, is called a boule. The cylindrical boule is moved from the furnace and cool; the boule is usually split along its vertical axis.

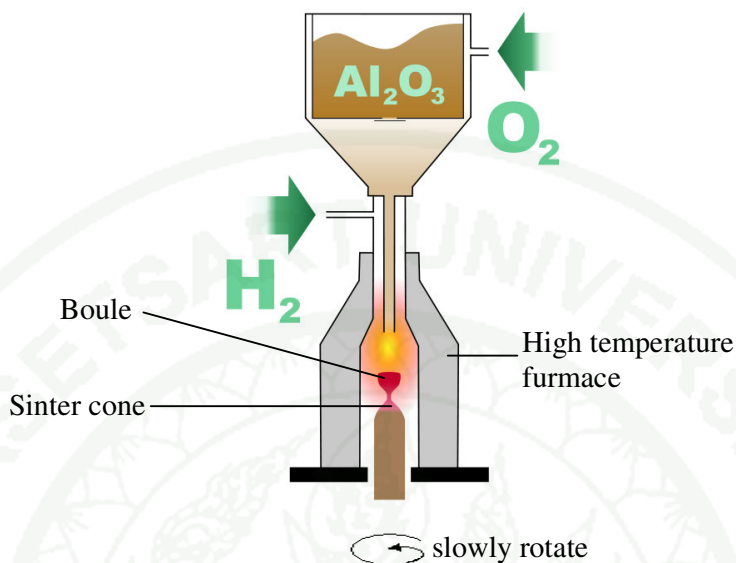


**Figure 4** The Verneuil process

**Source:** Hughes (2012)

### 3. Caused of colour in ruby

Ruby is the corundum containing traces of  $\text{Cr}^{3+}$  ions, which replace the  $\text{Al}^{3+}$  ions in its structure resulting in red colour that is described by the crystal field theory (Nassau, 1978).

The crystal field theory describes colours originating from the excitation of electrons in transition elements. When a transition metal ion has filled d-shell, the outer d-shell orbit electrons in the nucleus are unpaired. The surrounding ions of the crystal lattice create the crystal fields around the transition element, and the fields' strength determine which energy levels are available for the unpaired electrons.

The red colour presents in ruby when  $\text{Cr}^{3+}$  substitutes  $\text{Al}^{3+}$  in the  $\text{Al}_2\text{O}_3$ . In  $\text{Cr}^{3+}$ , the electron configuration is  $1s^2 2s^2 2p^6 3s^2 3p^6 3d^3$ ; there are only three unpaired electrons in the 3d shell which can interact with the visible light to produce the absorption and colour.

The crystal field around the chromium makes a few energy levels, which are available to the unpaired electrons. When white light enters a ruby, the unpaired electrons will absorb yellow-green and violet light, and these electrons now have sufficient energy to be excited to level of 2.23 eV corresponds with yellow-green light, and level of 3 eV corresponds with violet light. The colour which are not absorbed, determine the red colour of the ruby (Figure 5).

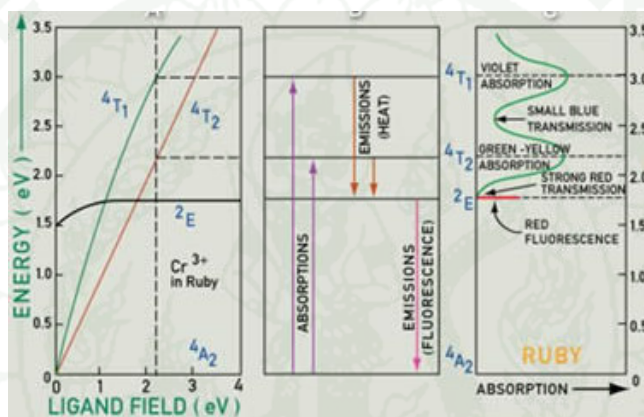


**Figure 5** The diagram of energy levels, transitions, and colour absorptions in ruby

**Source :** Webexhibits (2012)

#### 4. The cutting of natural and synthetic corundum

Finished boules usually split lengthwise along a parting plane. If a properly oriented seed rod is used, crystals can be grown with the *c* axis parallel to the boule's length. Nevertheless, if less care is taken in practice and the *c* axis may be inclined. The orientation of Verneuil synthetic corundum is of concern not only for industrial uses, but also to gemologists. Natural corundums are generally cut with the *c* axis close or perpendicular to the table facet. This is done for two reasons. First, due to the shape of most corundum gem rough, weight loss during cutting is minimized. However, of even greater importance is the fact that, in most varieties of corundum, natural or synthetic, the *o*-ray color is more intense and beautiful than the *e*-ray. Thus,

when a lapidary cuts natural corundum he usually tries to orient the gem with the table facet perpendicular to the c axis.

In contrast, the lapidary is rarely concerned with obtaining the best color when cutting the synthetic. Instead, convenience, speed, and weight retention dictate the stone orientation. Because boules are split the lengthwise, most cutters place the table parallel to the flat inner surface of the split. The c axis, which always lies in the plane of the split, is parallel to the table (Figure 6).

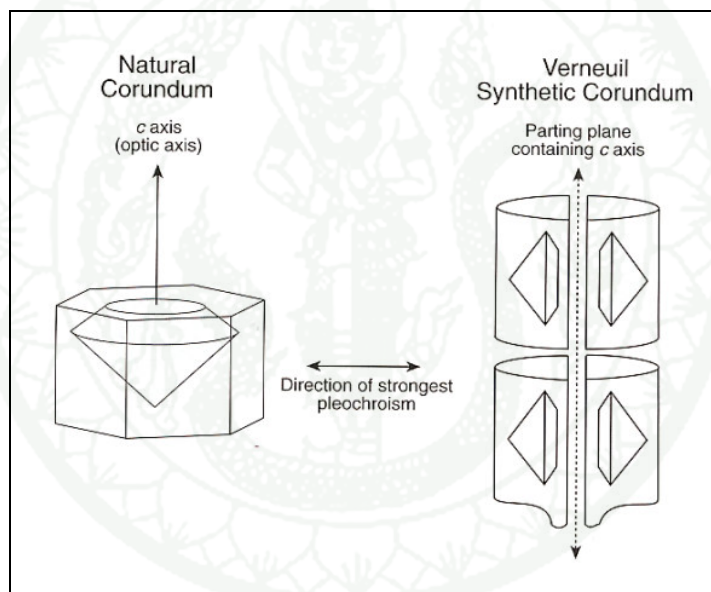


**Figure 6** The direction of intense colour in Verneuil synthetic corundum of the natural one, showing traditionally cut profile direction.

**Source:** Hughes (1997)

## 5. Surface images of corundum

Corundum crystallizes in the hexagonal system with a few crystal morphologies, i.e., tabular, hexagonal dipyramids. Previous studies were conducted mostly in the materials science experiments, which usually showed the annealed corundum surfaces with the atomic steps on the basal pinacoid, for applying in the growth of film (Kurnosikov *et al.*, 2000).

Yoshimoto *et al.* (1995) reported that the sapphire surface of [0001] annealed at 1000°C for 1 hour and at 1400°C for 1 hour in air; the step characteristic after heated at 1000°C is changed. The unheated sample surface has the small corrugation. The sample, which was heated at 1000°C show the atomically flat surfaces with the atomic steps about 0.22 nm (monostep), where as the large steps observed in the heated sample at 1400°C are larger. The large steps are formed by step-bunching through enhanced atom migration at high temperature. The terraces of 1400°C heated sample surface are smooth (Figure 7). These results indicate that atoms group characteristic of each surface migrated on the topmost surface during the thermal heating at high temperature.

Heffelfinger *et al.* (1997) prepared the alumina substrates by cutting and polishing a particular surface orientation from Crystal Systems for studying the alumina surface by AFM. The substrates were annealed at 1400°C for several hours in the air. The surface revealed the step heights to be commonly 2 and 3 multiples of  $c$  (double- and triple steps) and the junctions where two steps merge and form one larger step were found. Such step, where the number of smaller steps, are seen to join together to form a multiple step.

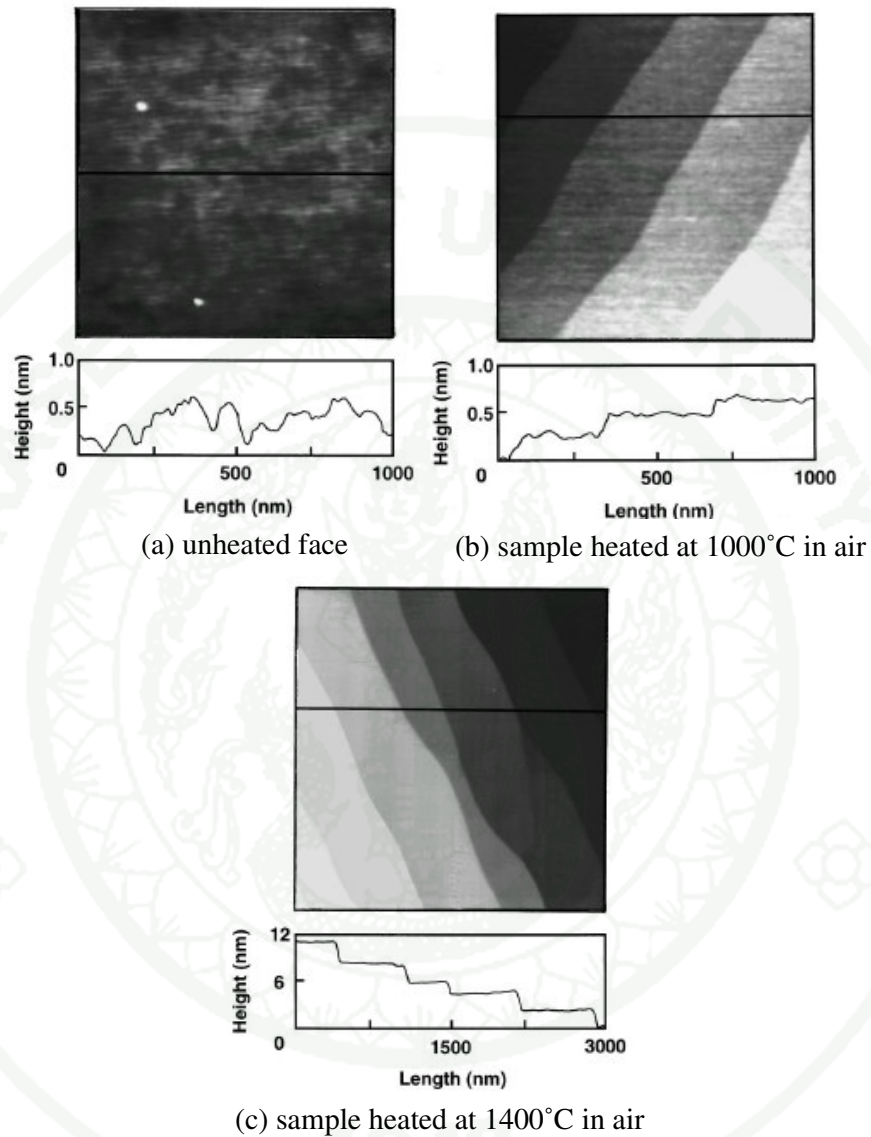


**Figure 7** The AFM images of [0001] sapphire: (a) unheated ( $1 \times 1 \mu\text{m}^2$ ), (b) heated at  $1000^\circ\text{C}$  for 1 hour ( $1 \times 1 \mu\text{m}^2$ ), (c) heated at  $1400^\circ\text{C}$  for 1 hour ( $3 \times 3 \mu\text{m}^2$ ) showing the image after heating at  $1400^\circ\text{C}$ ; the smooth step appear, and the step height increase.

**Source:** Yoshimoto *et al.* (1995)

Pham Van *et al.* (1998) reported that the steps with a height of 0.21 nm are present on clean vicinal [0001] alumina surfaces after mere polishing of the alumina samples. The height of the steps is determined by atomic structure of crystalline alumina and corresponds to the sixth fraction of the unit cell  $c$  in [0001] direction ( $c = 1.299$  nm). Hereafter, the steps on the alumina surface with the height value close to  $c/6$  value will be named as  $c/6$  steps.

Kurnosikov *et al.* (2000) reported that the surface of alumina at [0001] after heating in the air at  $1500^{\circ}\text{C}$  for 1 hour is explored by AFM in the air at room temperature. The step height equals to 0.22 nm (i.e.,  $c/6$  steps) were detected with the multiple steps (Figure 8).

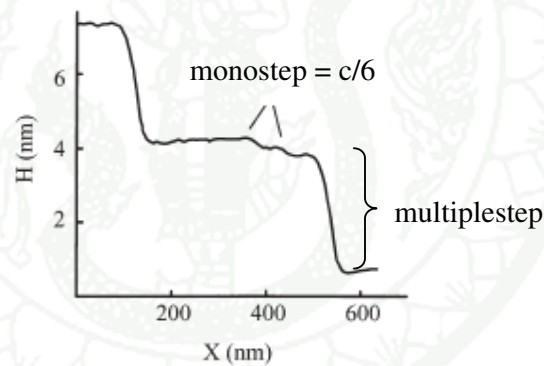


**Figure 8** The  $c/6$  step height of 0.22 nm with the multiple steps on the miscut [0001].

**Source:** Kurnosikov *et al.* (2000)

The atomic steps begin with 0.2 nm or  $c/6$  high steps called monostep ( $c$  is the unit cell height and equal 1.3 nm) (Heffelfinger *et al.*, 1997). The evolution of the step on the basal pinacoid is the increasing height of the atomic steps to be the multiple steps when annealing temperature increases. The multiple steps are caused by those undergo merging of two or many monosteps at high temperature annealing and the step edges become clearer than low temperature annealing. (Pham Van *et al.*, 1998)

Comparison of step height at different annealing temperatures is shown in Figure 9. The merging steps are shown in Figure 10.

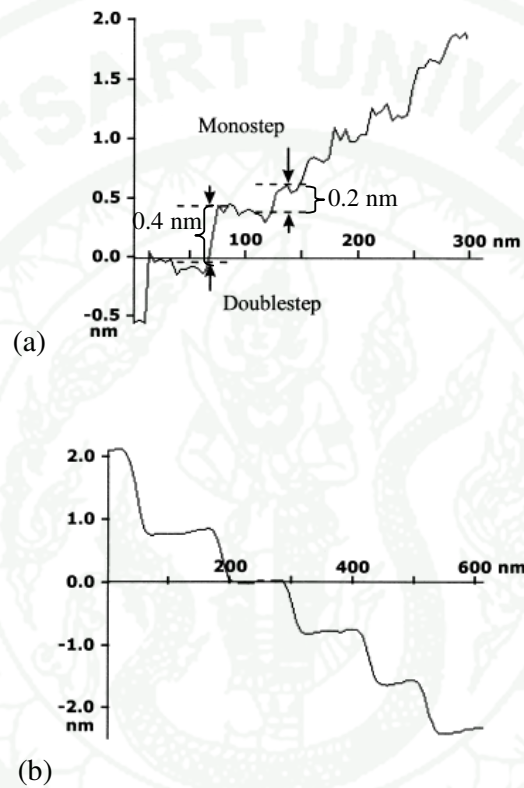


**Figure 9** The comparison of step height at 1100 and 1400°C respectively.

**Source:** Pham Van *et al.* (1998)

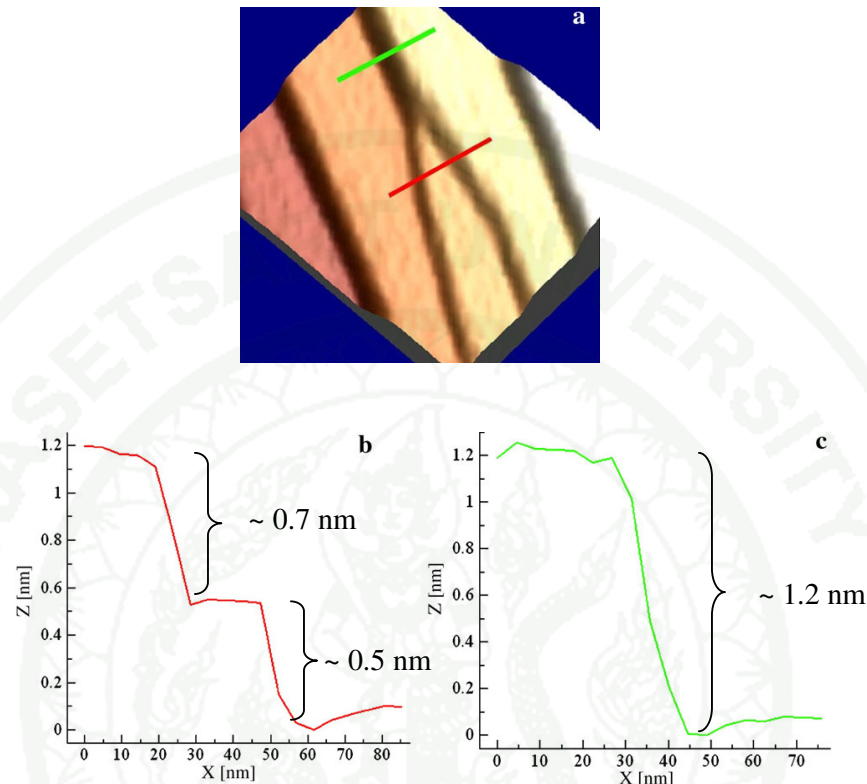


**Figure 10** Showing the merging step of two steps (b) become the higher step (c).

**Source:** After Cuccureddu *et al.* (2010)

Some orientations as c-, a- and m-surfaces after annealing show clearer steps than before annealing (Curiotto and Chatain, 2009). The surface structure of corundum at  $(11\bar{2}0)$  after high temperature annealing begins with monosteps like those of the basal pinacoid plane and becomes multiple step when the annealing temperature increased (Simeonov and Lederman, 2009).

The AFM study of basal pinacoid surface of corundum was shown in previous works (Heffelfinger and Carter, 1997, Pham Van *et al.*, 1998 and Yoshimoto *et al.*, 1995) but various other facets may yield the different results.

## MATERIALS AND METHODS

### Materials

Two flame-fusion synthetic corundum boules, a pink sapphire and a ruby for this research (Figure 11) were collected from Ruscgem Co., Ltd. Each boule was cut and polished as shown in Figures 12a-d. The samples of set 1 (pink sapphire) and set 2 (ruby) with different orientations were labeled and registered (Tables 1 and 2).

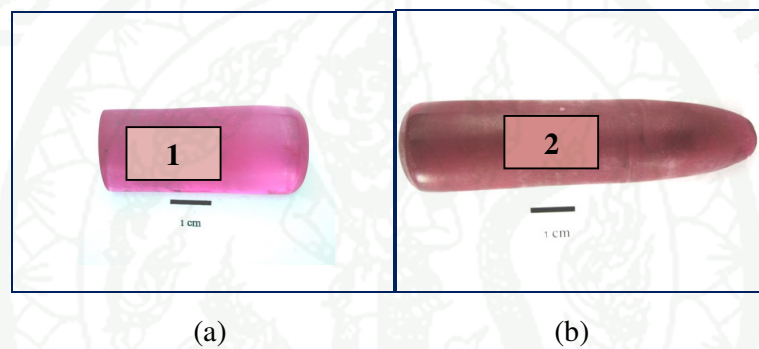


**Figure 11** A synthetic pink sapphire boule(a) and a synthetic ruby boule(b) before cutting and polishing

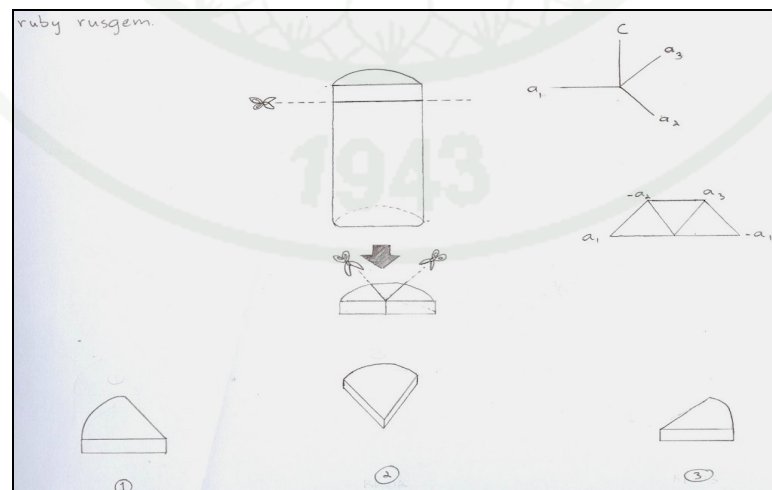


**Figure 12a** Perspective sketches showing sample orientations for cutting through  $a_1$ -,  $a_2$ - and  $a_3$ -axes.

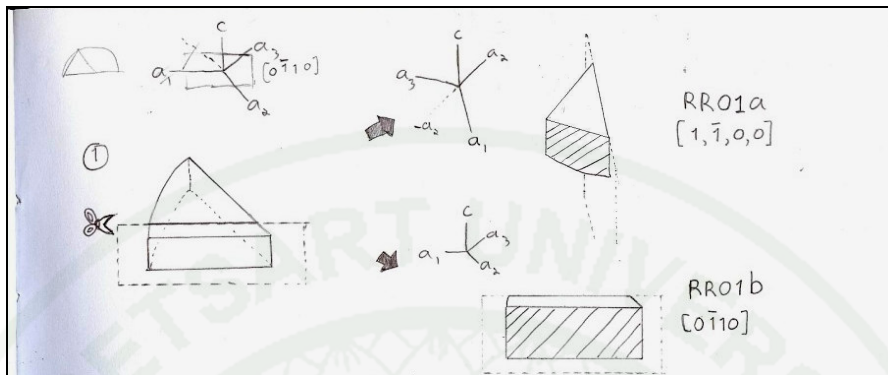


**Figure 12b** Sketches showing, how the first piece in the Figure 11a) was further cut in order to obtain samples with different orientations, for examples, the miscut of the prism  $[0\bar{1}10]$  face (sample RR01b), and the miscut of the prism  $[1\bar{1}00]$  face (sample RR01a).

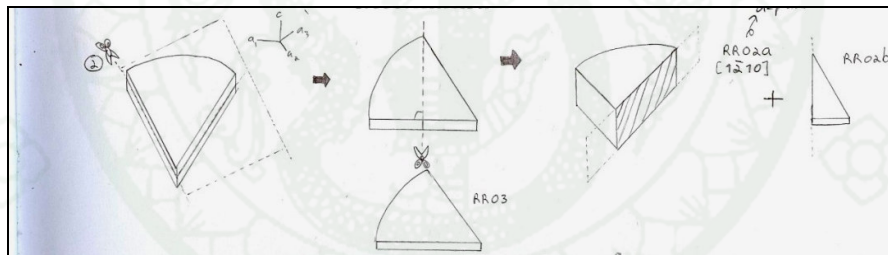


**Figure 12c** The miscut of  $[1\bar{2}10]$  from the second piece in the Figure 11a).

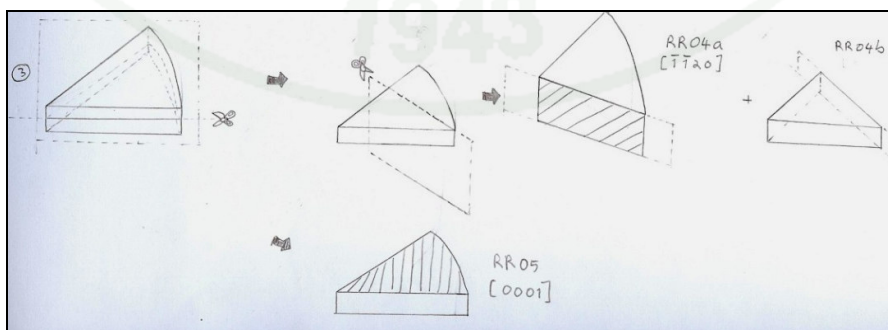


**Figure 12d** The miscut orientations of  $[\bar{1}\bar{1}20]$  and  $[0001]$  from the third piece in the Figure 11a).

**Table 1** Sample registration of set 1 (pink sapphire) after cutting and polishing

Sample	Picture	Weight (g)	Remark
RR01a		0.2966	$[1\bar{1}00]$
RR01b		0.1523	$[0\bar{1}10]$
RR01c		0.0581	$[0\bar{1}10]$
RR01d		0.0677	$[1\bar{1}00]$
RR02a		0.2589	$[1\bar{2}10]$
RR02c		0.0666	$[1\bar{2}10]$
RR04a		0.1196	$[\bar{1}\bar{1}20]$

**Table 1** (Continued)

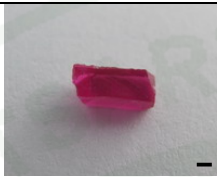
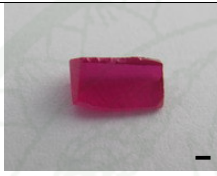
Sample	Picture	Weight (g)	Remark
RR04c		0.0696	$[\bar{1}\bar{1}20]$
RR05a		0.3528	$[0001]$
RR05e		0.1116	$[0001]$

**Remark:** Bar scale = 1 mm.

**Table 2** Sample registration of set 2 (ruby) after cutting and polishing

Sample	Picture	Weight (g)	Remark
RRb01a		0.2323	$[1\bar{1}00]$
RRb01b		0.1135	$[0\bar{1}10]$

**Table 2** (Continued)

Sample	Picture	Weight (g)	Remark
RRb01c		0.0921	$[0\bar{1}10]$
RRb01d		0.1647	$[1\bar{1}00]$
RRb02a		0.1926	$[1\bar{2}10]$
RRb02c		0.0995	$[1\bar{2}10]$
RRb04a		0.0534	$[\bar{1}\bar{1}20]$
RRb04c		0.0589	$[\bar{1}\bar{1}20]$
RRb05a		0.3715	$[0001]$

**Table 2** (Continued)

Sample	Picture	Weight (g)	Remark
RRb05e		0.1864	[0001]

**Remark:** Bar scale = 1 mm.

## Methods

The flow chart of research methodology is shown in Figure 13. The literatures surveys of corundum surfaces of both natural and synthetic as well as those undergone annealing at various temperatures were reviewed. The sample collection was designed by using two sets of sample, pink sapphire and ruby boules, i.e. containing different Cr content. The sample preparation includes cutting and mirror-shine polishing at a gemstone manufacture with respected to the different orientations. After that, physical properties, spectroscopic measurements and surface study by AFM were determined. The same pieces of the samples were cut and undergone annealing at 1650°C for 1 hour in an electrical furnace, i.e. in the oxidizing atmosphere. Again, the physical properties, spectroscopic measurements, and surface study by AFM of heated samples were determined. Finally, results, discussions and conclusions were made.

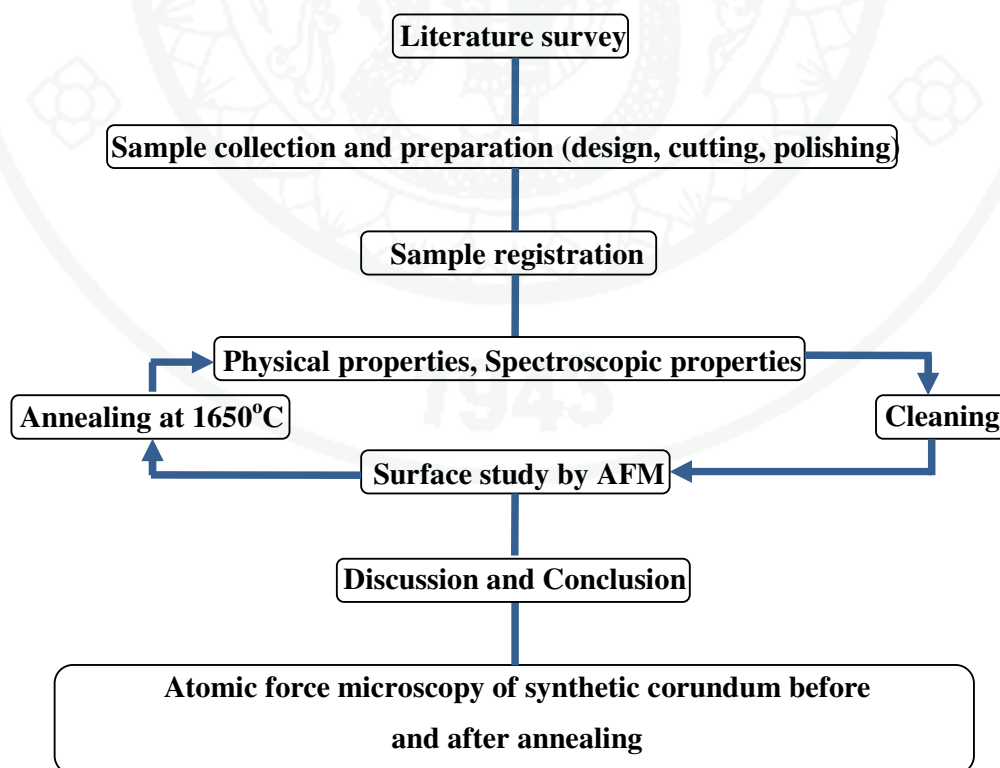


**Figure 13** Flow chart of research methodology

## 1. Basic property measurements

### 1.1 Specific gravity (S.G.)

The samples were weighed by electronic balance (Figure 14) for the sample weights in air ( $W_a$ ) and in water ( $W_w$ ). The specific gravity values of each sample were calculated by the equation below:

$$\text{S.G.} = W_a / (W_a - W_w) \quad (1)$$

When S.G. is a specific gravity,  $W_a$  is weight in air and  $W_w$  is weight in water.



**Figure 14** An electronic balance for measuring S.G. at Department of Earth Sciences, Faculty of Science, Kasetsart University

The specific gravity of a gemstone depends on the kind of mineral, and is usually constant for the same mineral even though the samples would have the different weights or shapes; therefore, it is used for basic identifying of a gemstone.

## 1.2 Refractive index (R.I.)

Refractive index value is a basic property of gemstone that is measured by the refractometer (Figure 15). The principle of refractive index (Figure 16) is related to the Snell's law (2) that depends on the light axis and the optical axis of a sample.

$$n_1 \sin \theta_1 = n_2 \sin \theta_2 \quad (2)$$

When  $n_1$  is the refractive index in air,  $n_2$  is the refractive index in a sample,  $\theta_1$  is an incident angle and  $\theta_2$  is a refraction angle.



**Figure 15** Refractometer, Rayner, and R.I. liquid at Department of Earth Sciences, Faculty of Science, Kasetsart University.

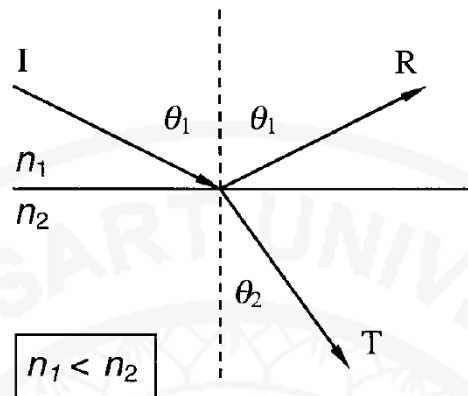


**Figure 16** Light beams reflected (R) and transmitted or refracted (T) at the interface between two refractive indexes,  $n_1$  and  $n_2$ , the second being greater than the first.

### 1.3 Optic axis

The polariscope (Figure 17) was used for finding the optical axis that assumed to be c-axis, before cutting the samples to many orientations for this research.

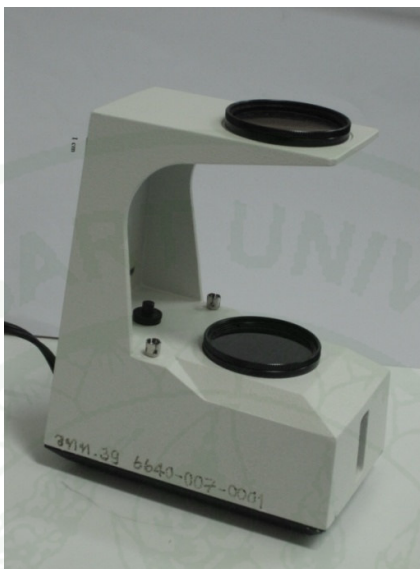


**Figure 17** Polariscope at Department of Earth Sciences, Faculty of Science, Kasetsart University.

#### 1.4 Sample preparation (cutting and polishing)

The sample preparation in this research by cutting at certain orientations was very important. The different orientations of samples were designed. Then the synthetic ruby boule was cut following the design by the local-made cutting machine. At first the sample boule was cut through  $a_1$ -,  $a_2$ - and  $a_3$ -axis, and three pieces of samples were obtained (Figure 12a). The first one of three pieces was then divided into two pieces; one was at the right side of the sample that was the miscut of the prism  $[0\bar{1}10]$ , and the other was at the rim of the sample that was the miscut of the prism  $[1\bar{1}00]$  face (Figure 12b).

The second of the three pieces was cut at the top right corner perpendicular to the opposite side; the surface parameter of this side is  $[1\bar{2}10]$  (Figure 12c). The last piece one was cut in the horizontal manner in order to obtain the top side being as the basal pinacoid or the  $[0001]$  face, and the lower part was shunted at the right corner of the triangle piece perpendicular to the opposite side, the surface of this side was used as the miscut  $[\bar{1}\bar{1}20]$  face (Figure 12d). Each piece was further cut into two pieces, one for heating at  $1650^{\circ}\text{C}$  in an electric furnace for one hour.

The samples were designed for experiments and cut following the design by Thai sawing and grinding machines (Figure 18). The samples were stuck with the bar and truncated to the easy shape for polishing by Thai local-made trim machine (Figure 19). After that, the samples were polished using Thai faceting machine (Figure 20). Thai faceting machine is the equipment for polishing the gemstone at lapidary quality. The annealing samples were made by heating at  $1650^{\circ}\text{C}$  for 1 hour in the electric furnace (Lenton, model UAF18/5) which placed at Earth Sciences Department, Kasetsart University, Bangkok (Figure 21).



**Figure 18** Thai sawing and grinding machines for sample cutting at Department of Earth Sciences, Faculty of Science, Kasetsart University.



**Figure 19** Sticking sample with the sample holder bar (left) then truncated by Thai local-made trim machine (right) at Department of Earth Sciences, Faculty of Science, Kasetsart University.



**Figure 20** The local-made polishing machine at Department of Earth Sciences, Faculty of Science, Kasetsart University.



**Figure 21** The high temperature electric furnace; Lenton, model UAF18/5 at Department of Earth Sciences, Kasetsart University, Bangkok

## 2. Optical Spectroscopy

### 2.1 Fourier Transform Infrared (FTIR) spectroscopy

The absorption and/or transmission spectra in the mid infrared range ( $400\text{-}4000\text{ cm}^{-1}$ ) were measured and recorded by Fourier Transform Infrared (FTIR) spectrophotometer. The infrared spectrum contains information on vibrations and bondings of light molecules in the samples, induced by IR. The structural vibrations depend on the molecular masses, bond lengths and bond angles between atoms. The FTIR spectrophotometer model NEXUS 470 was used in this study (Figure 22).



**Figure 22** NEXUS 470 FTIR spectrophotometer at Department of Earth Sciences, Faculty of Science, Kasetsart University.

## 2.2 UV-Vis-NIR Spectroscopy

The absorption spectra of UV-Vis-NIR of the samples were detected, and displayed by the monitor. UV-Vis-NIR spectroscopy relates to valent electronic transitions of transition trace elements or some structural defects in the sample. This study shows the absorption patterns obtained by UV-Vis-NIR spectrophotometer Perkin Elmer model LAMDA 900 (Figure 23) at the Department of Earth Sciences.



**Figure 23** UV-Vis-NIR spectroscopy Perkin Elmer model LAMDA 900 placed at Department of Earth Sciences, Faculty of Science, Kasetsart University.

### 3. Surface measurement

#### 3.1 Atomic Force Microscopy

Atomic Force Microscope (AFM) model MFP-3D-BIO from Asylum Research (Figure 24), placed at the Scientific Equipment Center, Faculty of Science, Kasetsart University, was used for studying the micro to nano scaled surface of the samples. Before measuring, the sample was cleaned in 10% Decon solution for 24 hours, washed with 1% NaOH and rinsed well with deionised water (Gan *et al.*, 2007). After drying the sample was kept in a clean box, and placed in a desiccator prior to AFM measurement.

Atomic Force Microscope usually referred to the scanning force microscope (SFM) that is the scanning probe microscope which is called SPM (Bowen and Hilal, 2009). The atomic force microscope was first invented and described by Gerd Binnig and Heinrich Rohrer; they were awarded the Nobel Prize in 1986 (Birdi, 2003). AFM was developed from the scanning tunneling microscope (STM) to measure the surface topography of both conducting and nonconducting samples.

The principle of AFM is working by the tiny tip with diameter about 7-10 nm under the nib of the cantilever whose function is creating the image while the surface moving under the tip. When placing the tip on the sample surface, there is a reaction force to the cantilever which is tilted by various degrees to the thickness of the steps. The step height can be detected by the laser that reflects from the top of the cantilever nib to the detector (Figure 25). The computer changes the signal to the picture shown on the computer screen. The roughness limit of measuring is not over 4 micrometer, and the large scan is not over 80  $\mu\text{m}$ .



**Figure 24** Atomic Force Microscope model MFP-3D-BIO AFM from Asylum Research based at the Scientific Equipment Center, Faculty of Science Kasetsart University, Bangkok.

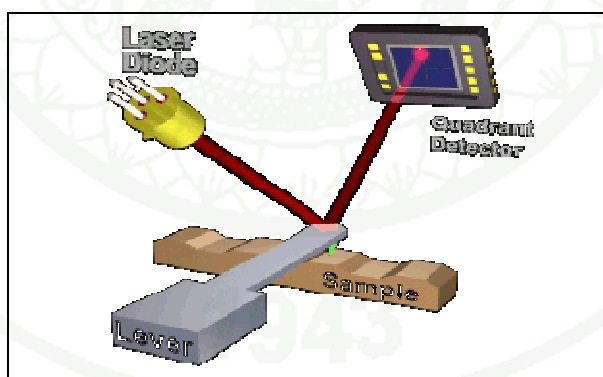


**Figure 25** The working principle of AFM tip sensing by the laser to present the image on the monitor

**Source:** Markiewicz (2011)

## RESULTS AND DISCUSSION

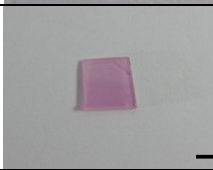
### Results

In this study, the surface features at micro-nanometre level of synthetic pink sapphire and ruby samples were determined by using Atomic Force Microscope (AFM). The basic physical properties of the samples were measured and recorded prior to the AFM measurement. The results are shown together with the sample registration in Tables 3 and 4.

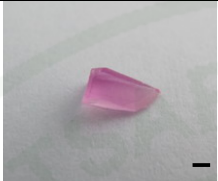
#### 1. Physical properties

The synthetic corundum samples were determined for their refractive index (R.I.) and specific gravity (S.G.) values. All the samples of both sets show their R.I. of 1.762 and 1.770 with the S.G. values varying between 3.83-4.01 for pink sapphires, and 3.93-4.00 for the ruby samples.

**Table 3** Physical properties of synthetic pink sapphires (set 1) at different surface orientations

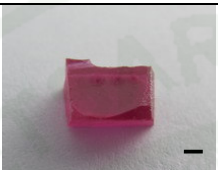
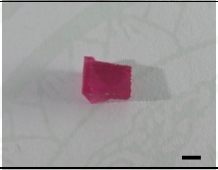
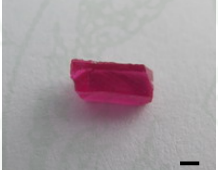
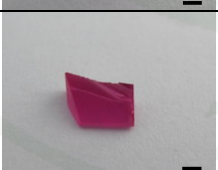
Sample	Picture	Wt. (g)	R.I.	S.G.	Remarks
RR01a		0.2966	1.762 1.770	3.92	miscut [1 $\bar{1}$ 00] unheated ( $\nabla$ )
RR01b		0.1523	1.762 1.770	4.01	miscut [0 $\bar{1}$ 10] unheated ( $\nabla$ )
RR01c		0.0581	1.762 1.770	3.92	miscut [0 $\bar{1}$ 10] heated ( $\Delta$ )

**Table 3** (Continued)

Sample	Picture	Wt. (g)	R.I.	S.G.	Remarks
RR01d		0.0677	1.762 1.770	3.98	miscut [1 $\bar{1}$ 00] heated ( $\Delta$ )
RR02a		0.2589	1.762 1.770	3.97	miscut [1 $\bar{2}$ 10] unheated ( $\nabla$ )
RR02c		0.0666	1.762 1.770	3.83	miscut [1 $\bar{2}$ 10] heated ( $\Delta$ )
RR04a		0.1196	1.762 1.770	3.95	miscut [ $\bar{1}$ $\bar{1}$ 00] unheated ( $\nabla$ )
RR04c		0.0696	1.762 1.770	4.00	miscut [ $\bar{1}$ $\bar{1}$ 00] unheated ( $\Delta$ )
RR05a		0.3528	1.762 1.770	3.96	miscut [0001] unheated ( $\nabla$ )
RR05e		0.1116	1.762 1.770	3.97	miscut [0001] heated ( $\Delta$ )

**Remarks:**  $\nabla$  = unheated,  $\Delta$  = heated; Bar scale = 1 mm.

**Table 4** Physical properties of synthetic ruby samples (set 2) at different surface orientations

Sample	Picture	Wt. (g)	R.I.	S.G.	Remark
RRb01a		0.2323	1.762 1.770	3.94	miscut [1 $\bar{1}$ 00] unheated ( $\Delta$ )
RRb01b		0.1135	1.762 1.770	3.93	miscut [0 $\bar{1}$ 10] unheated ( $\Delta$ )
RRb01c		0.0921	1.762 1.770	3.94	miscut [0 $\bar{1}$ 10] heated ( $\Delta$ )
RRb01d		0.1647	1.762 1.770	3.97	miscut [1 $\bar{1}$ 00] heated ( $\Delta$ )
RRb02a		0.1926	1.762 1.770	3.98	miscut [1 $\bar{2}$ 10] unheated ( $\Delta$ )
RRb02c		0.0995	1.762 1.770	4.00	miscut [1 $\bar{2}$ 10] heated ( $\Delta$ )
RRb04a		0.0534	1.762 1.770	3.98	miscut [ $\bar{1}$ $\bar{1}$ 00] unheated ( $\Delta$ )
RRb04c		0.0589	1.762 1.770	3.95	miscut [ $\bar{1}$ $\bar{1}$ 00] unheated ( $\Delta$ )

**Table 4** (Continued)

Sample	Picture	Wt. (g)	R.I.	S.G.	Remark
RRb05a		0.3715	1.762 1.770	3.98	miscut [0001] unheated ( $\nabla$ )
RRb05e		0.1864	1.762 1.770	3.99	miscut [0001] heated ( $\Delta$ )

**Remarks:**  $\nabla$  = unheated,  $\Delta$  = heated; Bar scale = 1 mm.

The results of R.I. and S.G. of the samples revealed that the samples seem to be the homogeneity.

## 2. Spectroscopy

FTIR and UV-Vis-NIR absorption spectra of synthetic corundum samples were recorded in order to distinguish the heated and unheated samples.

### 2.1 UV-Vis-NIR results

The samples show UV-Vis-NIR spectra with two  $\text{Cr}^{3+}$  absorptions centering at 405 and 555 nm (Figures 26-45); the red samples (set 2) show higher absorption intensities than those of the pink sapphires (set1) due to the higher Cr content. The synthetic ruby samples show the PL spectrum peak at 695 nm (Figure 36-45).

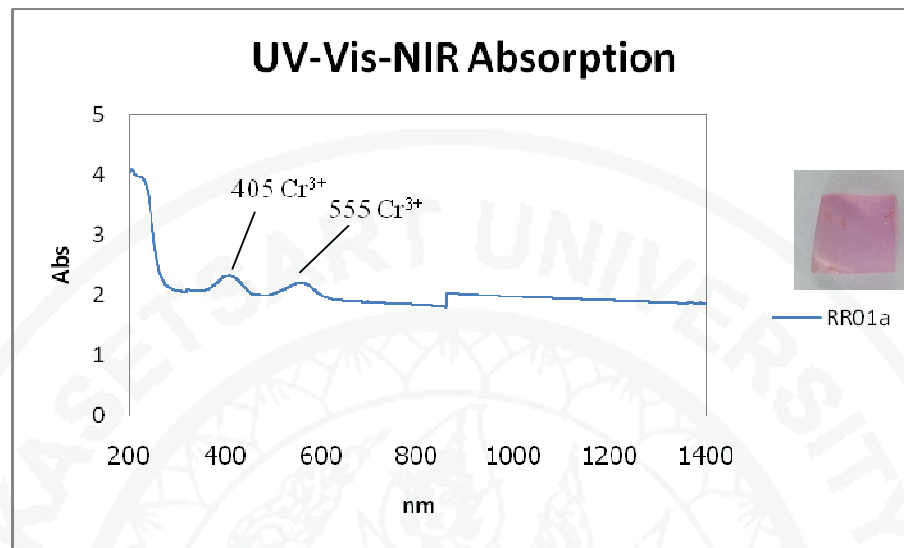


**Figure 26** UV-Vis-NIR absorption spectrum of the unheated synthetic pink sapphire sample set 1, the beam was perpendicular to the miscut prism  $[1\bar{1}00]$  face (RR01a).

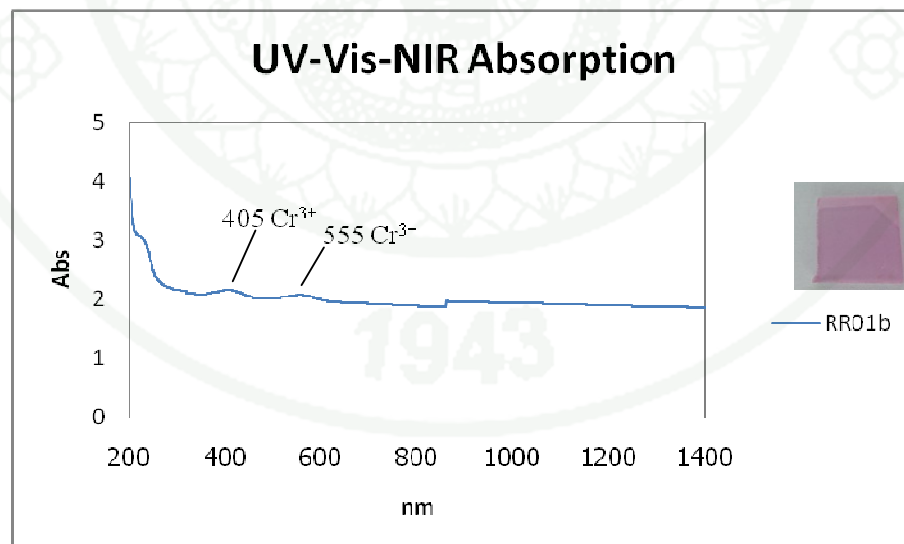


**Figure 27** UV-Vis-NIR absorption spectrum of the unheated synthetic pink sapphire sample set 1, the beam was perpendicular to the miscut prism  $[0\bar{1}10]$  face (RR01b).

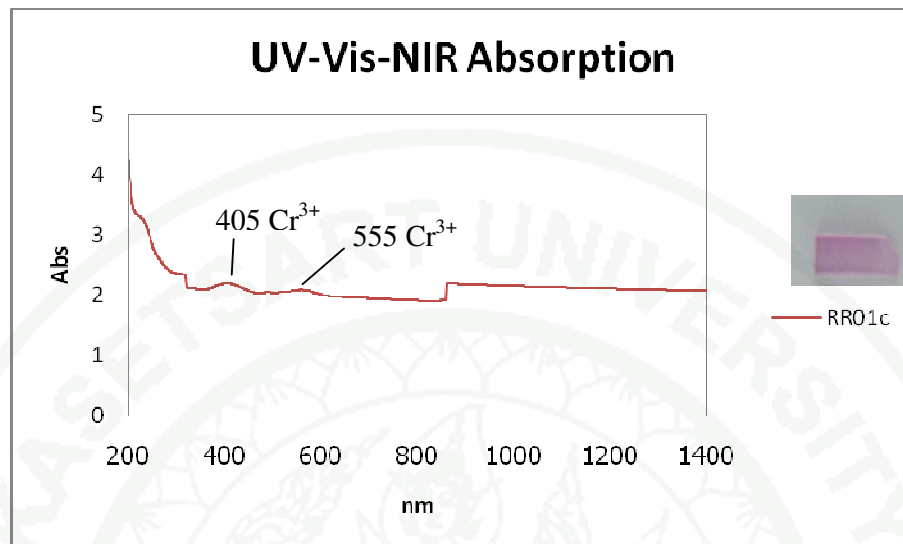


**Figure 28** UV-Vis-NIR absorption spectrum of the heated synthetic pink sapphire sample set 1, the beam was perpendicular to the miscut prism  $[0 \bar{1} 10]$  face (RR01c).

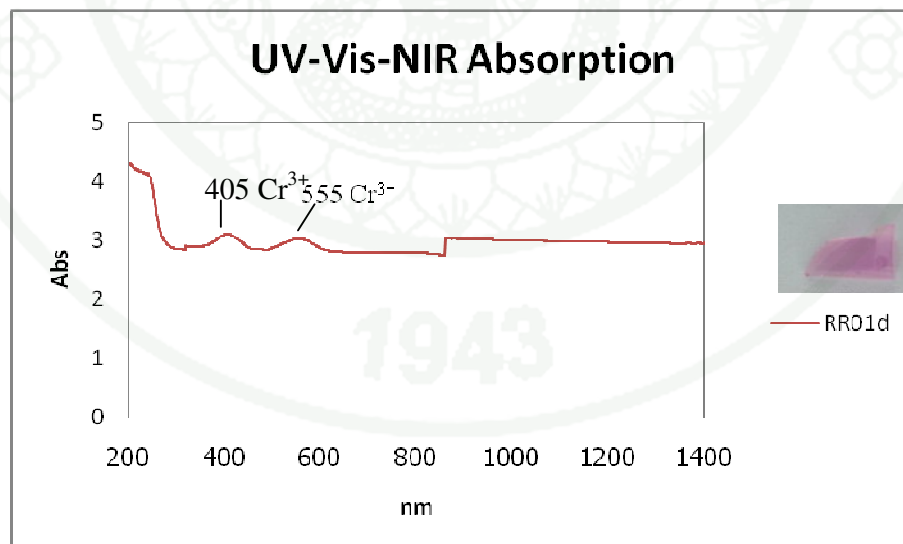


**Figure 29** UV-Vis-NIR absorption spectrum of the heated synthetic pink sapphire sample set 1, the beam was perpendicular to the miscut prism  $[1 \bar{1} 00]$  face (RR01d).

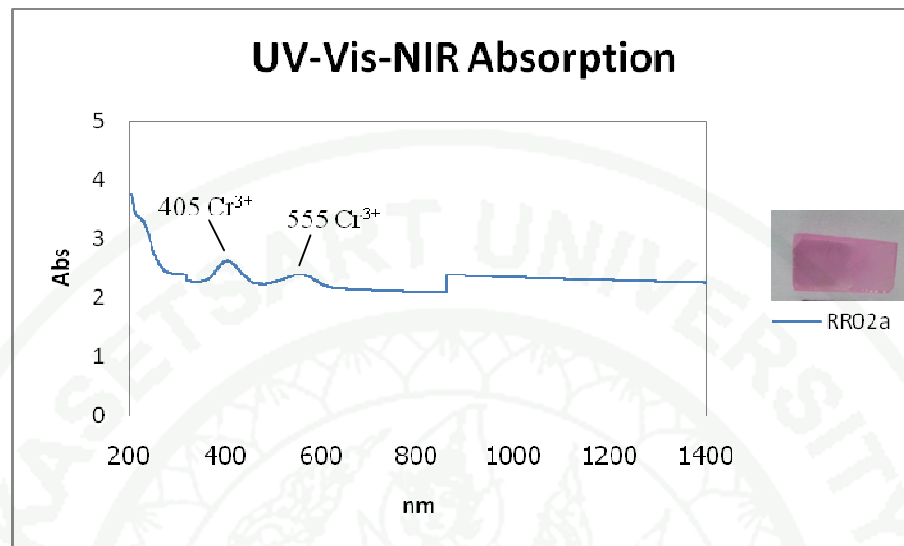


**Figure 30** UV-Vis-NIR absorption spectrum of the unheated synthetic pink sapphire sample set 1, the beam was perpendicular to the miscut prism  $[1\bar{2}10]$  face (RR02a).

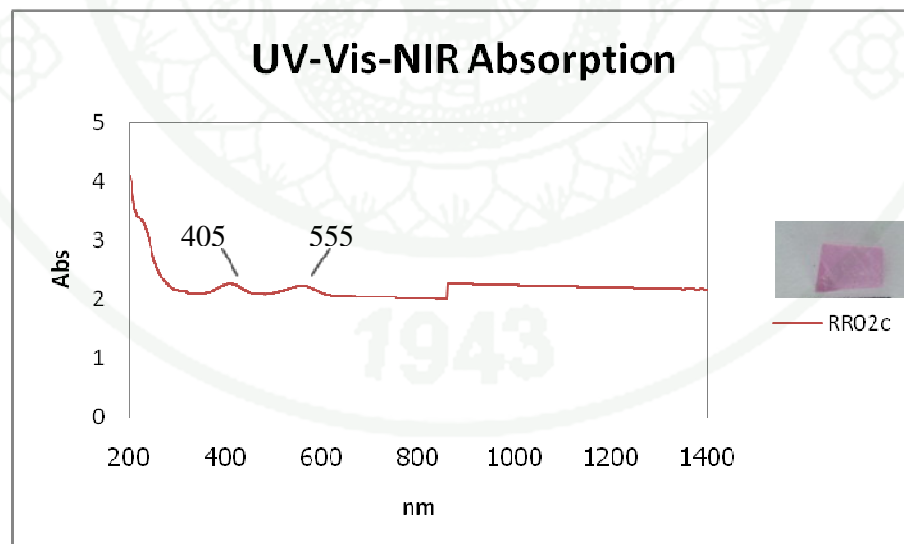


**Figure 31** UV-Vis-NIR absorption spectrum of the heated synthetic pink sapphire sample set 1, the beam was perpendicular to the miscut prism  $[1\bar{2}10]$  face (RR02c).

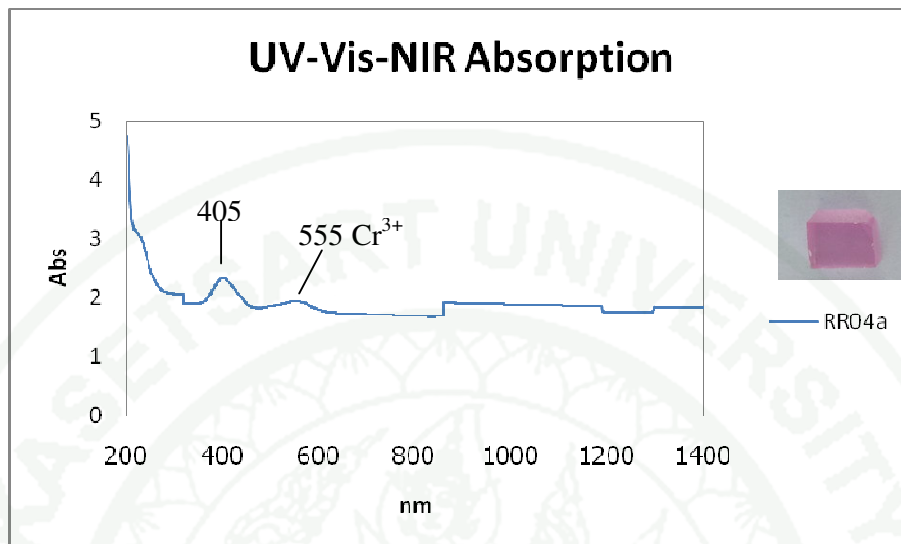


**Figure 32** UV-Vis-NIR absorption spectrum of the unheated synthetic pink sapphire sample set 1, the beam was perpendicular to the miscut prism  $[\bar{1}\bar{1}00]$  face (RR04a).

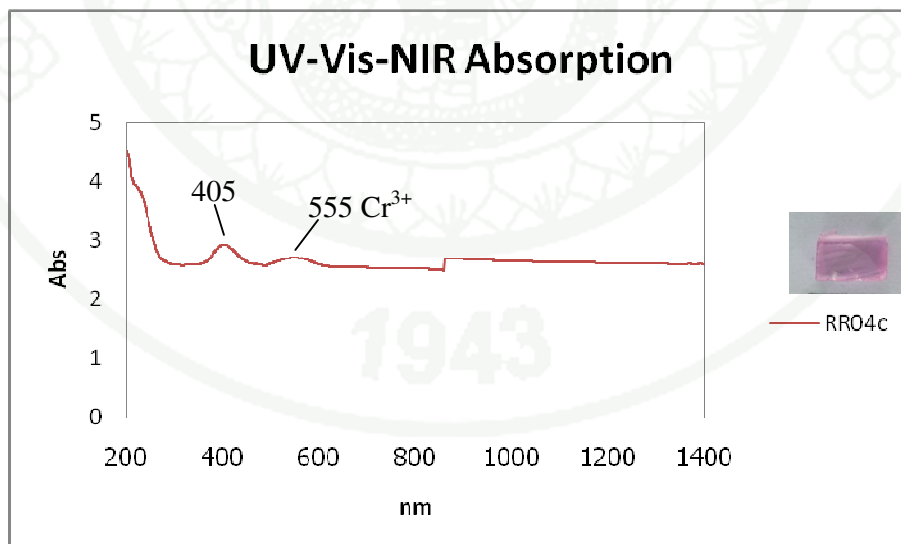


**Figure 33** UV-Vis-NIR absorption spectrum of the heated synthetic pink sapphire sample set 1, the beam was perpendicular to the miscut prism  $[\bar{1}\bar{1}00]$  face (RR04c).

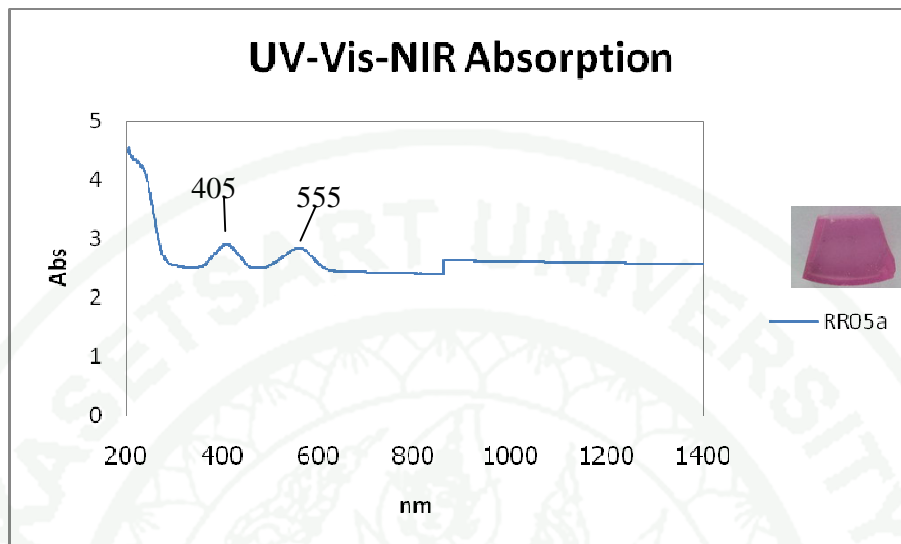


**Figure 34** UV-Vis-NIR absorption spectrum of the unheated synthetic pink sapphire sample set 1, the beam was perpendicular to the miscut pinacoid [0001] face (RR05a).

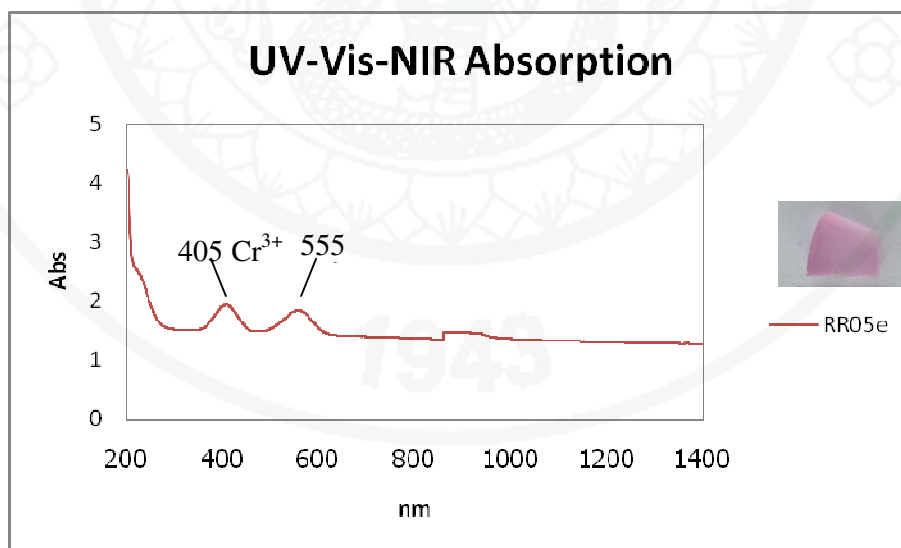


**Figure 35** UV-Vis-NIR absorption spectrum of the heated synthetic pink sapphire sample set 1, the beam was perpendicular to the miscut pinacoid [0001] face (RR05e).

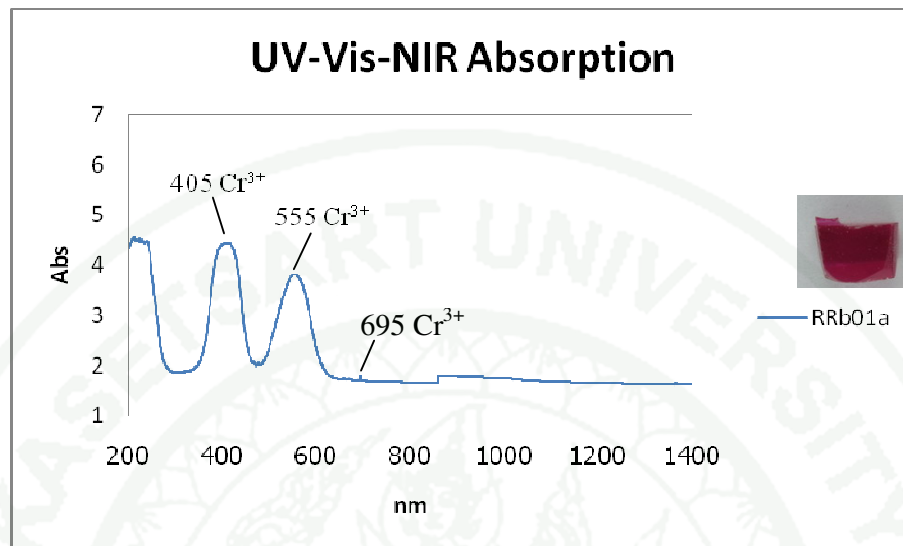


**Figure 36** UV-Vis-NIR absorption spectrum of the unheated synthetic ruby sample set 2, the beam was perpendicular to the miscut prism  $[1\bar{1}00]$  face (RRb01a).

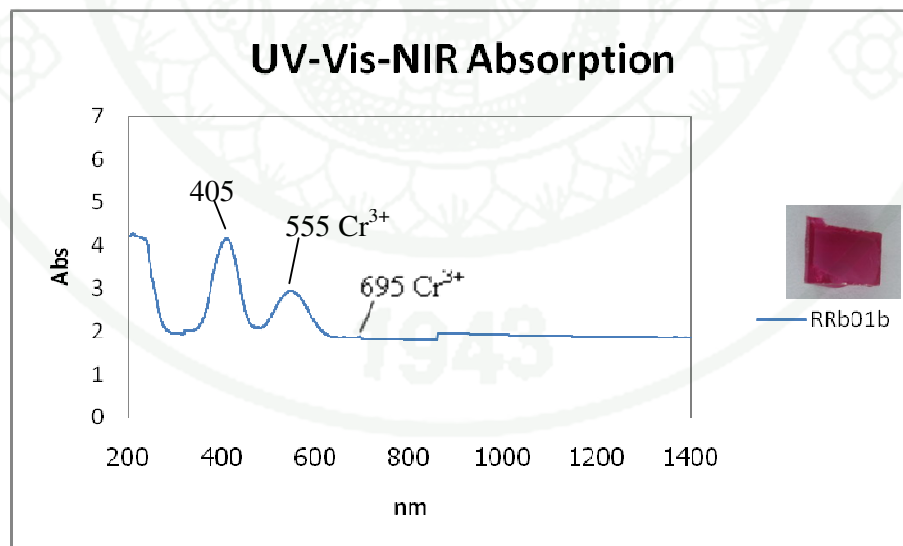


**Figure 37** UV-Vis-NIR absorption spectrum of the unheated synthetic ruby sample set 2, the beam was perpendicular to the miscut prism  $[0\bar{1}10]$  face (RRb01b).

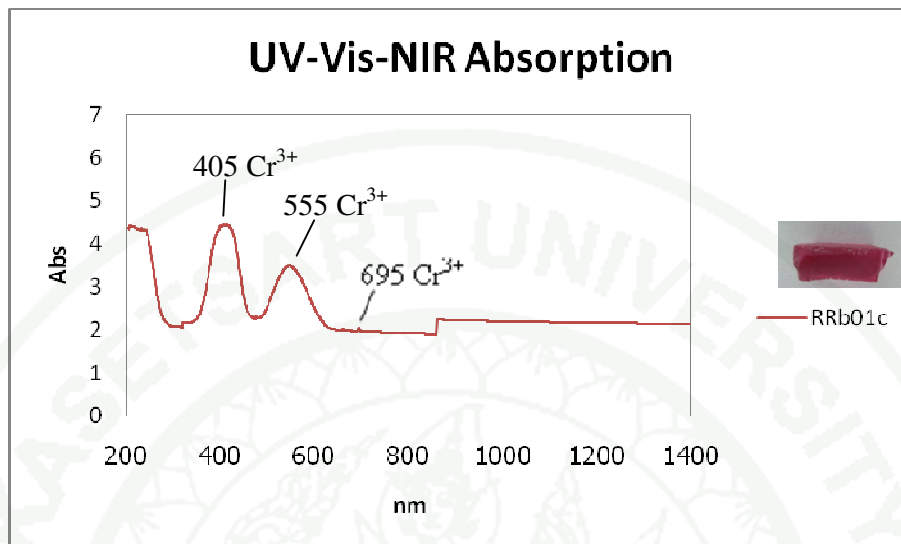


**Figure 38** UV-Vis-NIR absorption spectrum of the heated synthetic ruby sample set2, the beam was perpendicular to the miscut prism  $[0\bar{1}10]$  face (RRb01c).

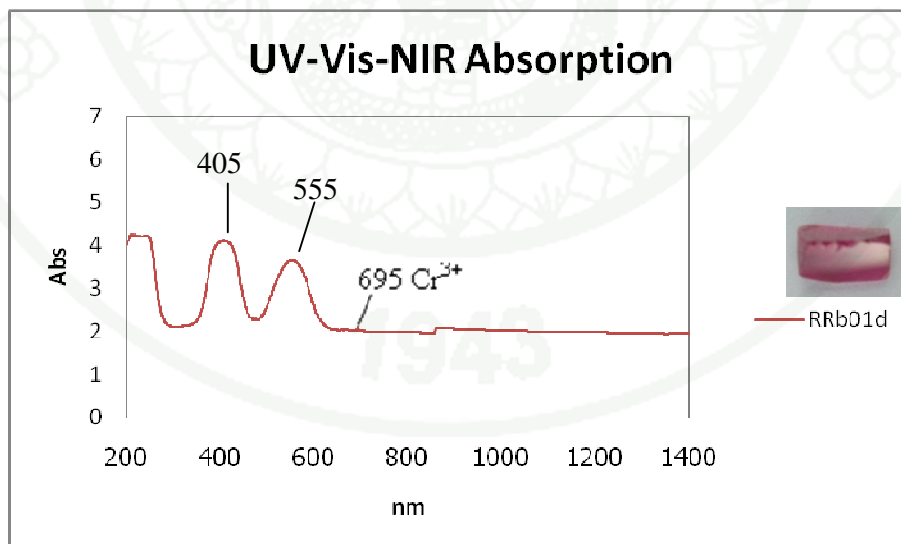


**Figure 39** UV-Vis-NIR absorption spectrum of the heated synthetic ruby sample set2, the beam was parallel to the miscut prism  $[1\bar{1}00]$  face (RRb01d).

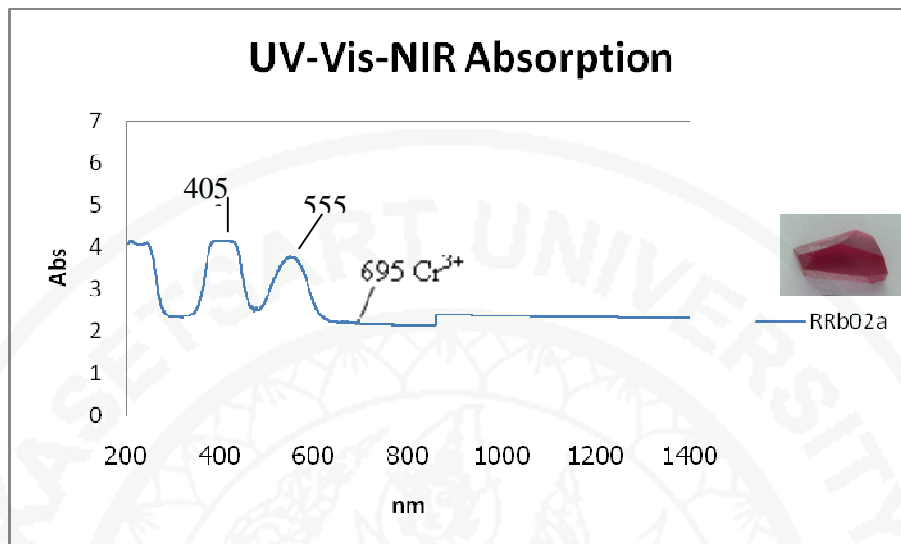


**Figure 40** UV-Vis-NIR absorption spectrum of the unheated synthetic ruby sample set 2, the beam was perpendicular to the miscut prism  $[1\bar{2}10]$  face (RRb02a).

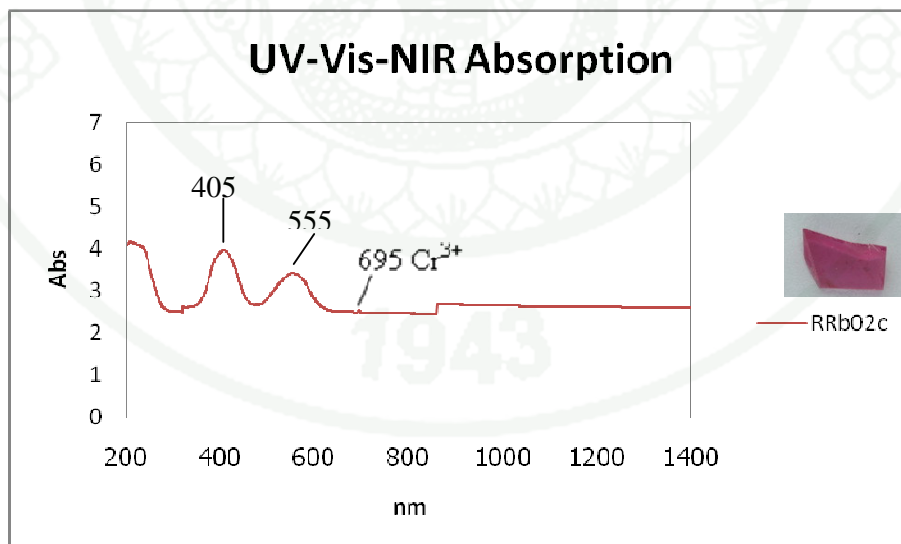


**Figure 41** UV-Vis-NIR absorption spectrum of the heated synthetic ruby sample set2, the beam was perpendicular to the miscut prism  $[1\bar{2}10]$  face (RRb02c).

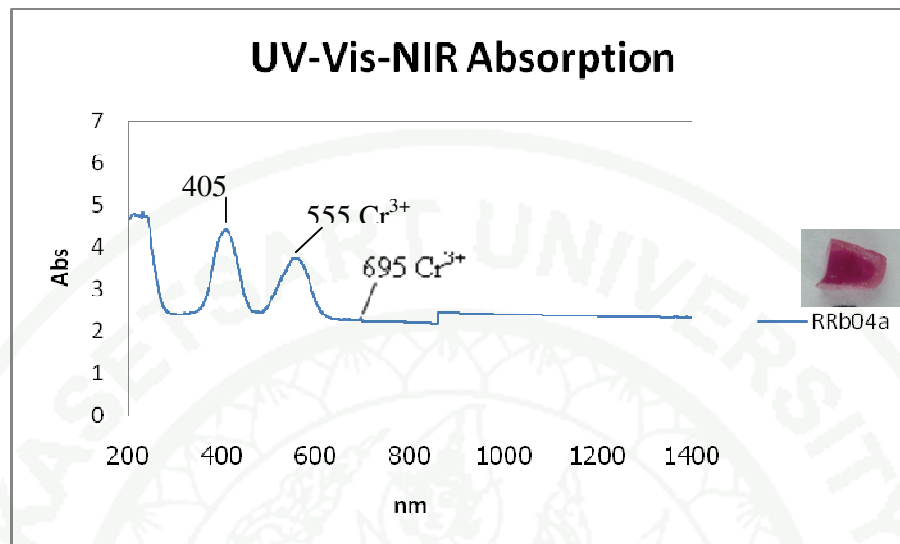


**Figure 42** UV-Vis-NIR absorption spectrum of the unheated synthetic ruby sample set 2, the beam was perpendicular to the miscut prism  $[\bar{1}\bar{1}00]$  face (RRb04a).

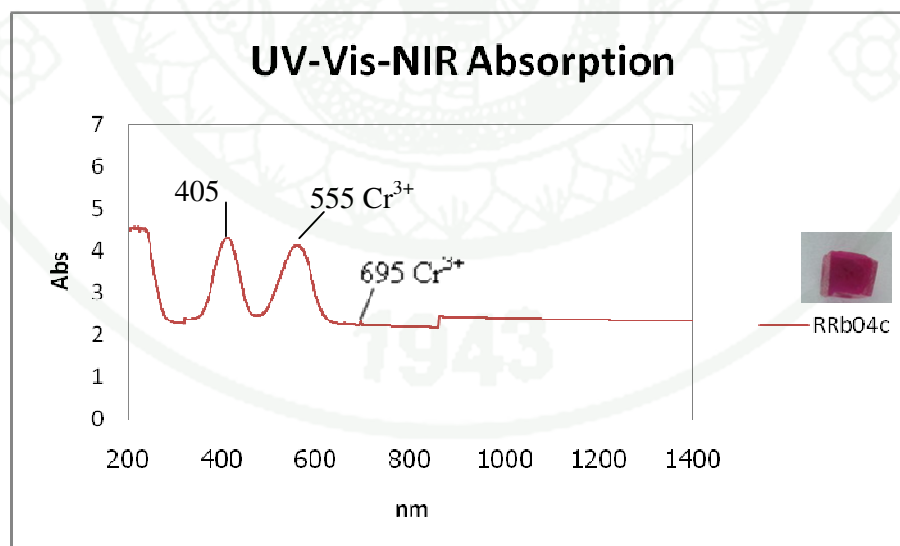


**Figure 43** UV-Vis-NIR absorption spectrum of the heated synthetic ruby sample set2, the beam was perpendicular to the miscut prism  $[\bar{1}\bar{1}00]$  face (RRb04c).

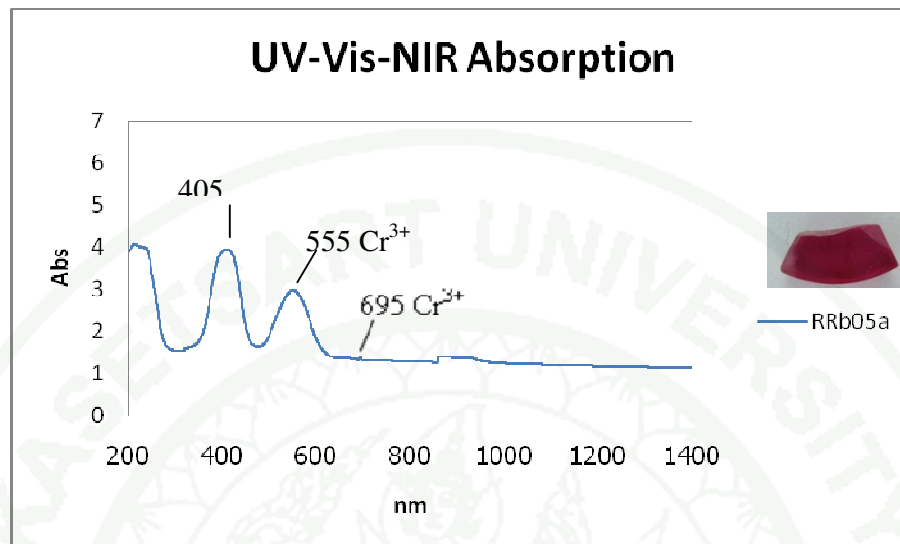


**Figure 44** UV-Vis-NIR absorption spectrum of the unheated synthetic ruby sample set 2, the beam was perpendicular to the miscut pinacoid [0001] face (RRb05a).

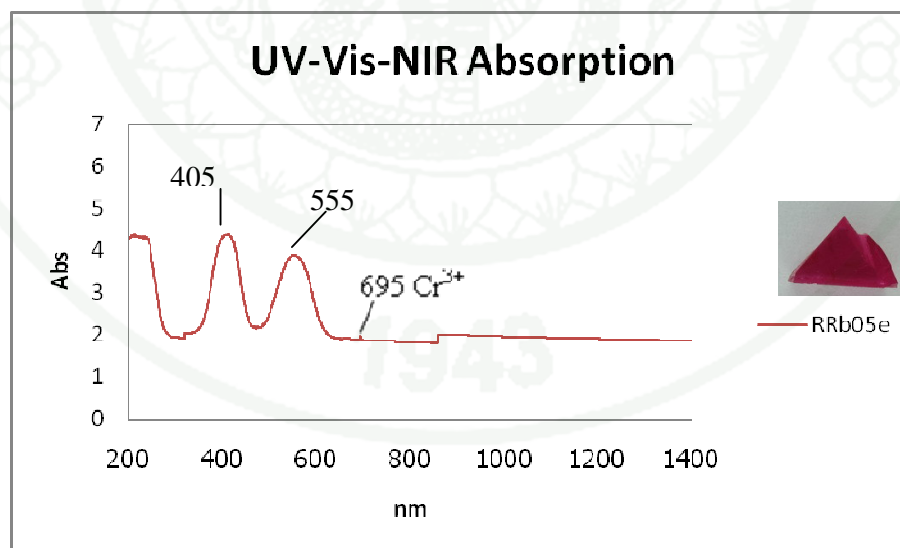


**Figure 45** UV-Vis-NIR absorption spectrum of the heated synthetic ruby sample set2, the beam was perpendicular to the miscut pinacoid [0001] face (RRb05e).

The UV-Vis-NIR absorption spectrum at the miscut pinacoid [0001] face of the heated synthetic pink sapphire sample has higher absorption than that of the unheated one about 3 times (Figure 46), whereas the absorption spectrum at the other miscut prism faces, for an example at the  $[1\bar{2}10]$  of the heated synthetic pink sapphire sample has lower absorption than that of the unheated sample about 1.5 times (Figure 47). The calculation of the absorbances based on the same path length gives better identical absorption peaks than those before applying the path length correction (Figure 48 of 49). UV-Vis-NIR results summarize in Table 5.

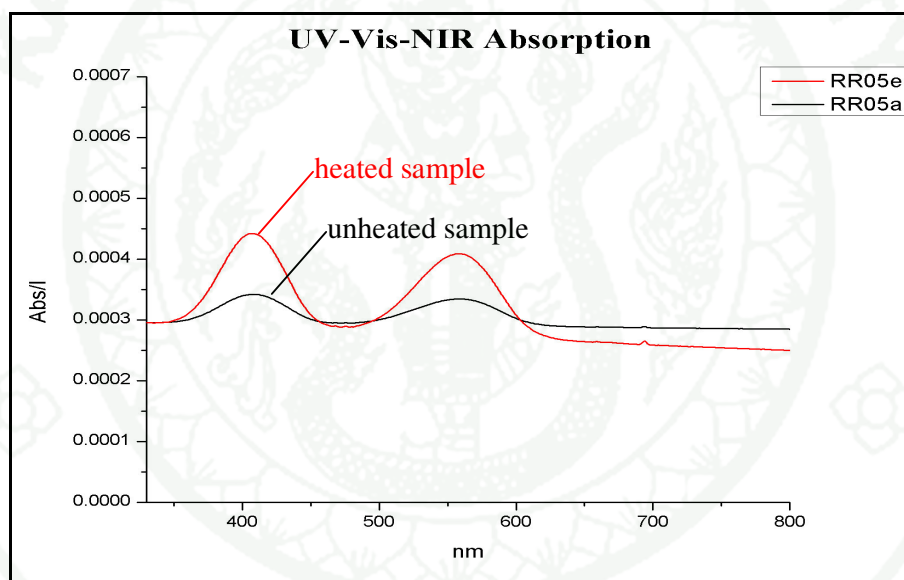


**Figure 46** UV-Vis-NIR spectra showing the higher absorption of the miscut pinacoid [0001] face of heated sample (RR05e) than that of the unheated one (RR05a).

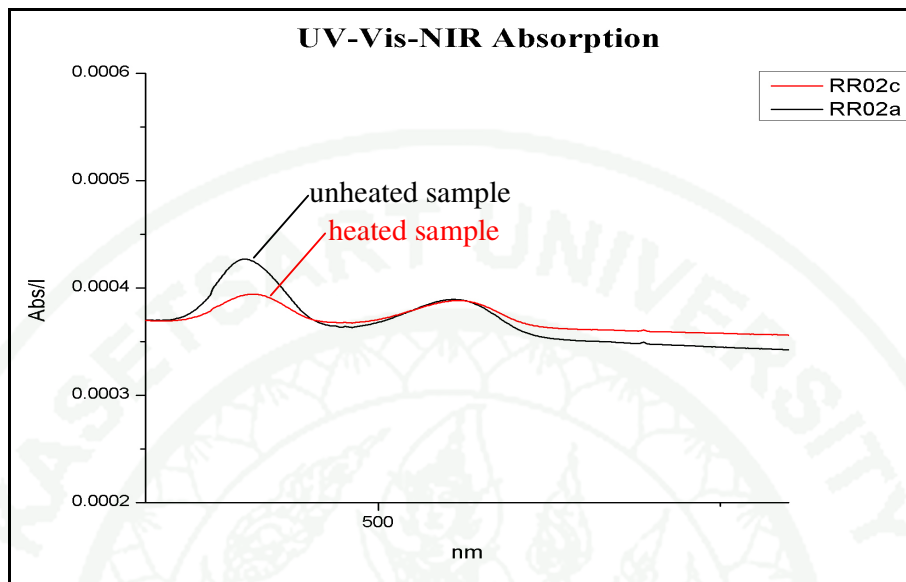


**Figure 47** UV-Vis-NIR spectra showing the lower absorption at the miscut prism  $[1\bar{2}10]$  face of heated sample (RR02c) than that of the unheated one (RR02a).

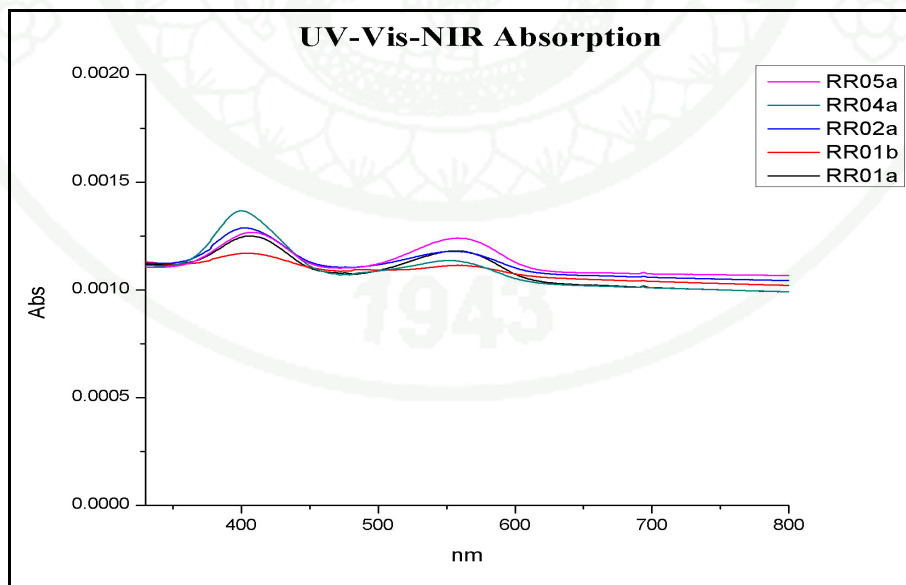


**Figure 48** UV-Vis-NIR absorption spectra of unheated synthetic pink sapphire samples before applying the path length correction.

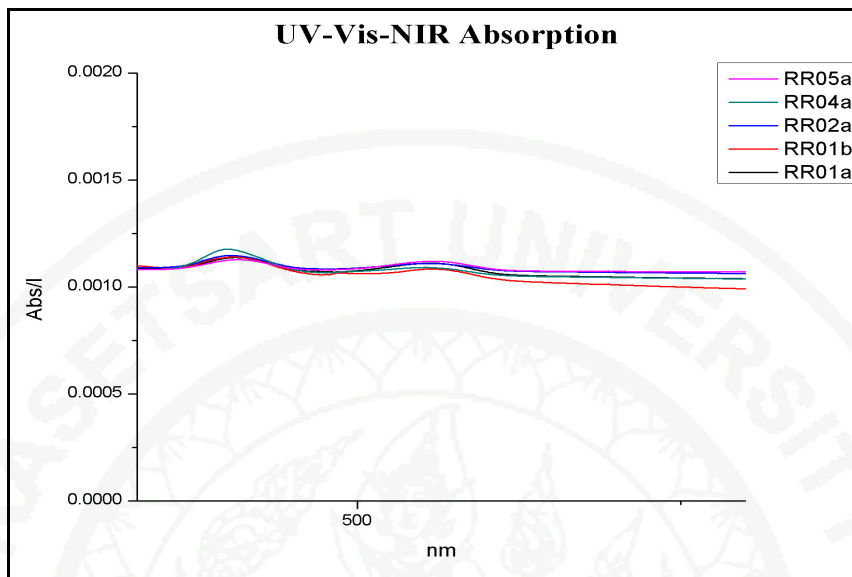


**Figure 49** UV-Vis-NIR absorption spectra of unheated synthetic pink sapphire samples after applying the pathlength correction.

**Table 5** The UV-Vis-NIR result conclusions of the synthetic pink sapphire and ruby samples

UV-Vis-NIR	Pink sapphire	Ruby
Absorption peaks	405, 555 nm.	405, 555, 695 nm.
Absorption at c-face	$\Delta > \text{\AA}$ (~3 times)	$\Delta > \text{\AA}$ (~1.5 times)
Absorption at prism face	$\text{\AA} > \Delta$ (~1.5 times)	$\text{\AA} > \Delta$ (~1.2 times)

**Remark:**  $\text{\AA}$  = unannealed sample,  $\Delta$  = annealed sample

## 2.2 FTIR results

FTIR results reveal absorption peaks of before and after annealing at 1650°C for 1 hour. The samples (both set 1 and set 2) show the absorption peak of CO<sub>2</sub> at 2345 cm<sup>-1</sup> for both heated and unheated samples due to the measuring environment, but the absorption peaks of structural OH at 3309, 3237, 3184cm<sup>-1</sup> present only in the samples before annealing (Figures 50). The 3309 and 3237 cm<sup>-1</sup> peaks were assigned for structural -Ti-OH and -V-OH, respectively (Volynet *et al.*, 1972), whereas the peak at 3184 cm<sup>-1</sup> has not yet been identified (Table 6).

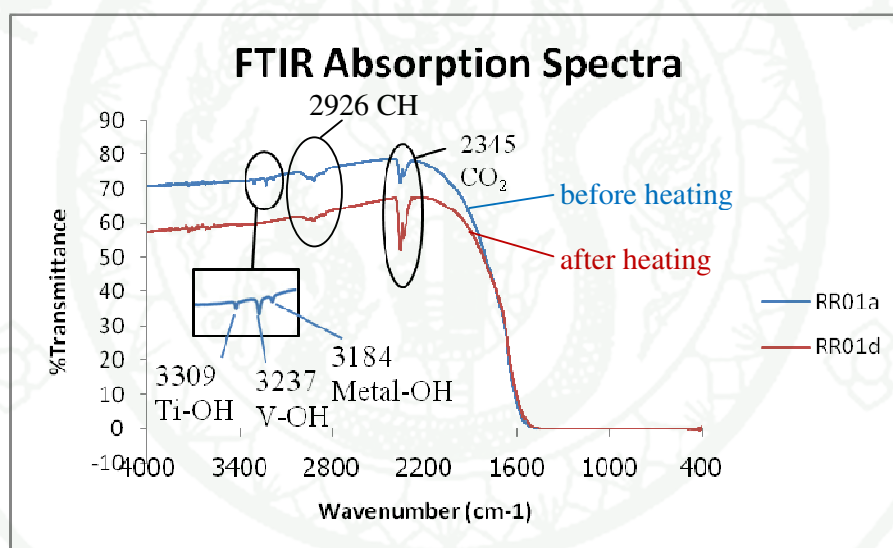


**Figure 50** FTIR spectra of synthetic pink sapphire samples set 1, through the miscut prism  $[1\bar{1}00]$  face of the samples (RR01a, RR01d).

**Table 6** The infrared absorbance characteristics of the samples.

Wavenumber (cm <sup>-1</sup> )	Characteristic (Wathanakul <i>et al.</i> , 2006)
2345	CO <sub>2</sub>
2926	CH stretching
3184	-Metal-OH
3237	-V-OH (Volynet <i>et al.</i> 1972)
3309	-Ti-OH (Volynet <i>et al.</i> 1972)

### 3. Chemical analysis

Based on the FTIR results, the LA-ICPMS analyses have been employed in order to compare the trace element results with the FTIR spectra. The analyses of both sample types are shown in Table 7. The results reveal the content of Ti and V that consistent with -Ti-OH and -V-OH absorption at 3309 and 3237 cm<sup>-1</sup>, respectively.

**Table 7** The concentrations in ppm of pink sapphire and ruby boules, which were detected by LA-ICPMS.

Chemical Substance	Concentration (ppm)	
	Pink sapphire (set 1)	Ruby (set 2)
Cr	356.38	3853.45
Ti	9.59	48.51
V	0.04	0.12
Fe	<0.73	<0.64
Ga	0.13	0.18

### 3. Atomic Force Microscopy

The surface scanning by using Atomic Force Microscope (AFM) was employed for this study. The areas selected for the step height measurement were taken from the smoothest surfaces (having almost the same false colour) in order to eliminate the error of polishing quality, and other possible surface impurities, etc. The line for measuring the step height should be perpendicular to the atomic steps. The results are shown in the Figure 51-130 below.

#### 3.1 RR01a (unheated)

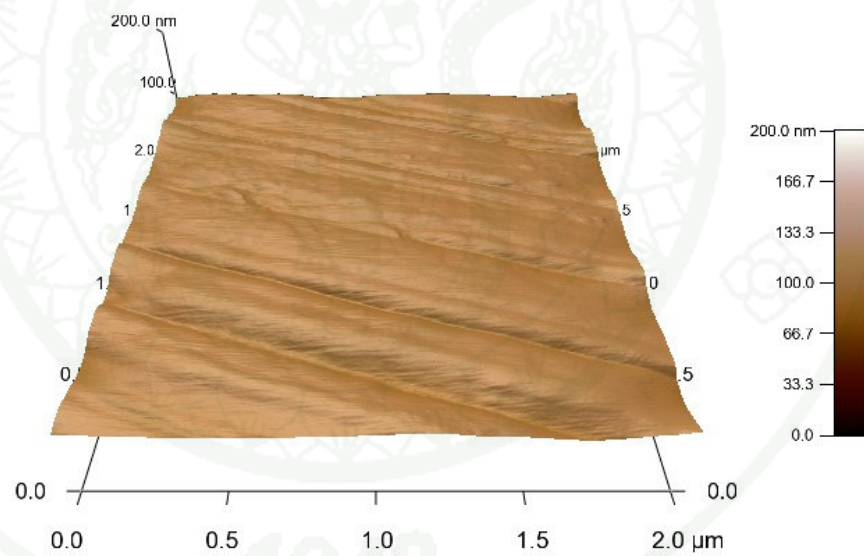


**Figure 51** 3D-Image ( $2.0 \times 2.0 \mu\text{m}^2$ ) of the unheated synthetic pink sapphire (set 1) on the miscut of the prism  $[1\bar{1}00]$  face of the sample RR01a

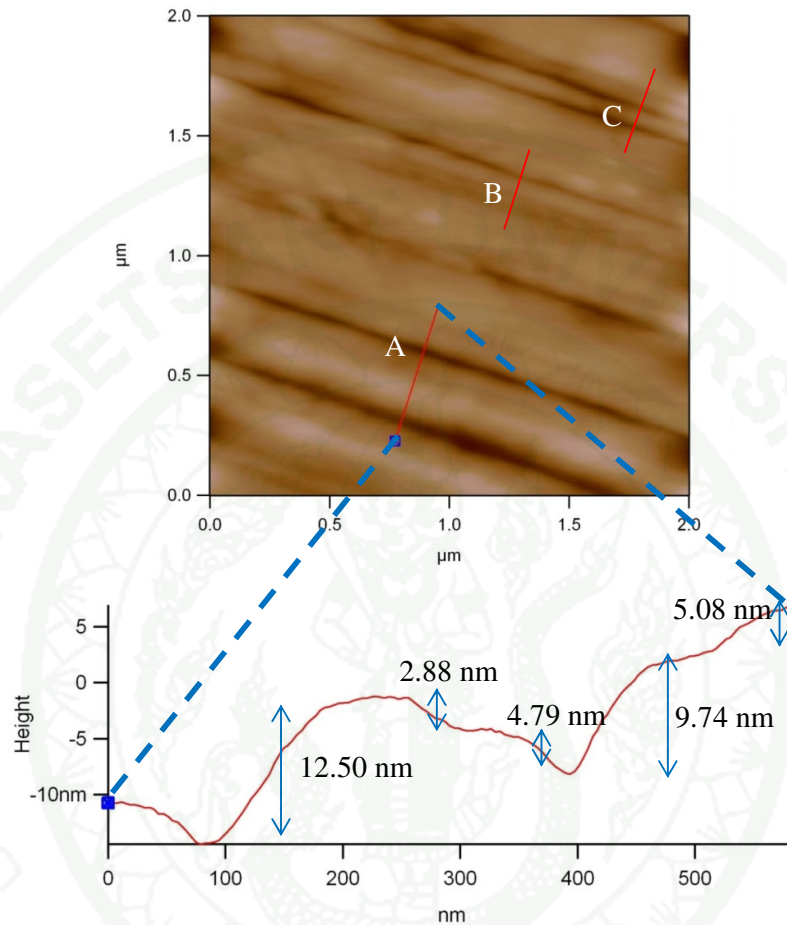


**Figure 52** Measurement of average step height of the unheated synthetic pink sapphire (set 1) sample (RR01a) on the miscut of the prism  $[1\bar{1}00]$  face

**Table 8** The average step height measurement obtained from the A, B and C lines on Figure 52.

Line	Step height (nm)
A	2.88, 4.79, 5.08, 9.74, 12.50
B	3.39, 0.89, 3.85
C	5.54, 6.48, 5.58, 4.79
Average	5.46

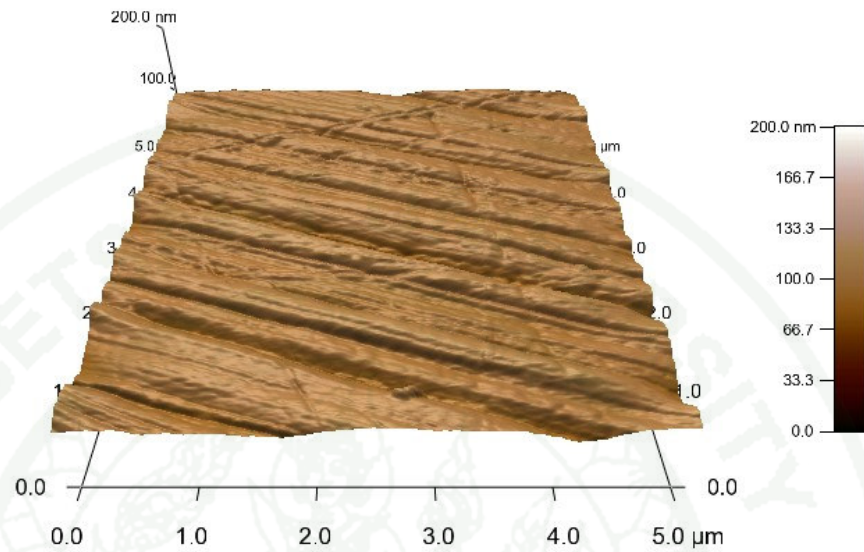


**Figure 53** 3D-Image ( $5.0 \times 5.0 \mu\text{m}^2$ ) of unheated synthetic pink sapphire (set 1) on the miscut of prism  $[1 \bar{1}00]$  face of the sample RR01a; note: some scratches on the surface.

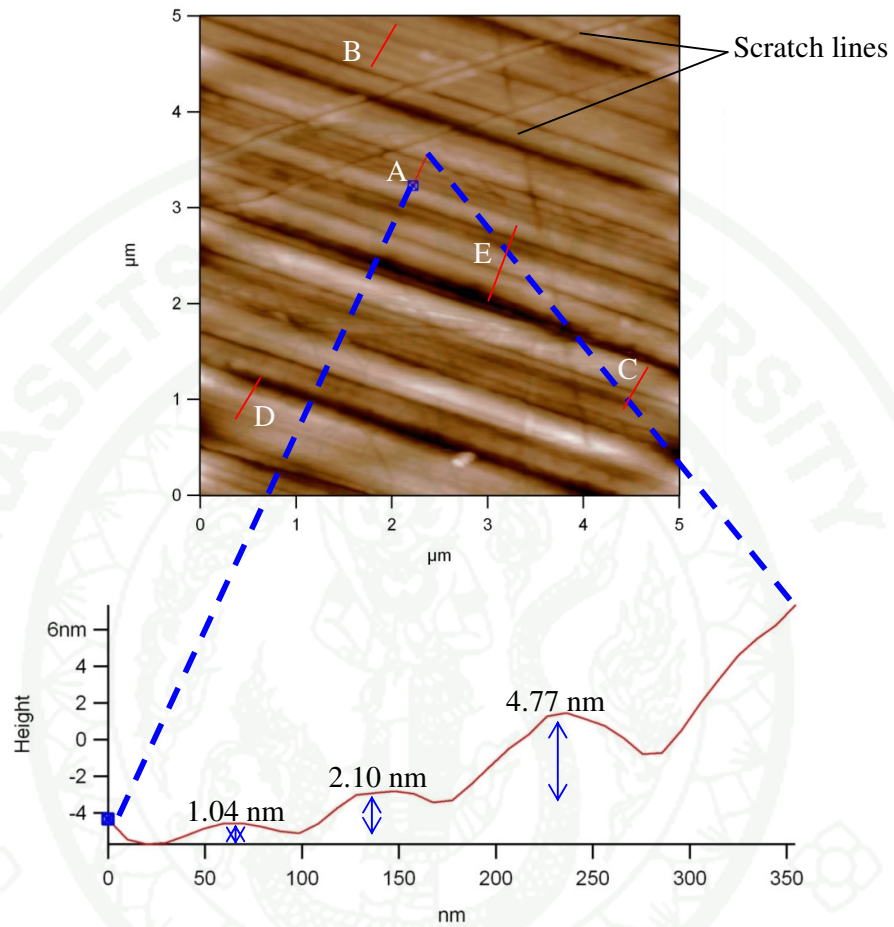


**Figure 54** Measurement of average step height of the unheated synthetic pink sapphire (set 1) sample (RR01a) on the miscut of prism  $[1\bar{1}00]$  face; note: the scratch lines

**Table 9** The average step height measurement obtained from the A, B, C, D and E lines on Figure 54.

Line	Step heights (nm)
A	1.04, 2.10, 4.77
B	2.12, 1.59, 2.53
C	8.19, 8.60
D	0.76, 2.40, 4.24
E	1.87, 2.85, 6.18, 7.22, 9.52, 9.94
Average	4.47

### 3.2 RR01d (heated)

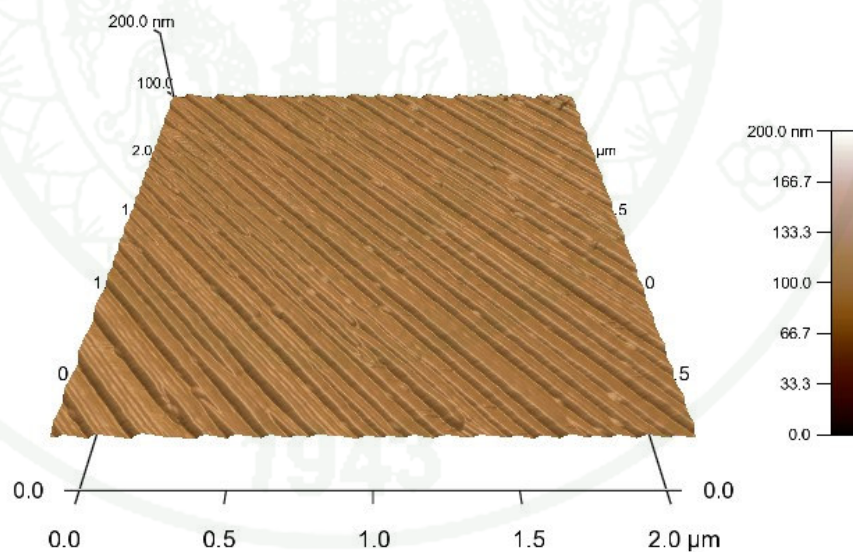


**Figure 55** 3D-Image ( $2.0 \times 2.0 \mu\text{m}^2$ ) of heated synthetic pink sapphire (set 1) on the miscut of prism  $[1\bar{1}00]$  face of the sample RR01d

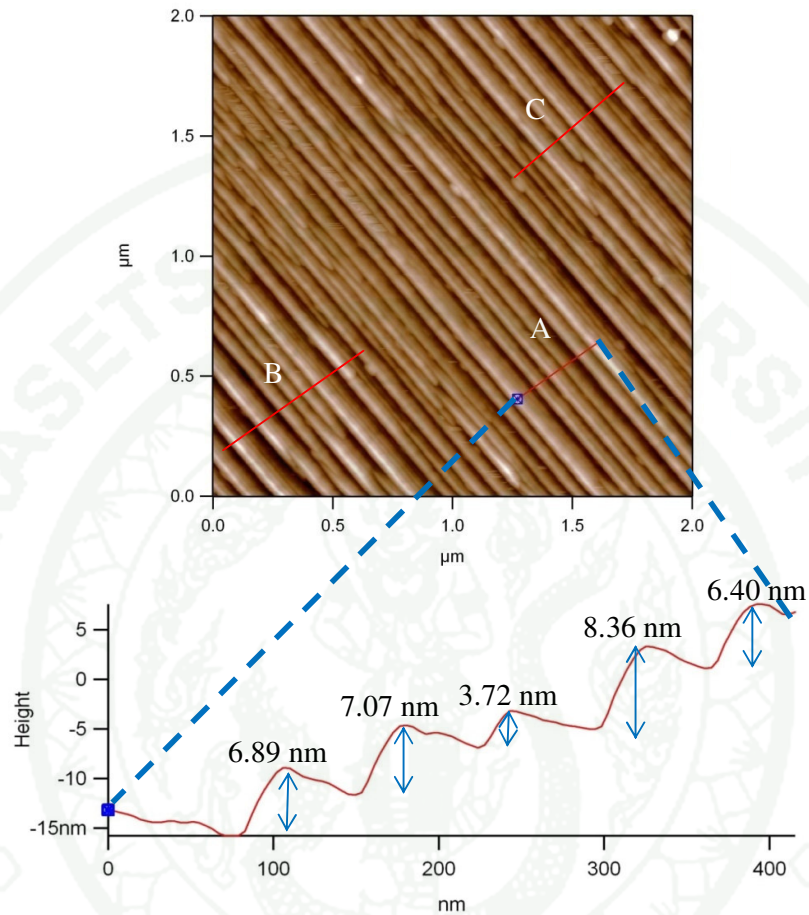


**Figure 56** Measurement of average step height of heated synthetic pink sapphire (set 1) sample (RR01d) on the miscut of prism  $[1\bar{1}00]$  face; note: the mismatched steps.

**Table 10** The average step height measurement obtained from the A, B and C lines on Figure 56

Line	Step heights (nm)
A	3.72, 6.40, 6.89, 7.07, 8.36
B	1.01, 1.26, 5.44, 5.87, 6.19, 6.94, 8.62, 9.48, 11.04, 11.35
C	1.42, 3.44, 3.55, 5.48, 5.96, 6.02, 6.32, 7.03
Average	6.04

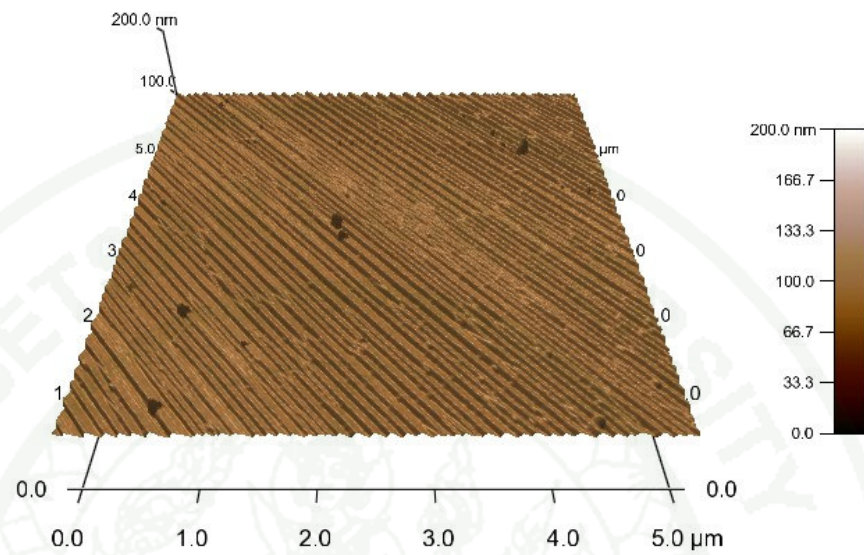


**Figure 57** 3D-Image ( $5.0 \times 5.0 \mu\text{m}^2$ ) of heated synthetic pink sapphire (set 1) on the miscut of prism  $[1\bar{1}00]$  face of the sample RR01d

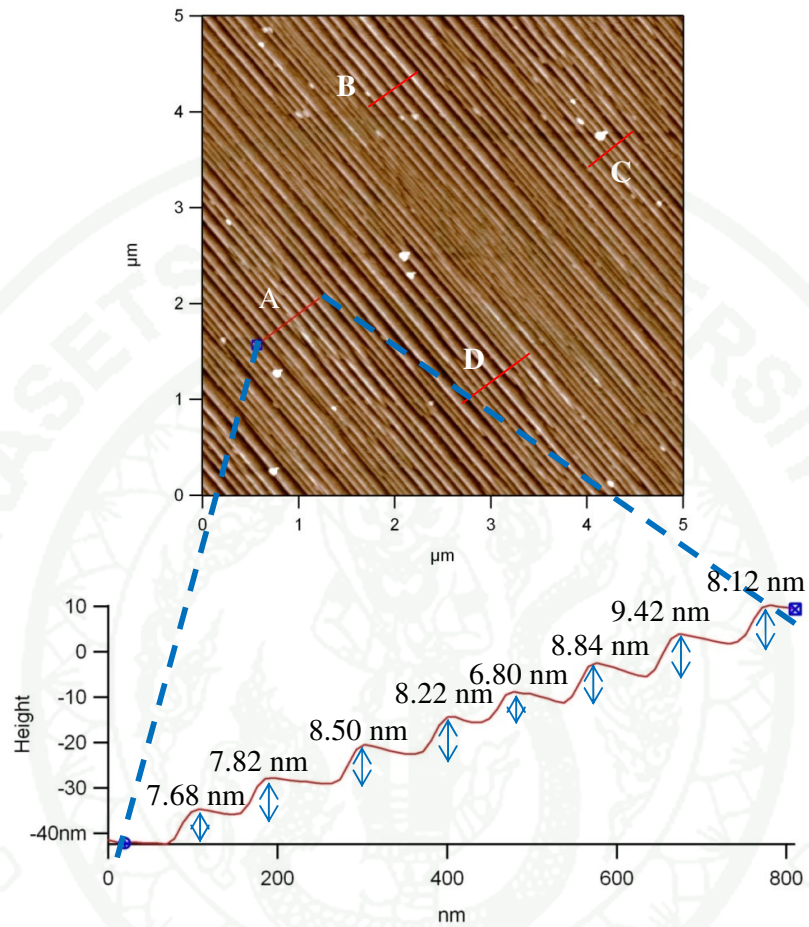


**Figure 58** Measurement of average step height of heated synthetic pink sapphire (set 1) sample (RR01d) on the miscut of prism  $[1\bar{1}00]$  face; note: the mismatched steps.

**Table 11** The average step height measurement obtained from the A, B, C and D lines on Figure 58

Line	Step heights (nm)
A	6.80, 7.68, 7.82, 8.12, 8.22, 8.50, 8.84, 9.42
B	6.07, 6.90, 7.05, 8.34, 8.62, 9.26
C	5.54, 6.07, 6.12, 6.80, 7.88, 8.04, 8.50, 8.86
D	3.97, 4.14, 4.69, 5.24, 6.65, 6.95, 7.11, 7.80, 9.25, 9.31
Average	7.33

### 3.3 RR01b (unheated)

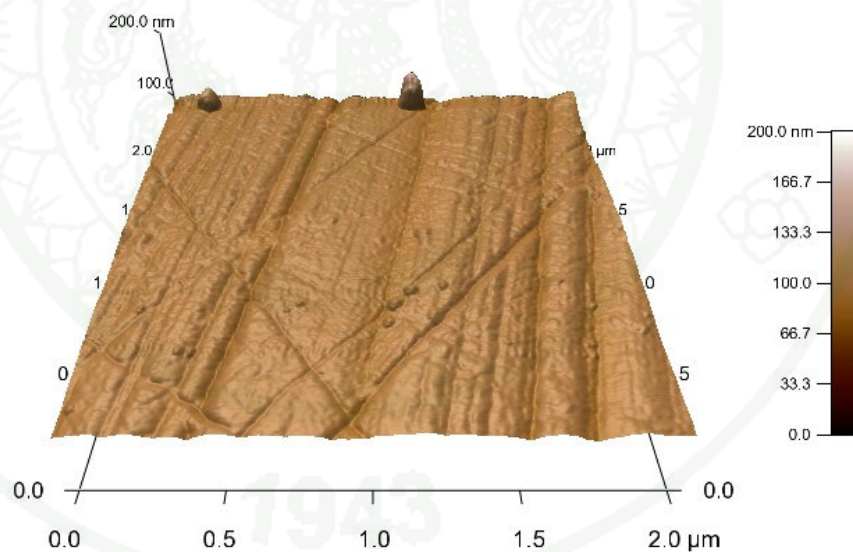


**Figure 59** 3D-Image ( $2.0 \times 2.0 \mu\text{m}^2$ ) of unheated synthetic pink sapphire (set 1) on the miscut of prism  $[0\bar{1}10]$  face of the sample RR01b; note: some surface scratches.

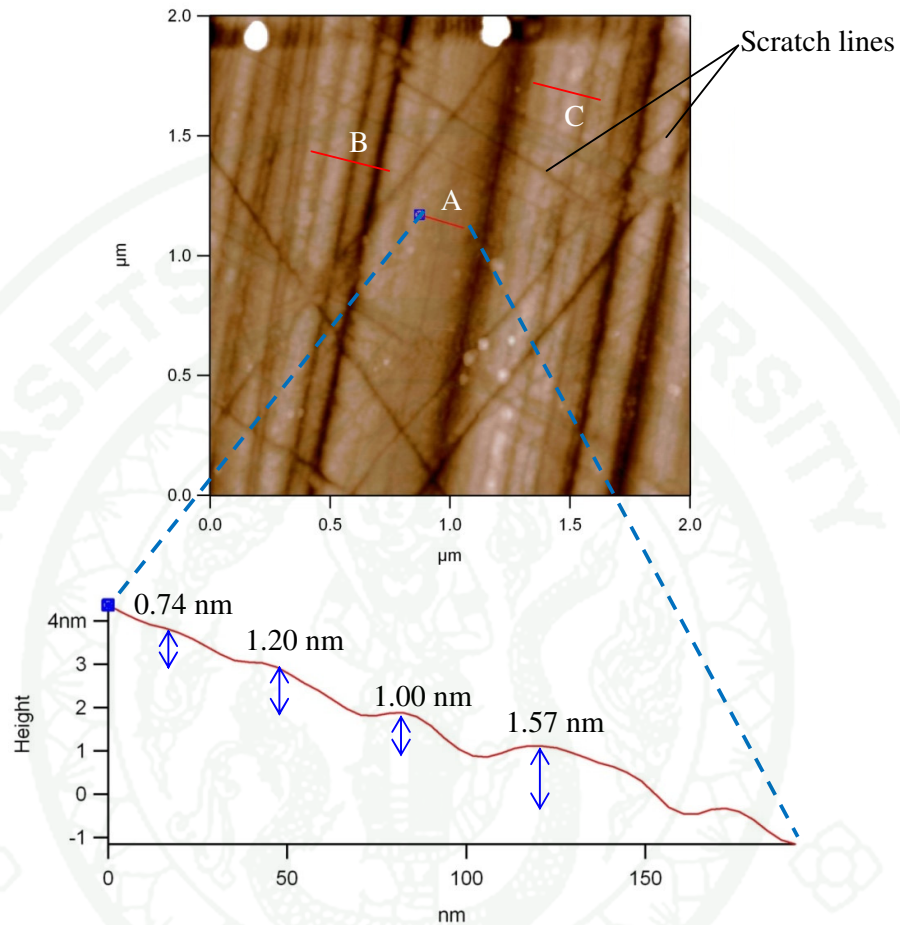


**Figure 60** Measurement of average step height of unheated synthetic pink sapphire (set 1) sample (RR01b) on the miscut of prism  $[0\bar{1}10]$  face; note: the scratch lines.

**Table 12** The average step height measurement obtained from the A, B and C lines on Figure 60

Line	Step heights (nm)
A	0.74, 1.00, 1.20, 1.57
B	4.14, 8.12, 8.44
C	1.44, 2.97, 5.74
Average	3.53

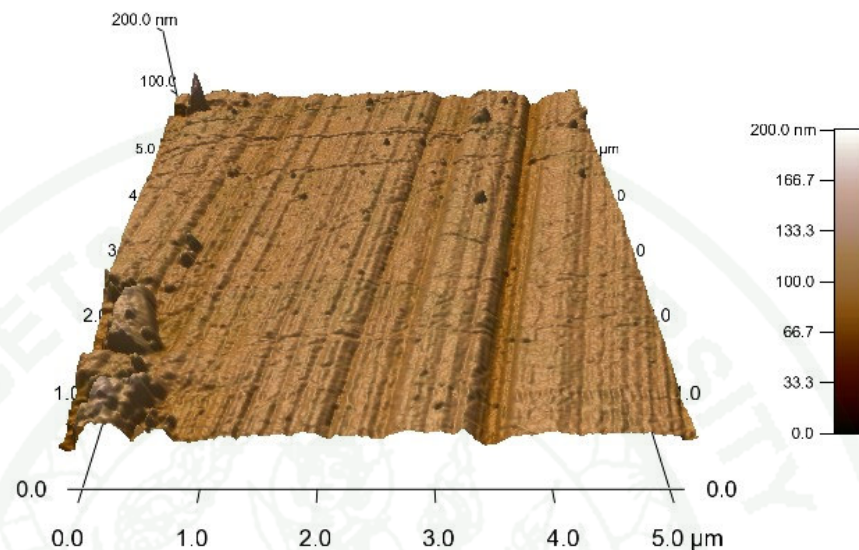


**Figure 61** 3D-Image ( $5.0 \times 5.0 \mu\text{m}^2$ ) of unheated synthetic pink sapphire (set 1) on the miscut of prism  $[0 \bar{1} 10]$  face of the sample RR01b; notes: some scratches and impurities.

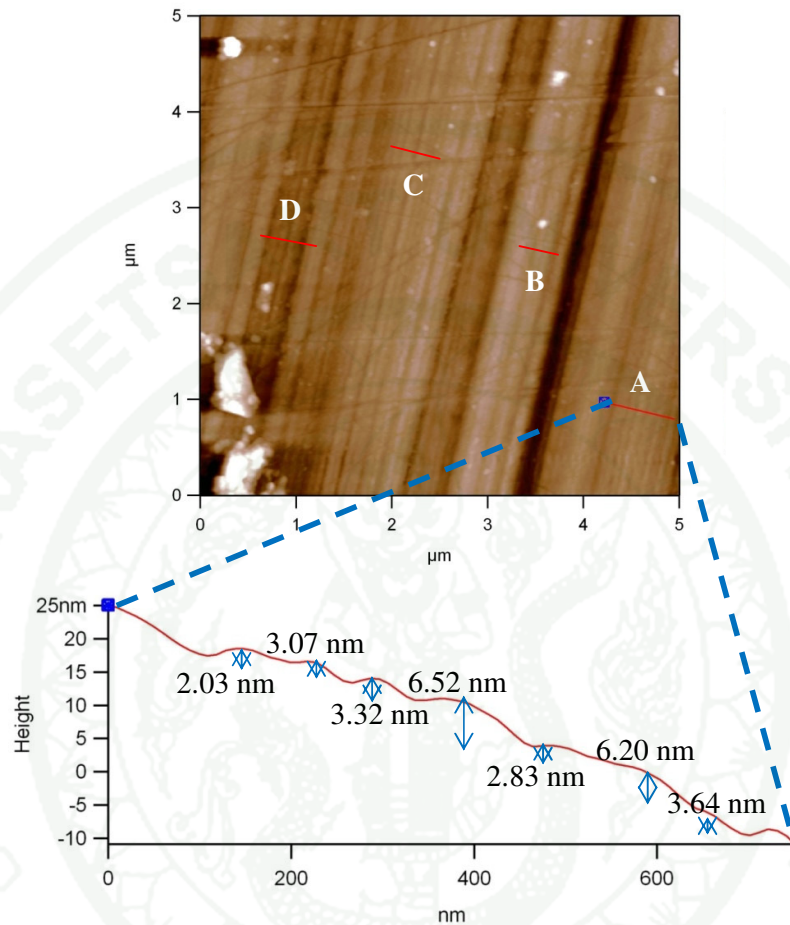


**Figure 62** Measurement of average step height of unheated synthetic pink sapphire (set 1) sample (RR01b) on the miscut of prism  $[0\bar{1}10]$  face; note: the scratch lines.

**Table 13** The average step height measurement obtained from the A, B, C and D lines on Figure 62

Line	Step heights (nm)
A	2.03, 2.83, 3.07, 3.32, 3.64, 6.20, 6.52
B	1.52, 1.62, 2.39, 7.97
C	1.93, 1.99, 3.19, 3.60, 5.38, 6.35
D	2.35, 2.35, 4.33, 5.70, 6.28, 9.13
Average	4.07

3.4 RR01c (heated)

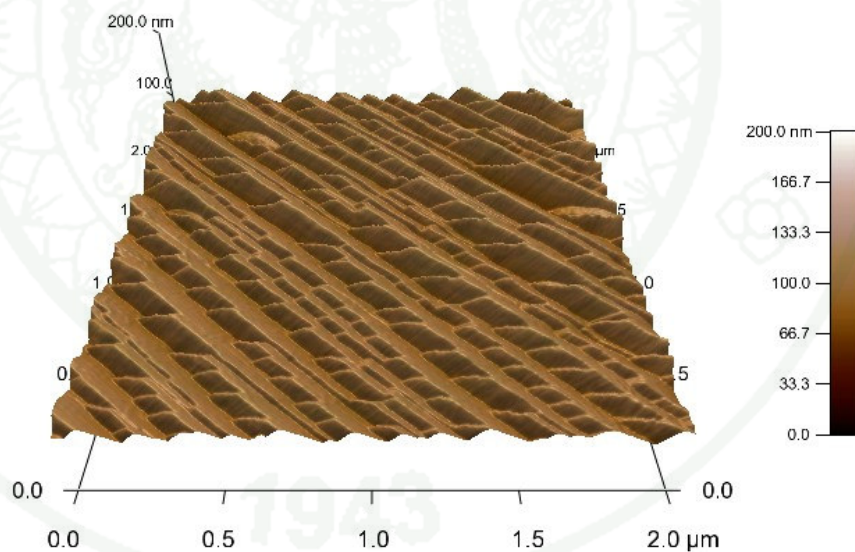


**Figure 63** 3D-Image ( $2.0 \times 2.0 \mu\text{m}^2$ ) of heated synthetic pink sapphire (set 1) on the miscut of prism  $[0\bar{1}10]$  face of the sample RR01c.

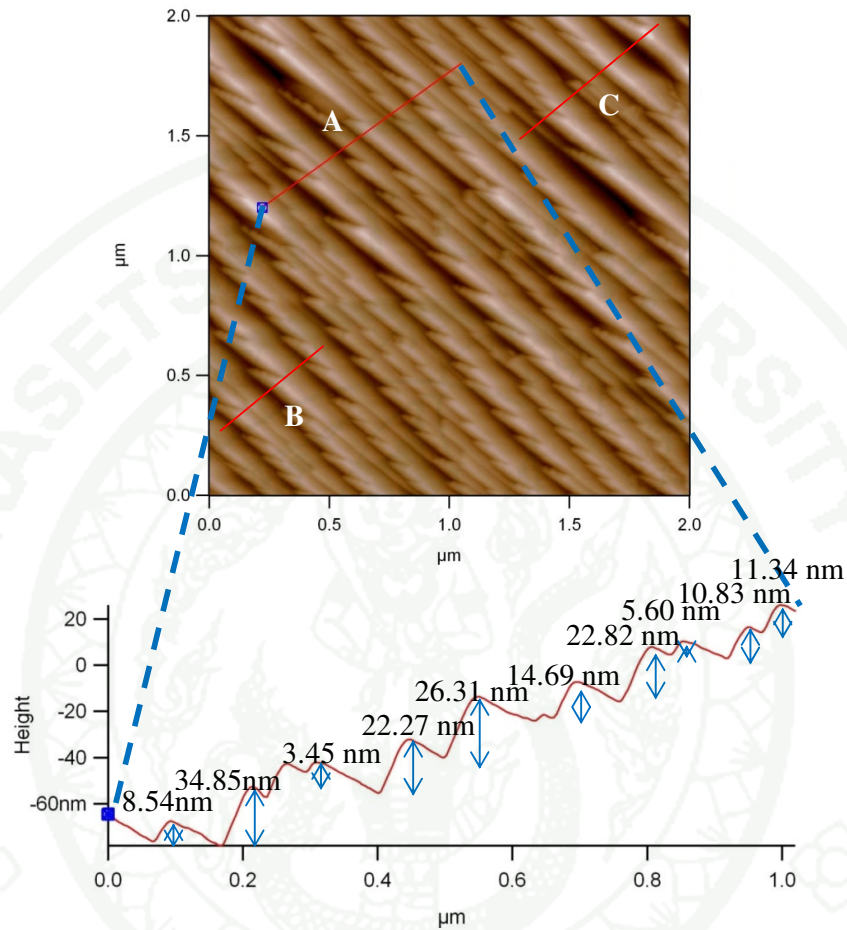


**Figure 64** Measurement of average step height of heated synthetic pink sapphire (set 1) sample (RR01c) on the miscut of prism  $[0\bar{1}10]$  face; note: the zigzag lines.

**Table 14** The average step height measurement obtained from the A, B and C lines on Figure 64

Line	Step heights (nm)
A	3.45, 5.60, 8.54, 10.83, 11.34, 14.69, 22.27, 22.82, 26.31, 34.85
B	3.26, 21.84, 27.44, 30.16
C	6.61, 8.68, 10.83, 25.30, 33.19, 43.93
Average	18.597

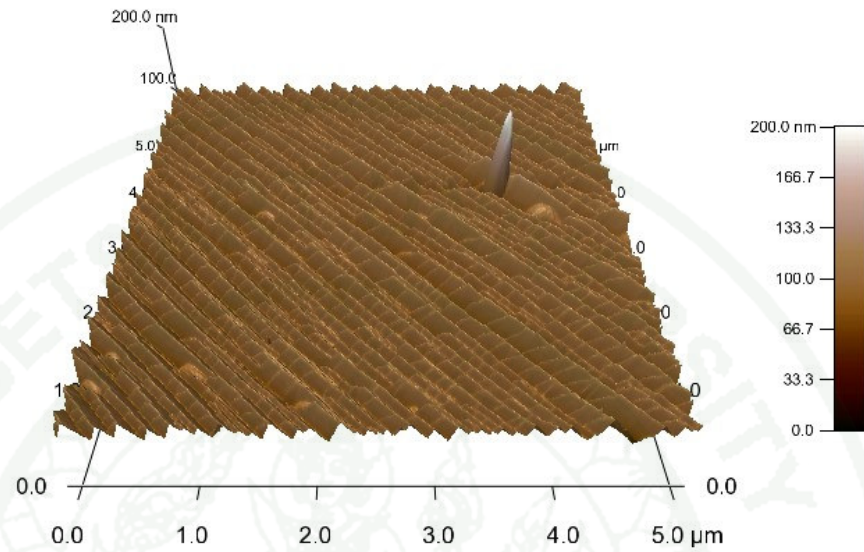


**Figure 65** 3D-Image ( $5.0 \times 5.0 \mu\text{m}^2$ ) of heated synthetic pink sapphire (set 1) on the miscut of prism  $[0\bar{1}10]$  face of the sample RR01c

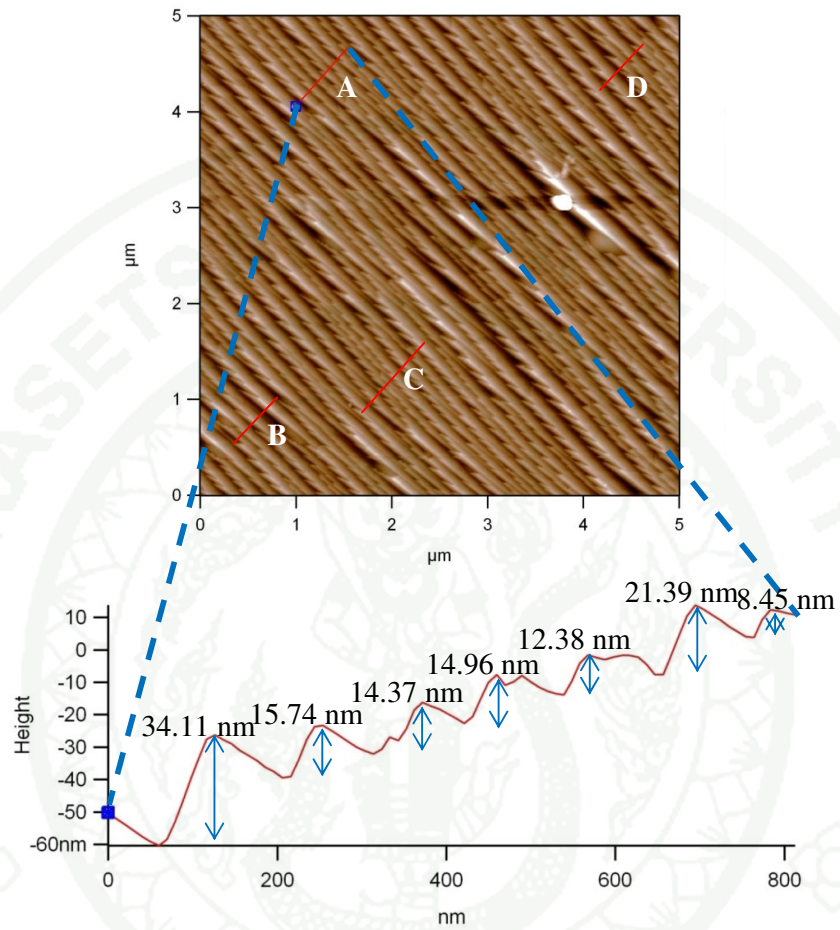


**Figure 66** Measurement of average step height of heated synthetic pink sapphire (set 1) sample (RR01c) on the miscut of prism  $[0\bar{1}10]$  face; note: the zigzag lines.

**Table 15** The average step height measurement obtained from the A, B, C and D lines on Figure 66

Line	Step heights (nm)
A	8.45, 12.38, 14.37, 14.96, 15.74, 21.39, 34.11
B	4.03, 17.33, 20.04, 27.44, 39.45
C	8.12, 11.06, 11.82, 16.29, 18.36, 22.97, 24.19, 26.85
D	4.76, 15.66, 15.72, 17.31, 23.89, 26.84
Average	18.21

3.5 RR02a (unheated)

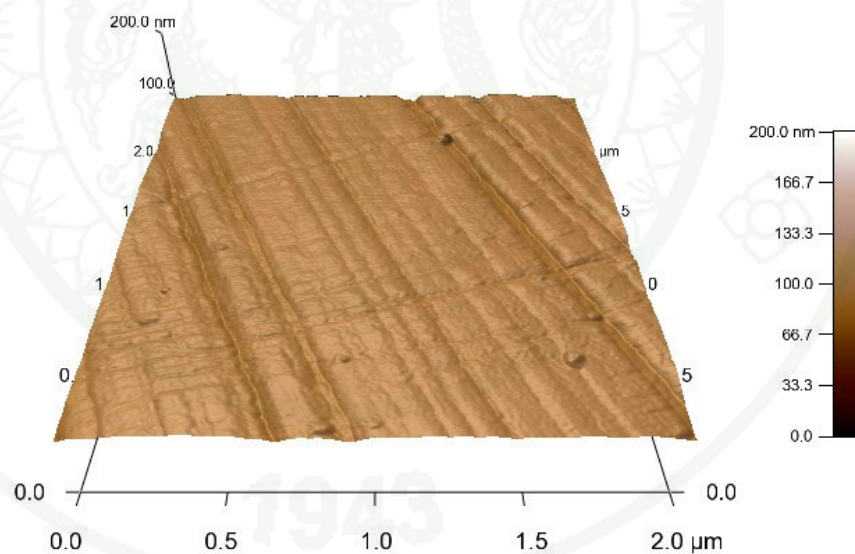


**Figure 67** 3D-Image ( $2.0 \times 2.0 \mu\text{m}^2$ ) of unheated synthetic pink sapphire (set 1) on the miscut of prism  $[1\bar{2}10]$  face of the sample RR02a; note: some scratch lines.

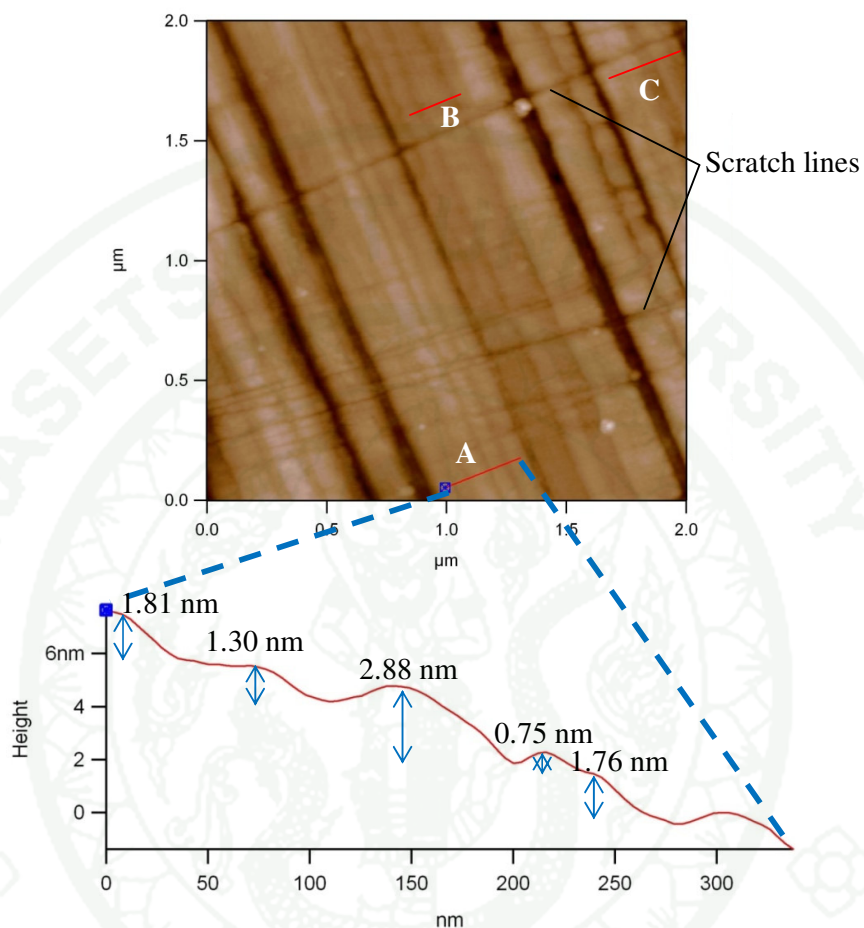


**Figure 68** Measurement of average step height of unheated synthetic pink sapphire (set 1) sample (RR02a) on the miscut of prism  $[1\bar{2}10]$  face; note: the scratch lines

**Table 16** The average step height measurement obtained from the A, B and C lines on Figure 68

Line	Step heights (nm)
A	0.75, 1.30, 1.76, 1.81, 2.88
B	0.69, 0.84, 0.84, 1.17, 2.01
C	0.52, 1.78, 1.88
Average	1.40

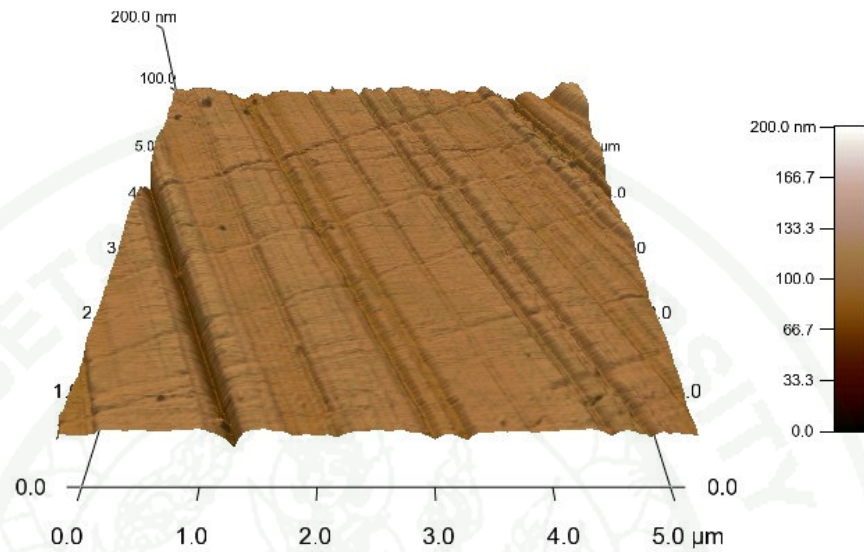


**Figure 69** 3D-Image ( $5.0 \times 5.0 \mu\text{m}^2$ ) of unheated synthetic pink sapphire (set 1) on the miscut of prism  $[1\bar{2}10]$  face of the sample RR02a; note: some scratch lines.

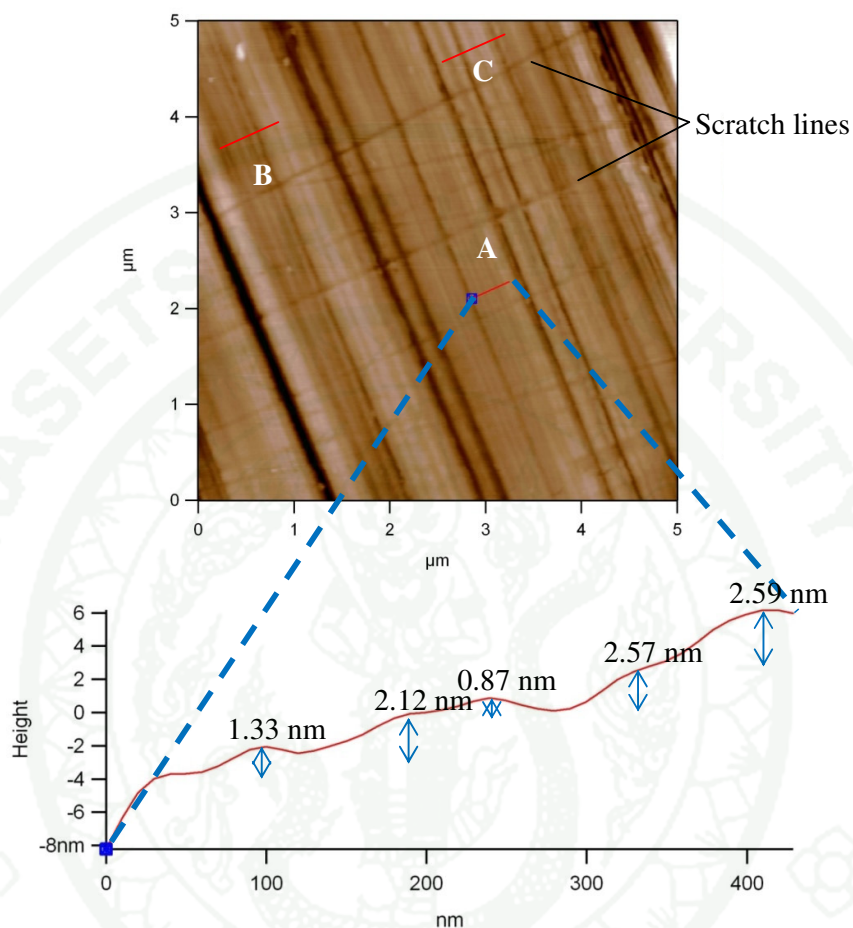


**Figure 70** Measurement of average step height of unheated synthetic pink sapphire (set 1) sample (RR02a) on the miscut of prism  $[1\bar{2}10]$  face; note: the scratch lines

**Table 17** The average step height measurement obtained from the A, B and C lines on Figure 70

Line	Step heights (nm)
A	0.87, 1.33, 2.12, 2.57, 2.59
B	3.28, 3.53, 3.55, 4.72, 5.58, 6.17
C	2.97, 5.72, 6.11, 8.66, 14.44
Average	4.63

## 3.6 RR02c (unheated)

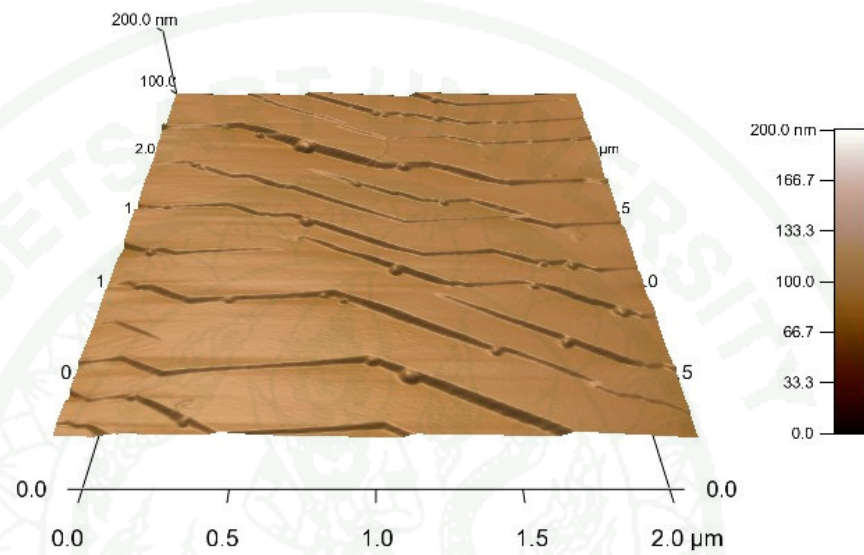


**Figure 71** 3D-Image ( $2.0 \times 2.0 \mu\text{m}^2$ ) of heated synthetic pink sapphire (set 1) on the miscut of prism  $[1\bar{2}10]$  face of the sample RR02c; note: the zigzag lines.

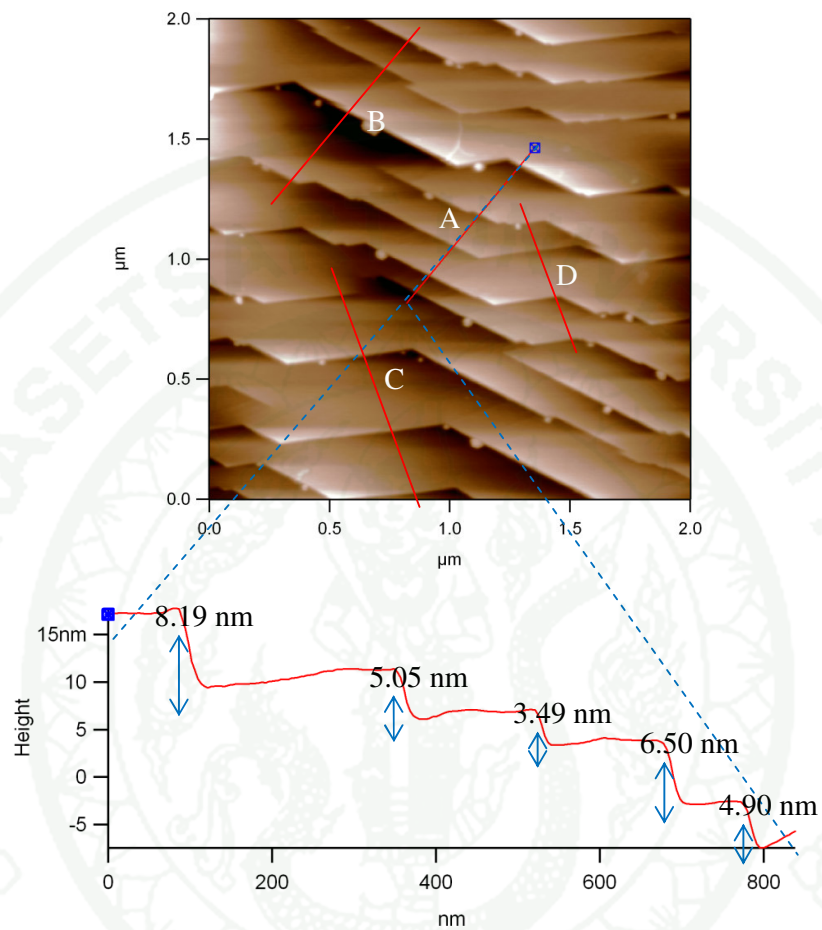


**Figure 72** Measurement of average step height of heated synthetic pink sapphire (set 1) sample (RR02c) on the miscut of prism  $[1\bar{2}10]$  face; note: the zigzag lines.

**Table 18** The average step height measurement obtained from the A, B, C and D lines on Figure 72

Line	Step heights (nm)
A	3.49, 4.90, 5.05, 6.50, 8.19
B	3.14, 4.22, 6.38, 11.81
C	1.65, 3.59, 3.84, 4.82
D	1.96, 3.52, 3.97, 3.97
Average	4.76

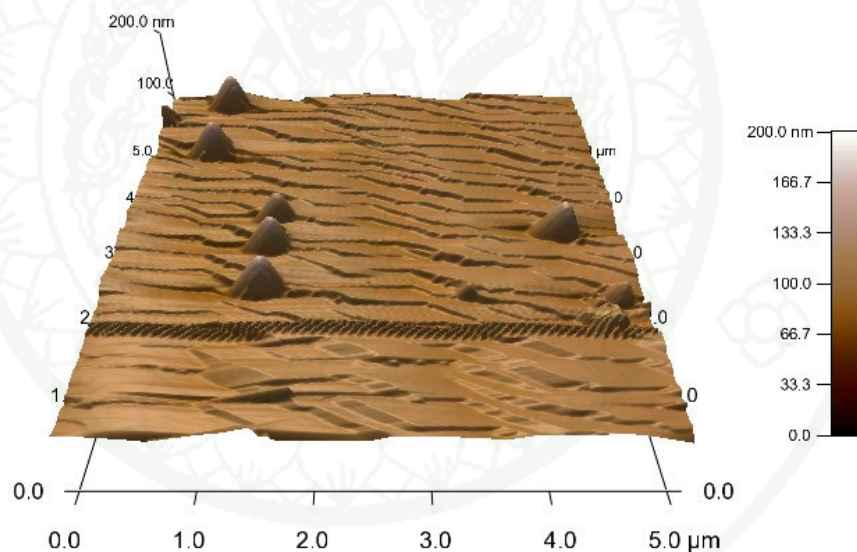


**Figure 73** 3D-Image ( $5.0 \times 5.0 \mu\text{m}^2$ ) of heated synthetic pink sapphire (set 1) on the miscut of prism  $[1\bar{2}10]$  face of the sample RR02c; note: some interruption line and hillock artifacts occurring by the measurement.

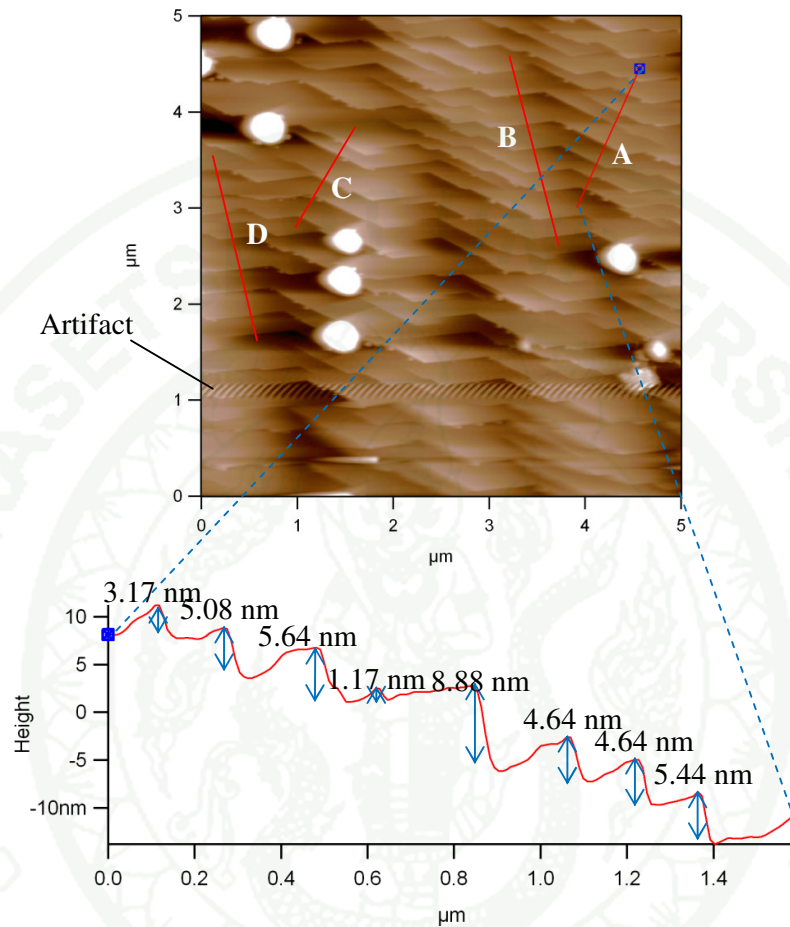


**Figure 74** Measurement of average step height of heated synthetic pink sapphire (set 1) sample (RR02c) on the miscut of prism  $[1\bar{2}10]$  face; note: the artifact.

**Table 19** The average step height measurement obtained from the A, B, C and D lines on Figure 74.

Line	Step heights (nm)
A	1.17, 3.17, 4.64, 4.64, 5.08, 5.44, 5.64, 8.88
B	1.55, 3.12, 3.25, 3.99, 4.12, 4.12, 4.35, 5.77
C	4.14, 5.29, 6.81, 8.65, 8.92
D	2.15, 2.56, 2.64, 3.02, 3.53, 4.02, 4.53, 5.47
Average	4.51

## 3.7 RR04a (unheated)

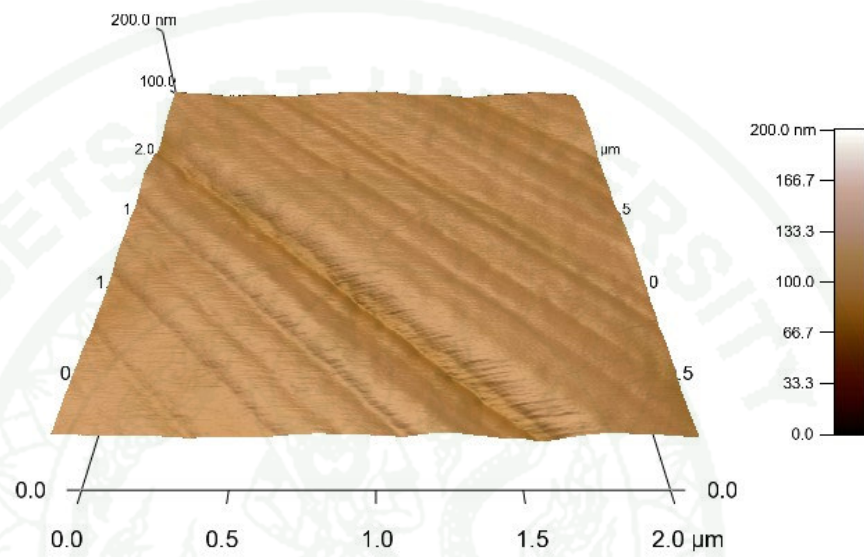


**Figure 75** 3D-Image ( $2.0 \times 2.0 \mu\text{m}^2$ ) of unheated synthetic pink sapphire (set 1) on the miscut of prism  $[\bar{1}\bar{1}20]$  face of the sample RR04a.

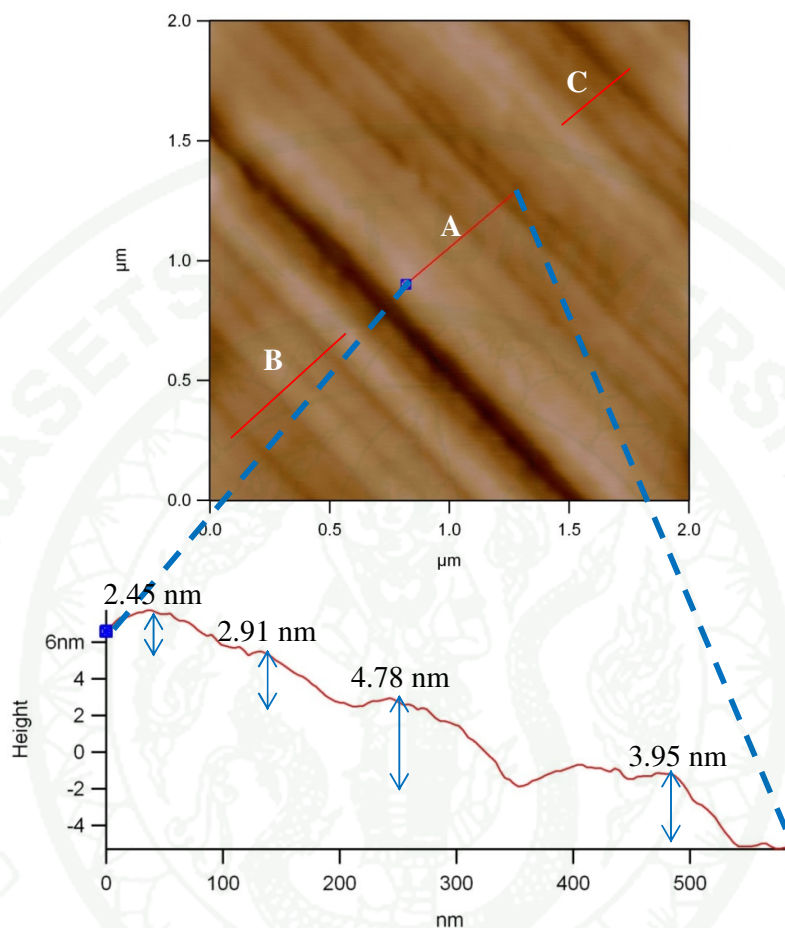


**Figure 76** Measurement of average step height of unheated synthetic pink sapphire (set 1) sample (RR04a) on the miscut of prism  $[\bar{1}\bar{1}20]$  face.

**Table 20** The average step height measurement obtained from the A, B and C lines on Figure 76.

Line	Step heights (nm)
A	2.45, 2.91, 3.95, 4.78
B	1.66, 3.68, 6.28, 8.84
C	3.25, 4.58
Average	4.24

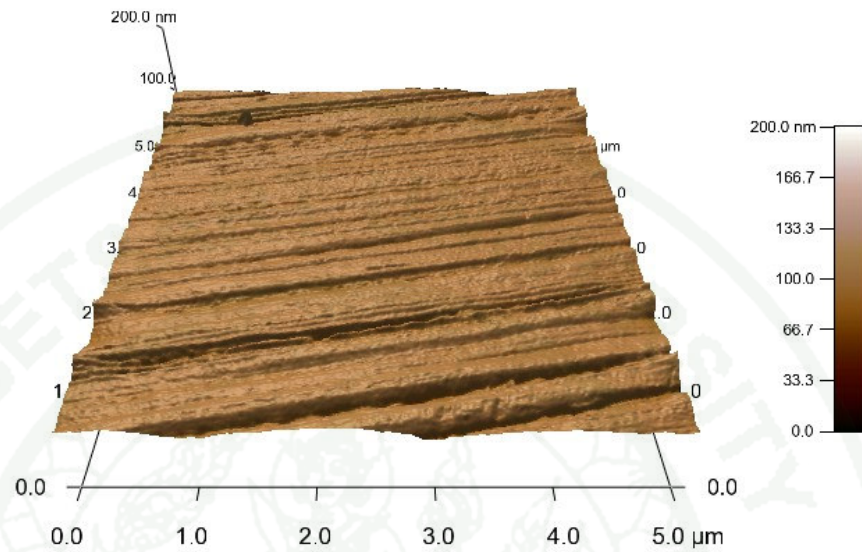


**Figure 77** 3D-Image ( $5.0 \times 5.0 \mu\text{m}^2$ ) of unheated synthetic pink sapphire (set 1) on the miscut of prism  $[\bar{1}\bar{1}20]$  face of the sample RR04a

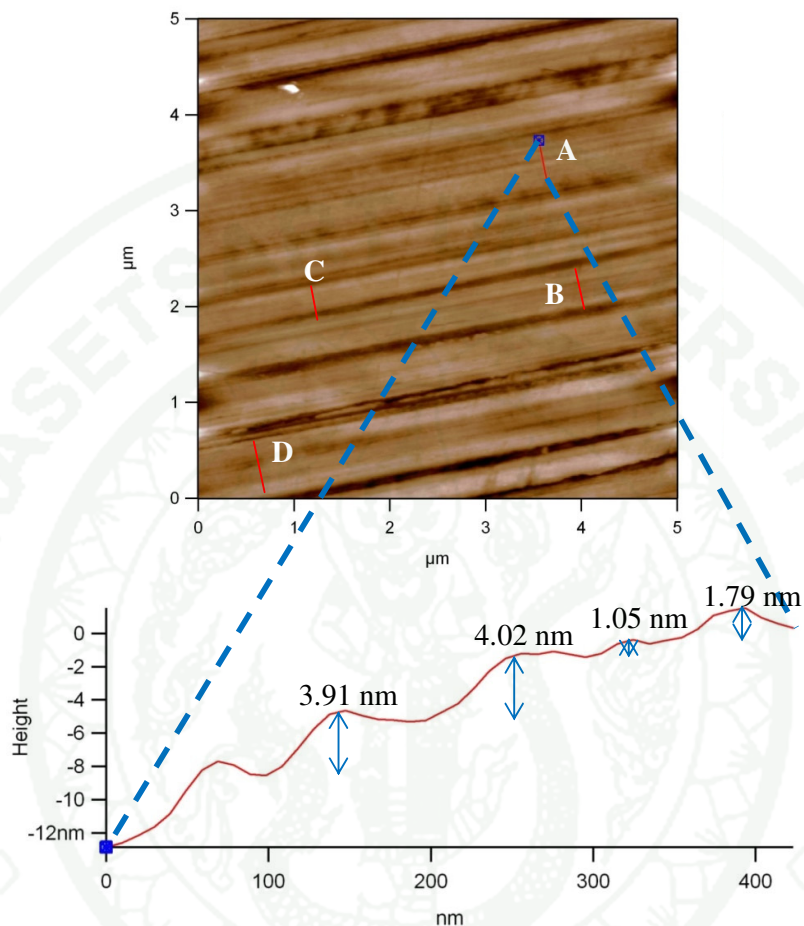


**Figure 78** Measurement of average step height of unheated synthetic pink sapphire (set 1) sample (RR04a) on the miscut of prism  $[\bar{1}\bar{1}20]$  face.

**Table 21** The average step height measurement obtained from the A, B, C and D lines on Figure 78

Line	Step heights (nm)
A	1.05, 1.79, 3.91, 4.02
B	0.85, 1.10, 1.96, 2.28
C	1.16, 1.16, 2.03, 2.31, 5.15
D	0.88, 1.00, 1.46, 1.52, 2.08, 2.81, 4.05
Average	2.13

## 3.8 RR04c (heated)

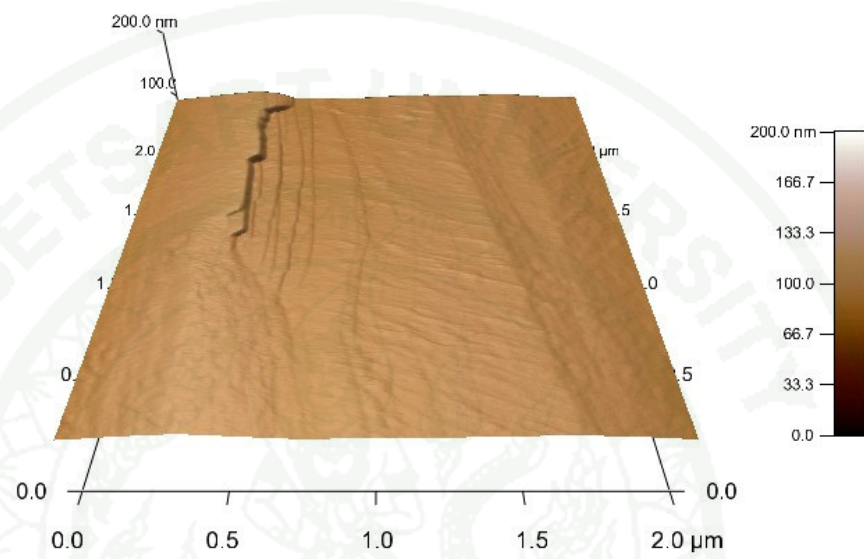


**Figure 79** 3D-Image ( $2.0 \times 2.0 \mu\text{m}^2$ ) of heated synthetic pink sapphire (set 1) on the miscut of prism  $[\bar{1}\bar{1}20]$  face of the sample RR04c.

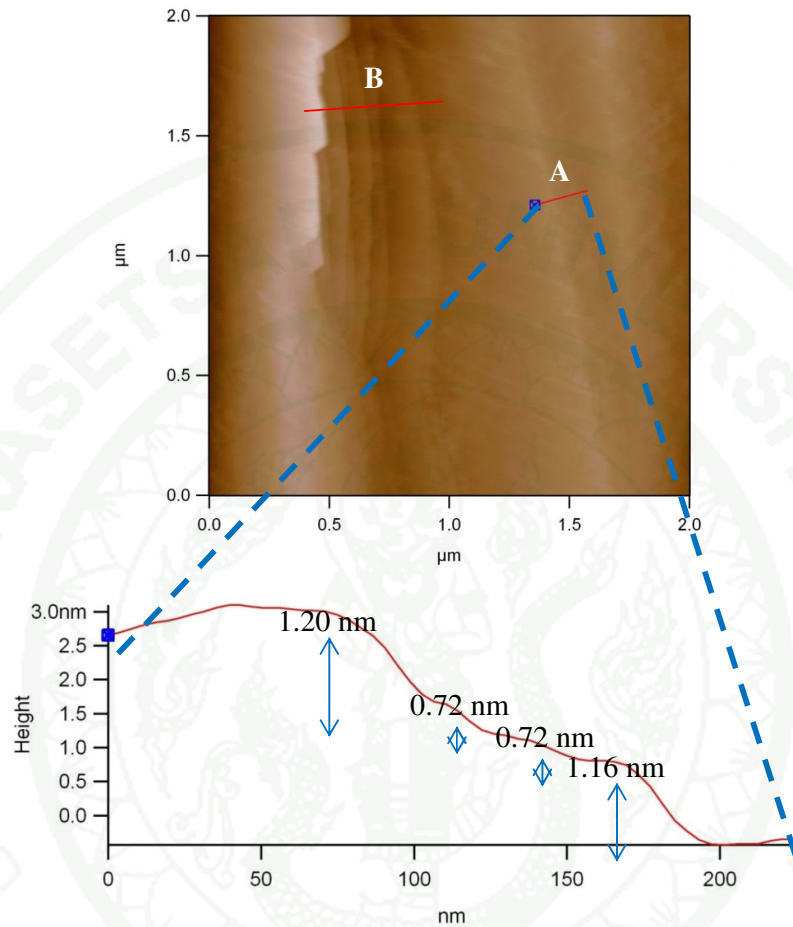


**Figure 80** Measurement of average step height of heated synthetic pink sapphire (set 1) sample (RR04c) on the miscut of prism  $[\bar{1}\bar{1}20]$  face.

**Table 22** The average step height measurement obtained from the A and B lines on Figure 80

Line	Step heights (nm)
A	0.72, 0.72, 1.16, 1.20
B	1.25, 1.47, 1.47, 2.88
Average	1.36

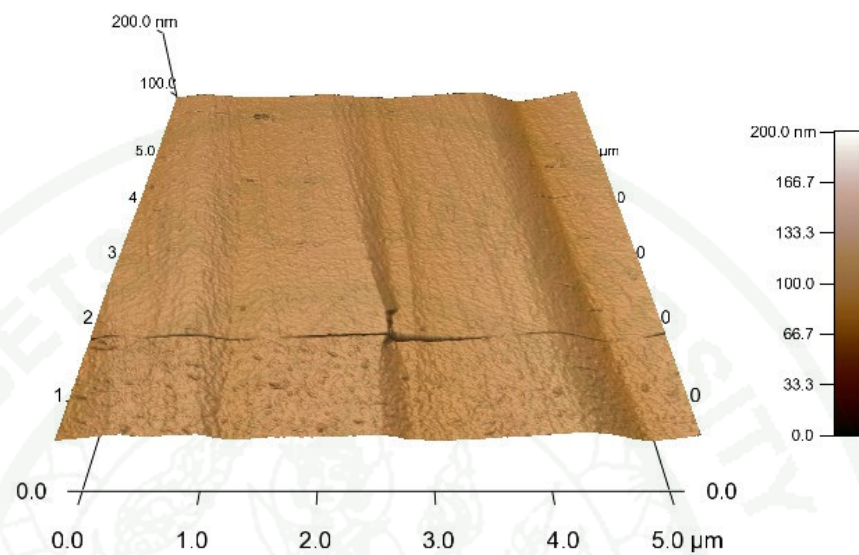


**Figure 81** 3D-Image ( $5.0 \times 5.0 \mu\text{m}^2$ ) of heated synthetic pink sapphire (set 1) on the miscut of prism  $[\bar{1}\bar{1}20]$  face of the sample RR04c.

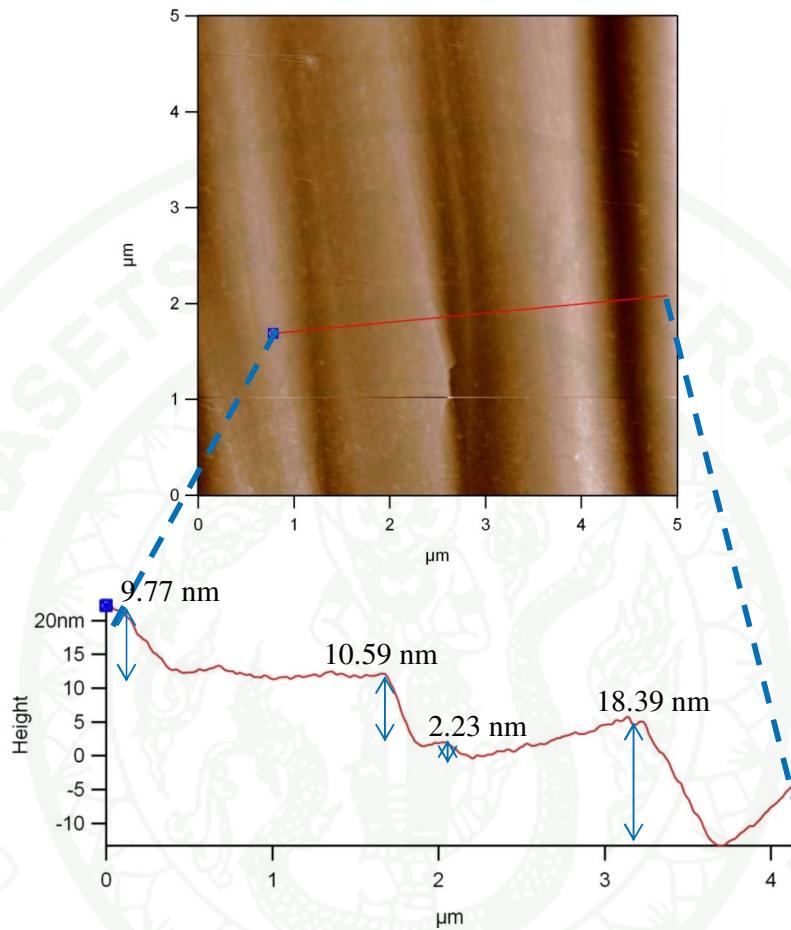


**Figure 82** Measurement of average step height of heated synthetic pink sapphire (set 1) sample (RR04c) on the miscut of prism  $[\bar{1}\bar{1}20]$  face.

**Table 22** The average step height measurement obtained from the A line on Figure 82

Line	Step heights (nm)
A	2.23, 9.77, 10.59, 18.39
Average	10.24

## 3.9 RR05a (unheated)

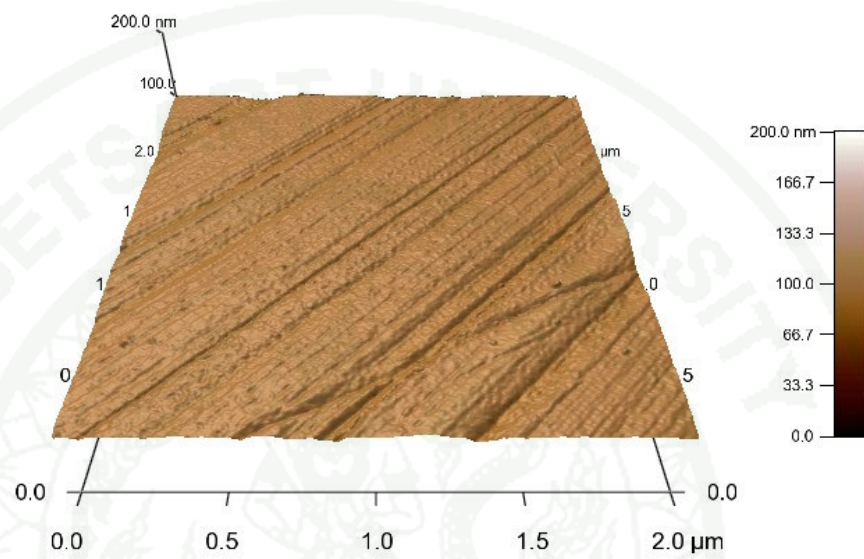


**Figure 83** 3D-Image ( $2.0 \times 2.0 \mu\text{m}^2$ ) of unheated synthetic pink sapphire (set 1) on the miscut of pinacoid [0001] face of the sample RR05a.

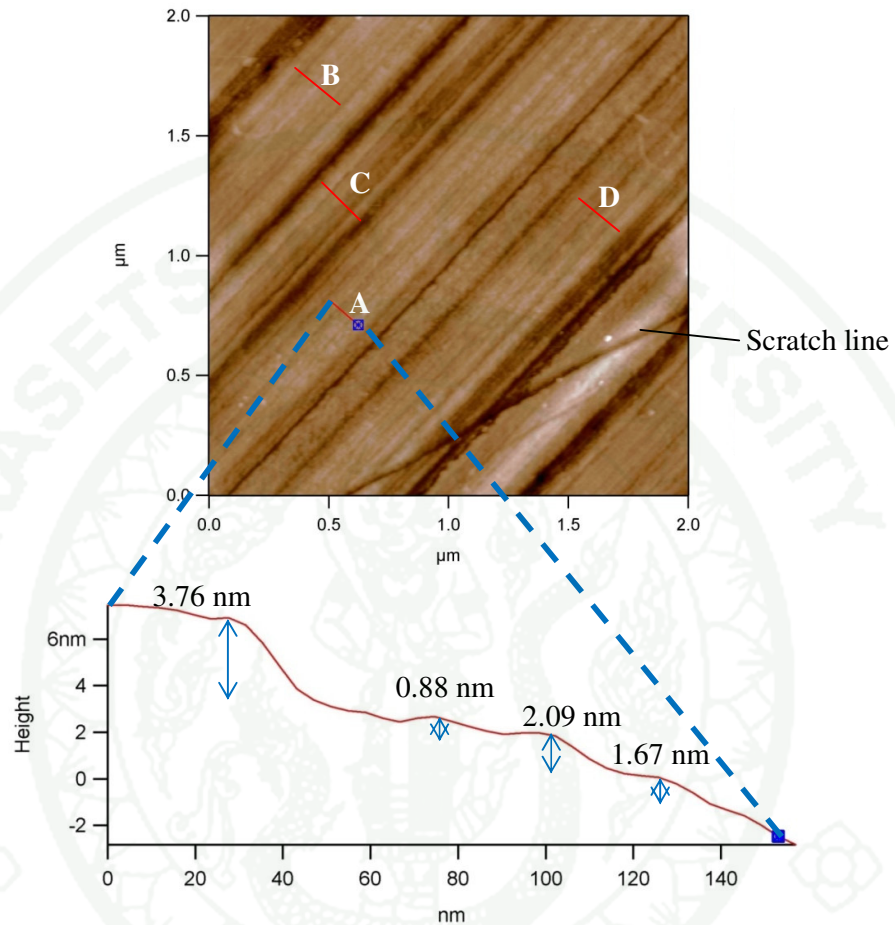


**Figure 84** Measurement of average step height of unheated synthetic pink sapphire (set 1) sample (RR05a) on the miscut of pinacoid [0001] face; note: the scratch line

**Table 24** The average step height measurement obtained from the A, B, C and D lines on Figure 84.

Line	Step heights (nm)
A	0.88, 1.67, 2.09, 3.76
B	0.20, 0.60, 0.85, 0.85, 1.00, 1.00, 1.00, 1.23
C	3.40, 3.78, 4.10, 5.38, 6.70, 13.27
D	0.20, 0.58, 0.89, 0.92, 1.10
Average	2.41

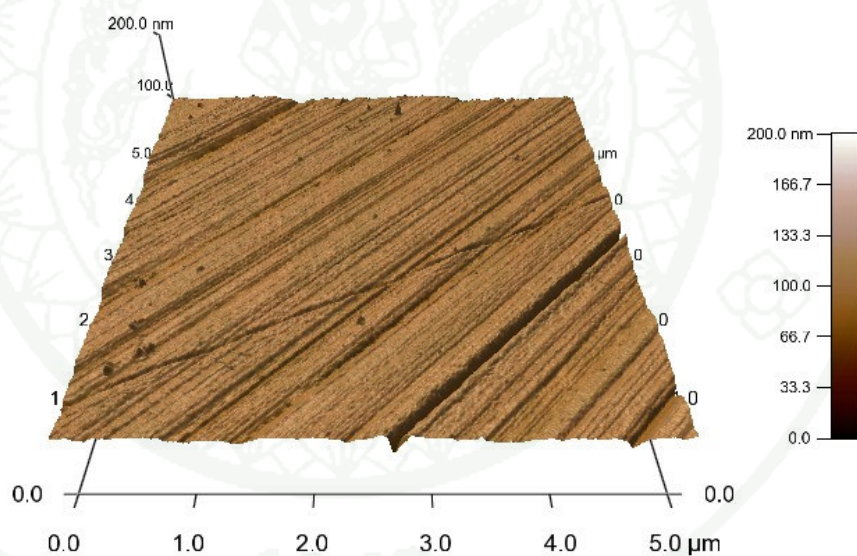


**Figure 85** 3D-Image ( $5.0 \times 5.0 \mu\text{m}^2$ ) of unheated synthetic pink sapphire (set 1) on the miscut of pinacoid [0001] face of the sample RR05a.

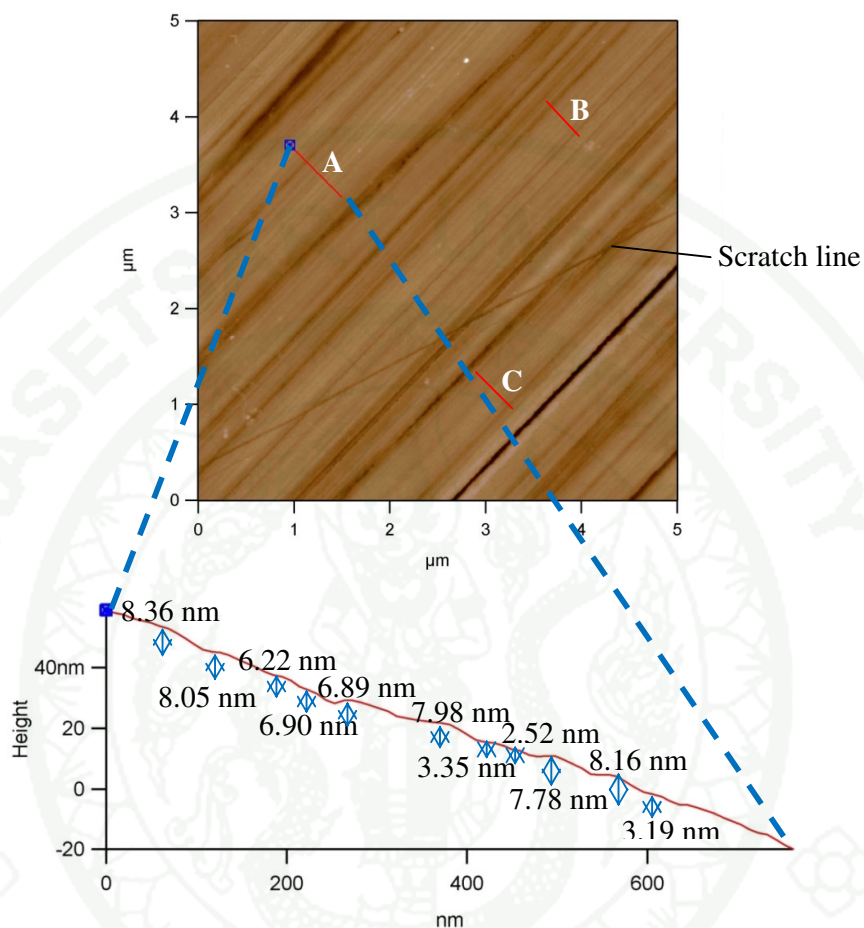


**Figure 86** Measurement of average step height of unheated synthetic pink sapphire (set 1) sample (RR05a) on the miscut of pinacoid [0001] face; note: the scratch line.

**Table 25** The average step height measurement obtained from the A, B and C lines on Figure 86

Line	Step heights (nm)
A	2.52, 3.19, 3.35, 6.22, 6.89, 6.89, 7.78, 7.98, 8.05, 8.16, 8.36
B	0.42, 0.55, 1.12, 1.17, 1.69, 3.02, 3.60
C	0.81, 1.04, 1.10, 1.46, 1.46, 1.50, 2.15, 2.20, 2.24, 2.24
Average	3.47

## 3.10 RR05e (heated)

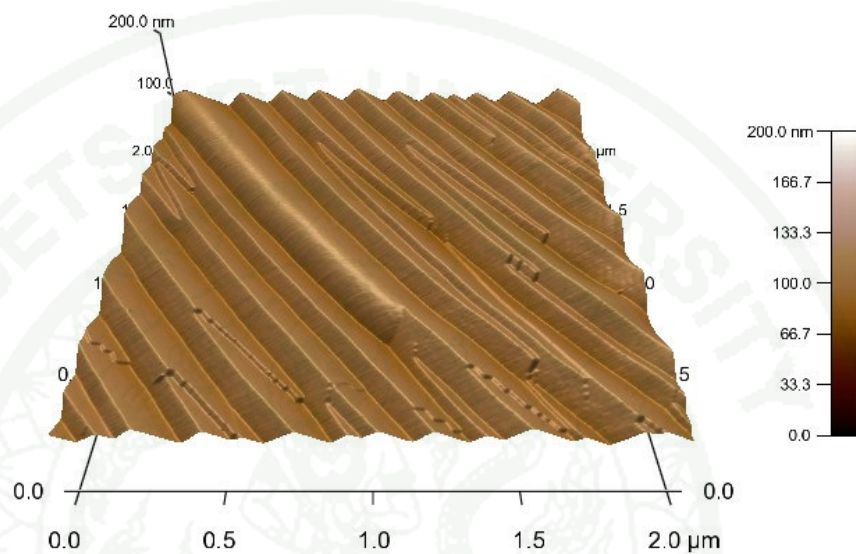


**Figure 87** 3D-Image ( $2.0 \times 2.0 \mu\text{m}^2$ ) of heated synthetic pink sapphire (set 1) on the miscut of pinacoid [0001] face of the sample RR05e; note: this pinacoid face shows the junction point that also found by Cuccureddu *et al.*, 2010.

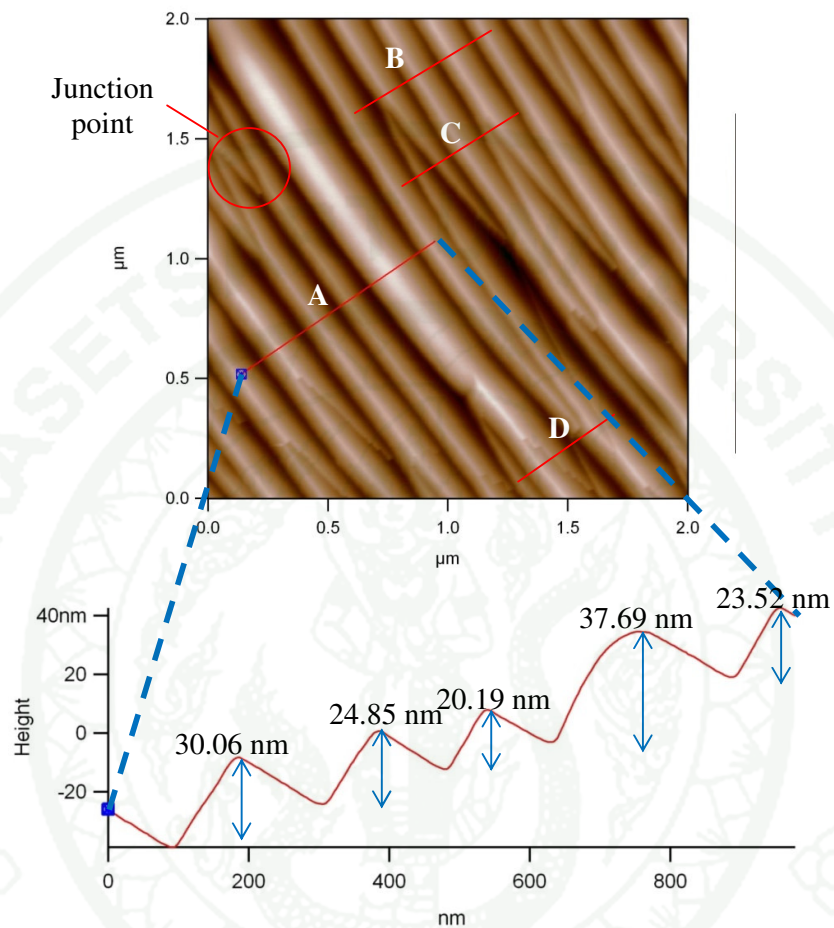


**Figure 88** Measurement of average step height of heated synthetic pink sapphire (set 1) sample (RR05e) on the miscut of pinacoid [0001] face; note: the junction point.

**Table 26** The average step height measurement obtained from the A, B, C and D lines on Figure 88

Line	Step heights (nm)
A	20.19, 23.52, 24.85, 30.06, 37.69
B	19.14, 20.87, 23.30, 23.86
C	9.50, 10.81, 10.99, 12.56, 20.84
D	1.06, 1.82, 2.25, 19.42, 25.39
Average	17.80

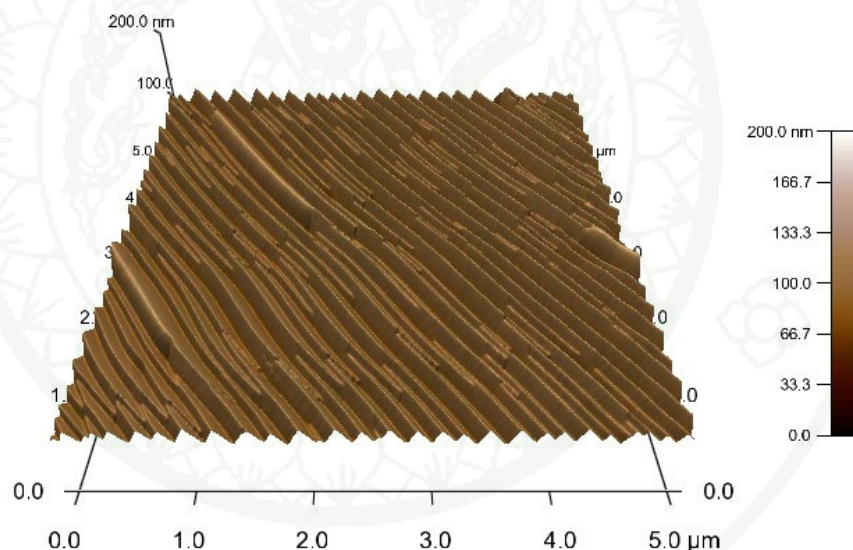


**Figure 89** 3D-Image ( $5.0 \times 5.0 \mu\text{m}^2$ ) of heated synthetic pink sapphire (set 1) on the miscut of pinacoid [0001] face of the sample RR05e; note: this pinacoid face shows the junction point that also found by Cuccureddu *et al.*, 2010.

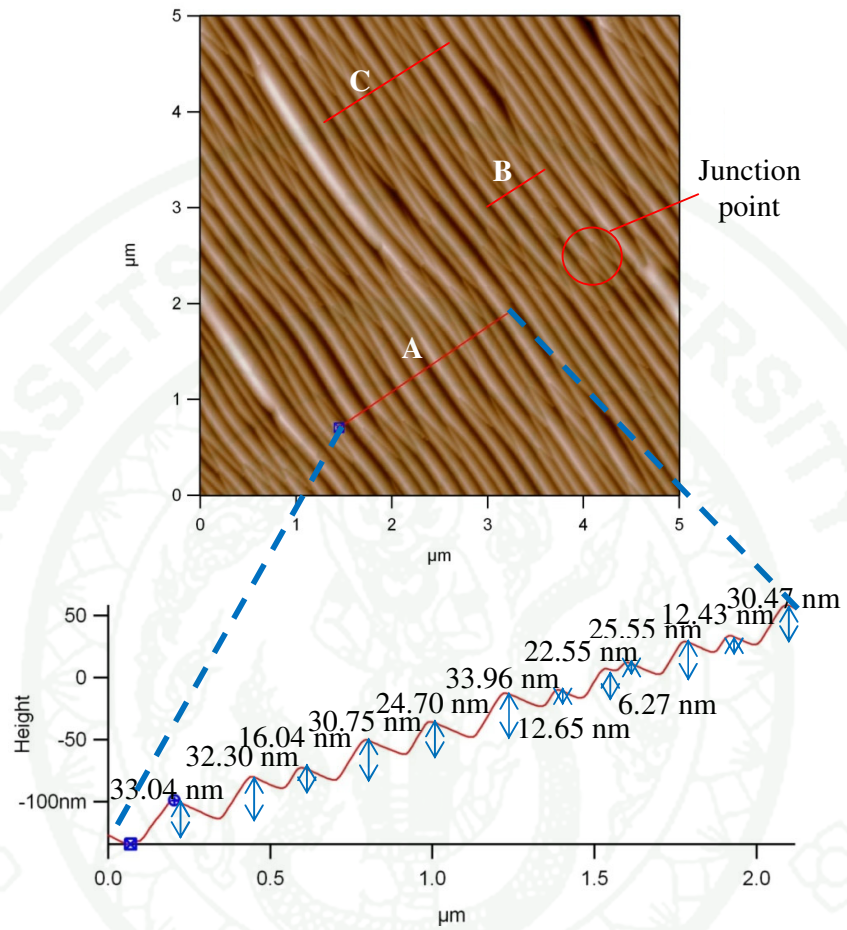


**Figure 90** Measurement of average step height of heated synthetic pink sapphire (set 1) sample (RR05e) on the miscut of pinacoid [0001] face; note: the junction point.

**Table 27** The average step height measurement obtained from the A, B and C lines on Figure 89

Line	Step heights (nm)
A	6.27, 12.43, 12.65, 16.04, 22.55, 24.70, 25.55, 30.47, 30.75, 32.30, 33.04, 33.96,
B	22.10, 26.44, 26.84, 29.85
C	10.91, 13.93, 17.06, 18.47, 18.97, 19.42, 20.85, 22.30, 23.86, 26.70
Average	22.25

### 3.11 RRb01a (unheated)

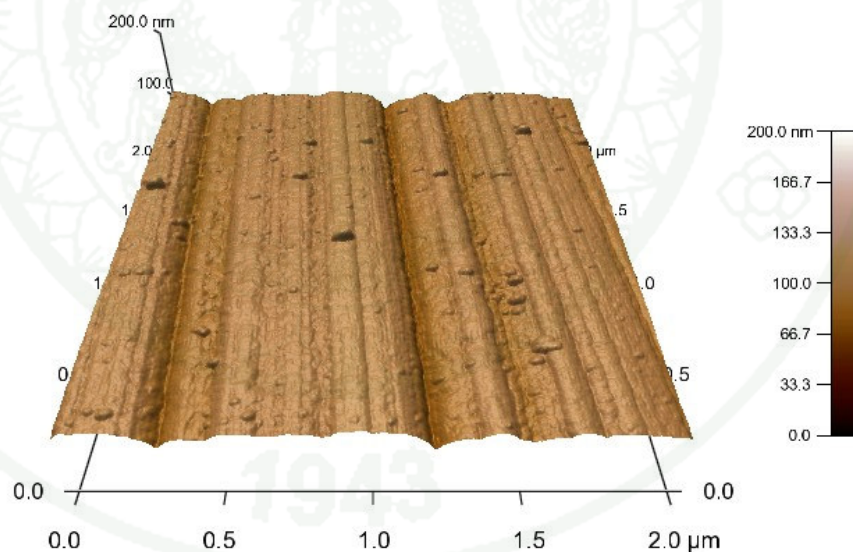


**Figure 91** 3D-Image ( $2.0 \times 2.0 \mu\text{m}^2$ ) of unheated synthetic ruby (set 2) on the miscut of prism  $[1\bar{1}00]$  face of the sample RRb01a; notes; some impurities

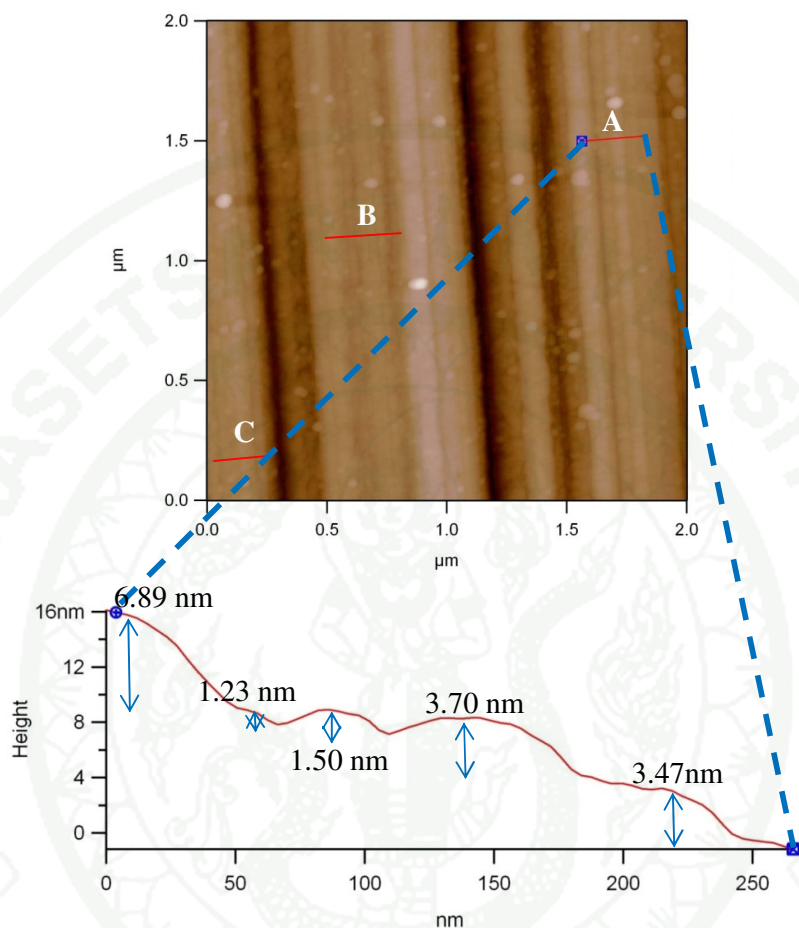


**Figure 92** Measurement of average step height of unheated synthetic ruby (set 2) sample (RRb01a) on the miscut of prism  $[1 \bar{1}00]$  face

**Table 28** The average step height measurement obtained from the A, B and C lines on Figure 92

Line	Step heights (nm)
A	1.23, 1.50, 3.47, 3.70, 6.89
B	0.95, 1.17, 1.17, 1.28, 1.76, 1.94, 3.71, 4.38
C	1.19, 2.19, 2.36, 2.92, 3.62
Average	2.32

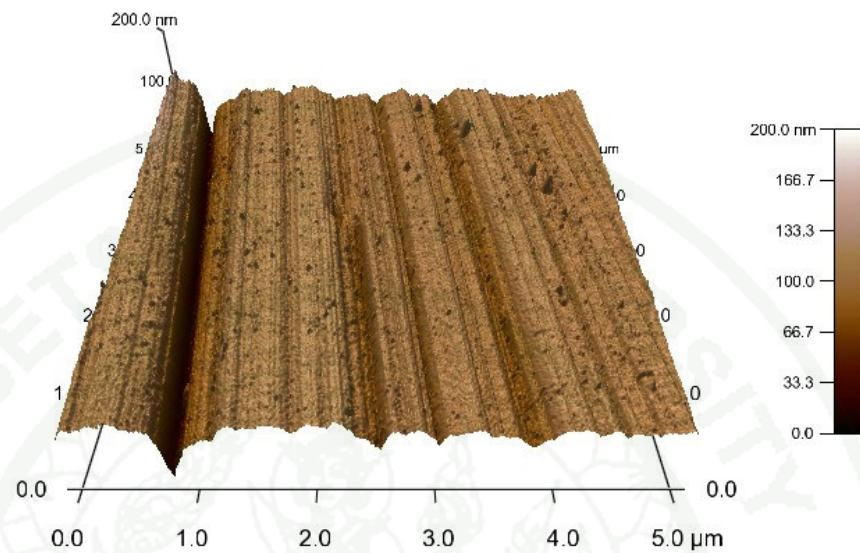


**Figure 93** 3D-Image ( $5.0 \times 5.0 \mu\text{m}^2$ ) of unheated synthetic ruby (set 2) on the miscut of prism  $[1\bar{1}00]$  face of the sample RRb01a

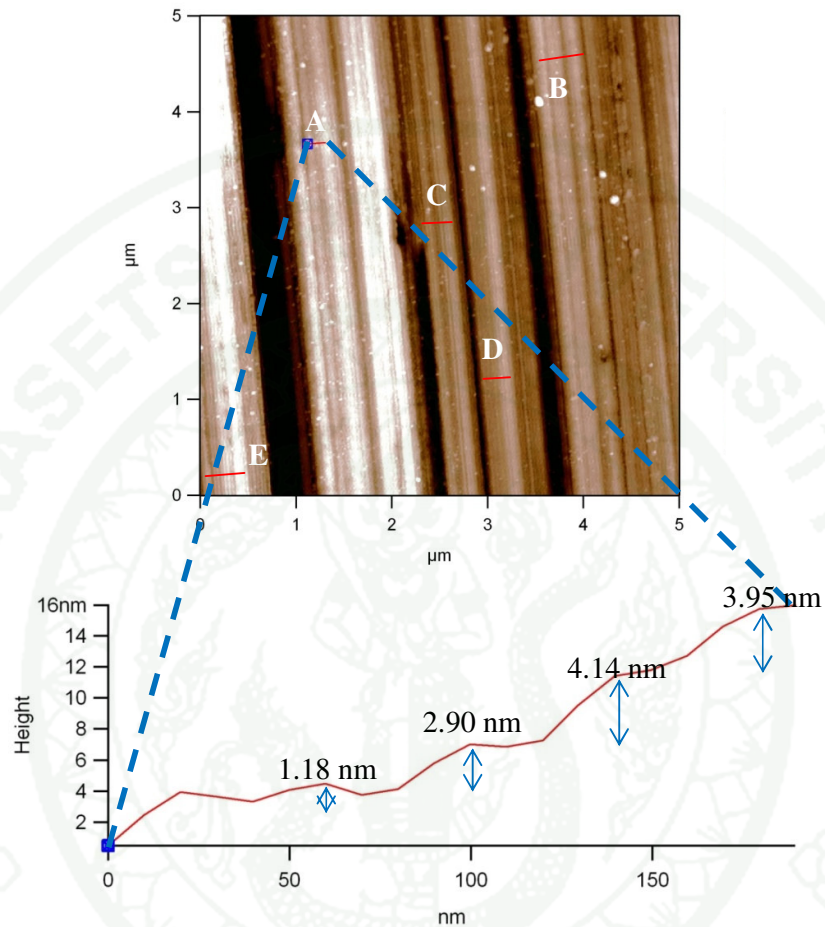


**Figure 94** Measurement of average step height of unheated synthetic ruby (set 2) sample (RRb01a) on the miscut of prism  $[1\bar{1}00]$  face

1943

**Table 29** The average step height measurement obtained from the A, B, C, D and E lines on Figure 94

Line	Step heights (nm)
A	1.18, 2.90, 3.95, 4.14
B	1.65, 2.81, 3.26, 3.82, 4.32, 4.42
C	1.70, 3.76, 4.27, 4.43, 4.45, 6.14, 6.22
D	2.69, 3.57, 5.86, 7.94, 11.71
E	1.19, 3.38, 3.81, 4.82, 5.64, 6.12, 13.88
Average	4.62

### 3.12 RRb01d (heated)

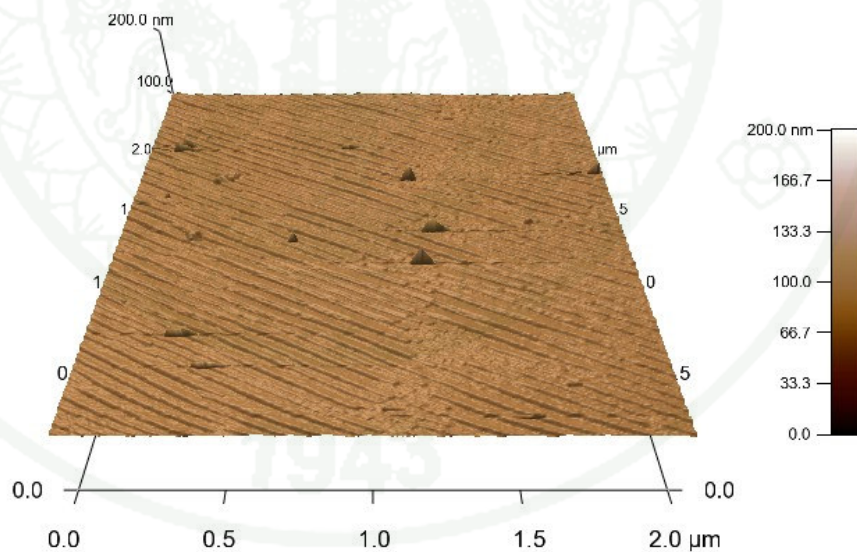


**Figure 95** 3D-Image ( $2.0 \times 2.0 \mu\text{m}^2$ ) of heated synthetic ruby (set 2) on the miscut of prism  $[1\bar{1}00]$  face of the sample RRb01d

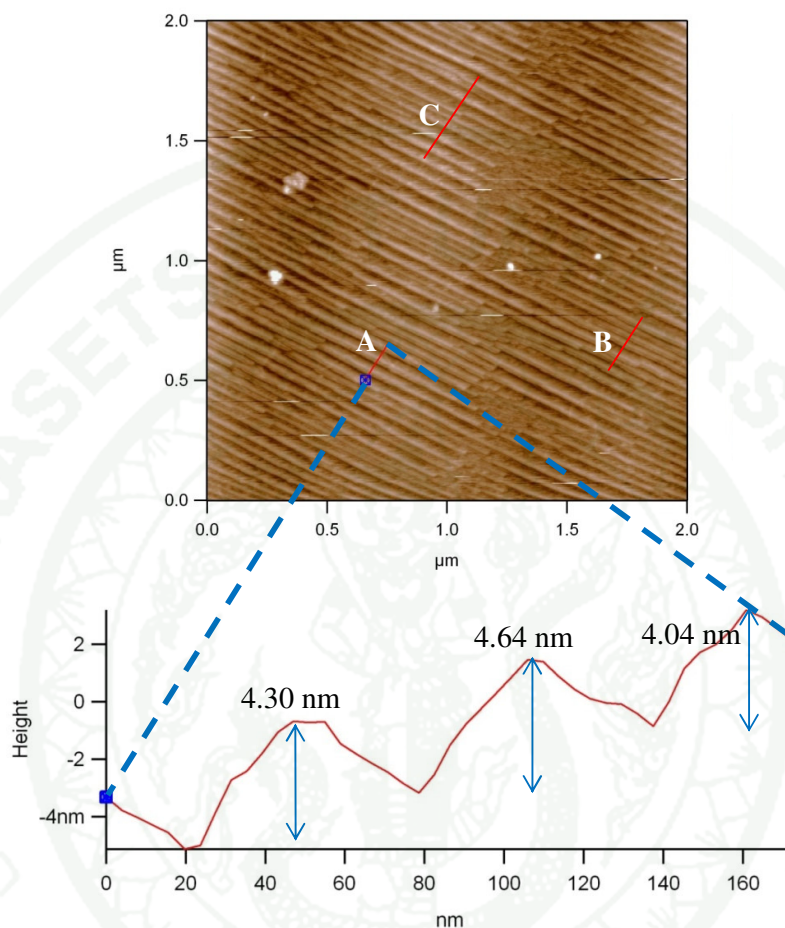


**Figure 96** Measurement of average step height of heated synthetic ruby (set 2) sample (RRb01d) on the miscut of prism  $[1 \bar{1}00]$  face

**Table 30** The average step height measurement obtained from the A, B and C lines on Figure 96

Line	Step heights (nm)
A	4.04, 4.30, 4.64
B	1.65, 2.08, 2.18, 2.80, 2.85, 3.26, 3.32
C	1.47, 2.64, 3.14, 3.42, 3.64, 3.80, 4.28, 4.34
Average	3.21

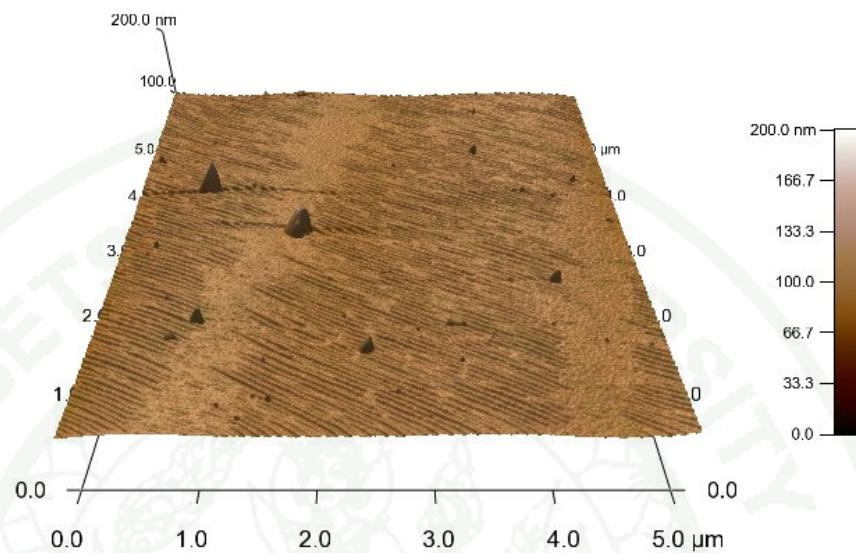


**Figure 97** 3D-Image ( $5.0 \times 5.0 \mu\text{m}^2$ ) of heated synthetic ruby (set 2) on the miscut of prism  $[1\bar{1}00]$  face of the sample RRb01d

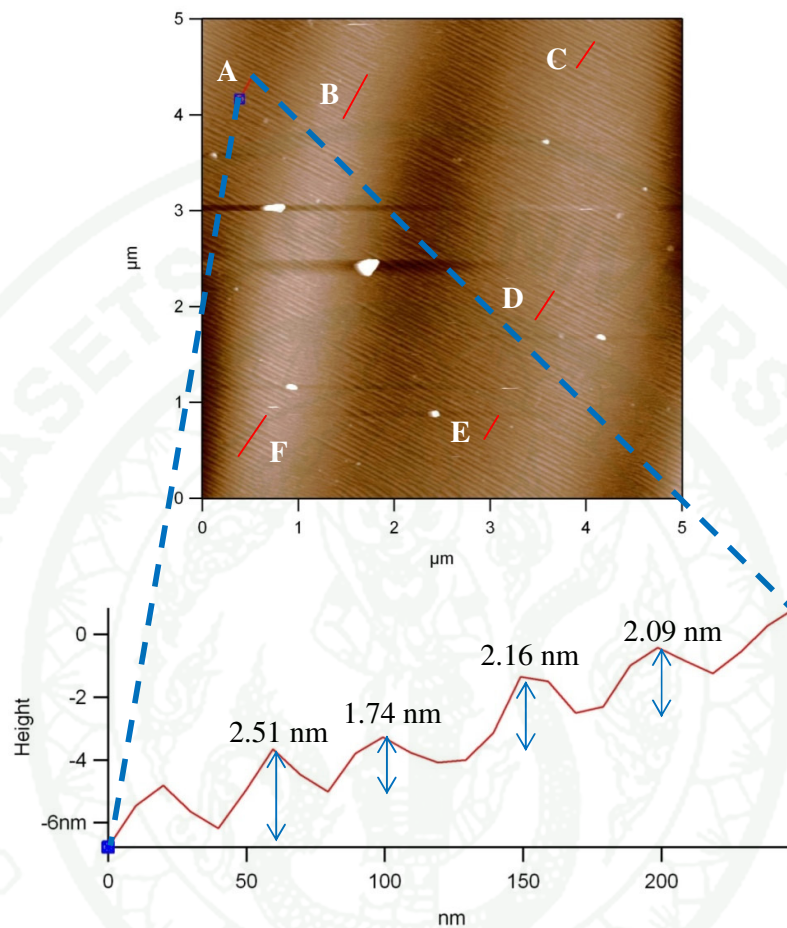


**Figure 98** Measurement of average step height of heated synthetic ruby (set 2) sample (RRb01d) on the miscut of prism  $[1 \bar{1}00]$  face

1943

**Table 31** The average step height measurement obtained from the A, B, C, D, E and F lines on Figure 98

Line	Step heights (nm)
A	1.74, 2.09, 2.16, 2.51
B	1.00, 1.00, 1.28, 1.34, 1.36, 1.58, 1.89, 2.64, 2.73, 2.95
C	1.17, 2.16, 2.54, 2.63, 3.53
D	2.31, 2.72, 3.19, 3.22, 3.29
E	1.12, 1.22, 1.38, 1.80, 1.85, 1.85, 2.14, 2.58
F	1.10, 1.57, 1.91, 2.06, 2.17, 2.17, 2.23, 2.48, 2.72, 3.45, 3.64
Average	2.15

### 3.13 RRb01b (unheated)

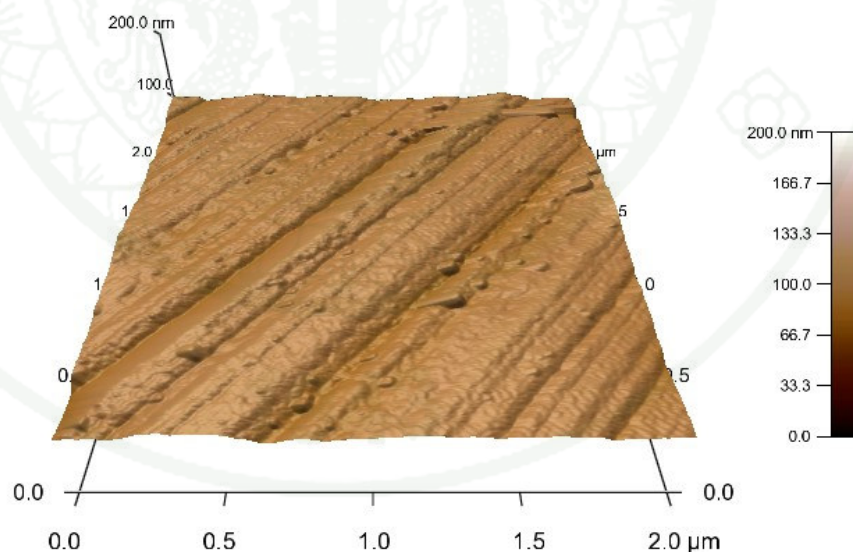


**Figure 99** 3D-Image ( $2.0 \times 2.0 \mu\text{m}^2$ ) of unheated synthetic ruby (set 2) on the miscut of prism  $[0\bar{1}10]$  face of the sample RRb01b

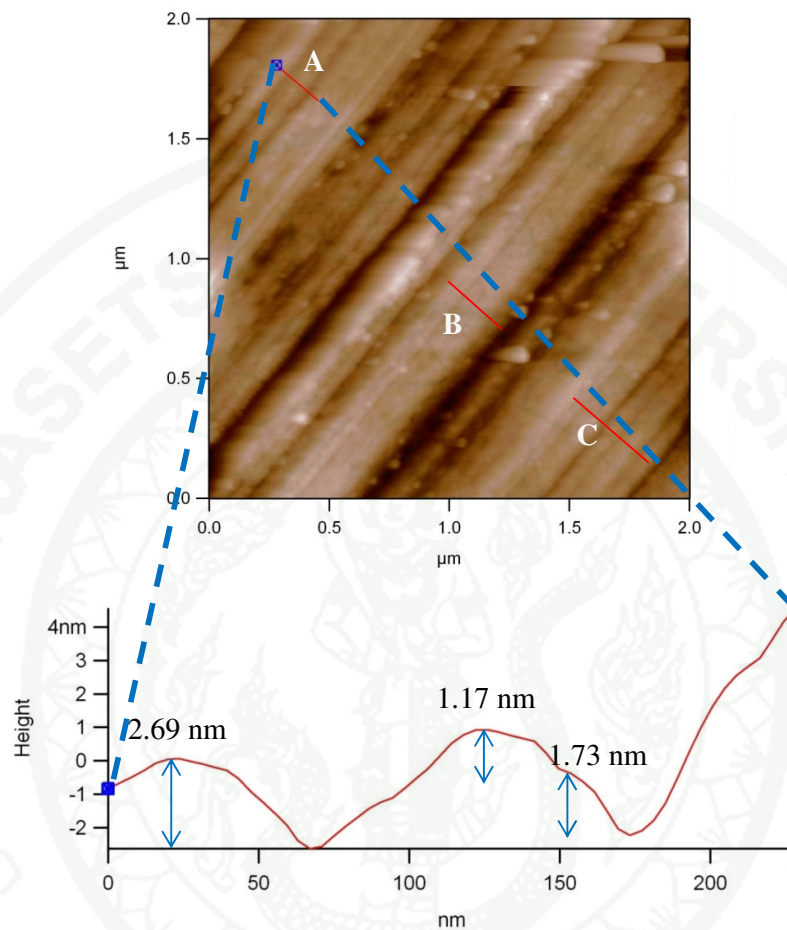


**Figure 100** Measurement of average step height of unheated synthetic ruby (set 2) sample (RRb01b) on the miscut of prism  $[0\bar{1}10]$  face

**Table 32** The average step height measurement obtained from the A, B and C lines on Figure 100

Line	Step heights (nm)
A	1.17, 1.73, 2.69
B	0.42, 0.61, 1.06, 1.45, 2.28
C	1.11, 1.46, 1.58, 2.62, 5.38
Average	1.81

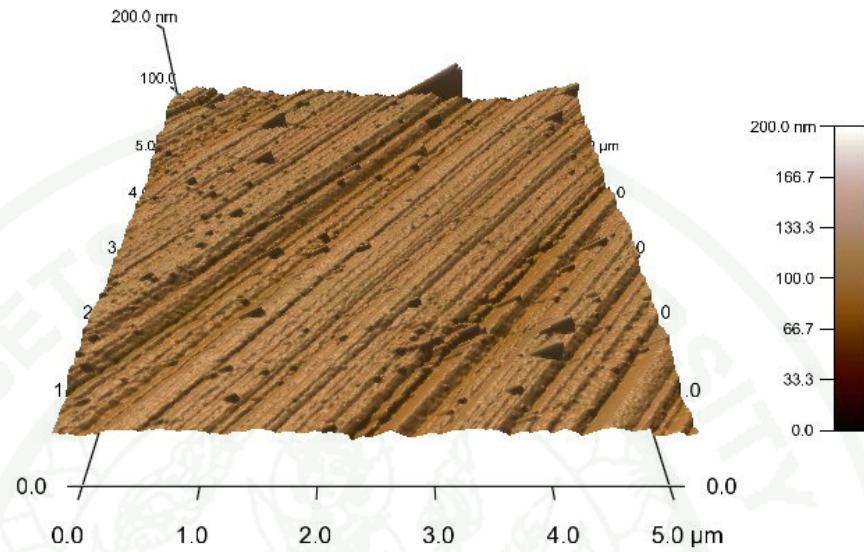


**Figure 101** 3D-Image ( $5.0 \times 5.0 \mu\text{m}^2$ ) of unheated synthetic ruby (set 2) on the miscut of prism  $[0\bar{1}10]$  face of the sample RRb01b

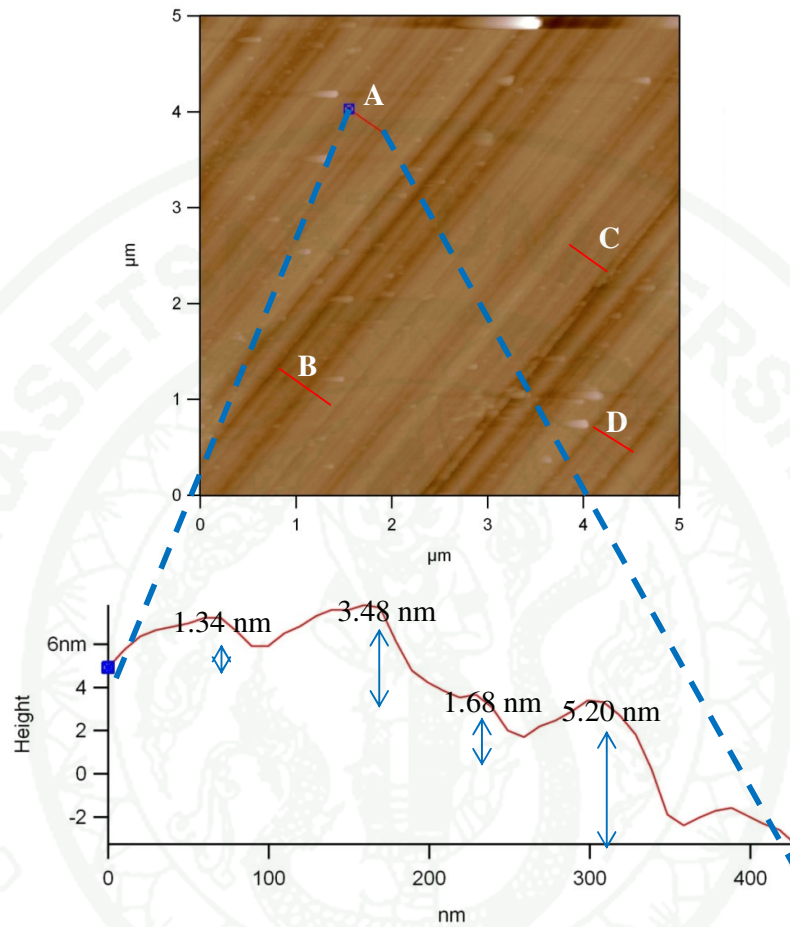


**Figure 102** Measurement of average step height of unheated synthetic ruby (set 2) sample (RRb01b) on the miscut of  $[0\bar{1}10]$  face

1943

**Table 33** The average step height measurement obtained from the A, B, C and D lines on Figure 102

Line	Step heights (nm)
A	1.34, 1.68, 3.48, 5.20
B	1.36, 1.81, 4.44, 5.21, 5.94
C	0.83, 1.96, 2.38, 4.94
D	1.51, 1.54, 4.22
Average	2.99

3.14 RRb01c (heated)

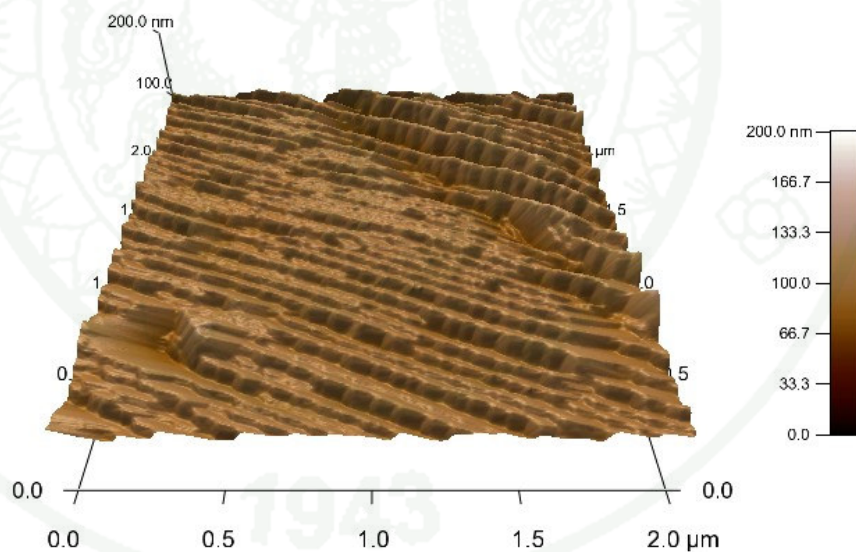


**Figure 103** 3D-Image ( $2.0 \times 2.0 \mu\text{m}^2$ ) of heated synthetic ruby (set 2) on the miscut of prism  $[0\bar{1}10]$  face of the sample RRb01c; note: the zigzag lines

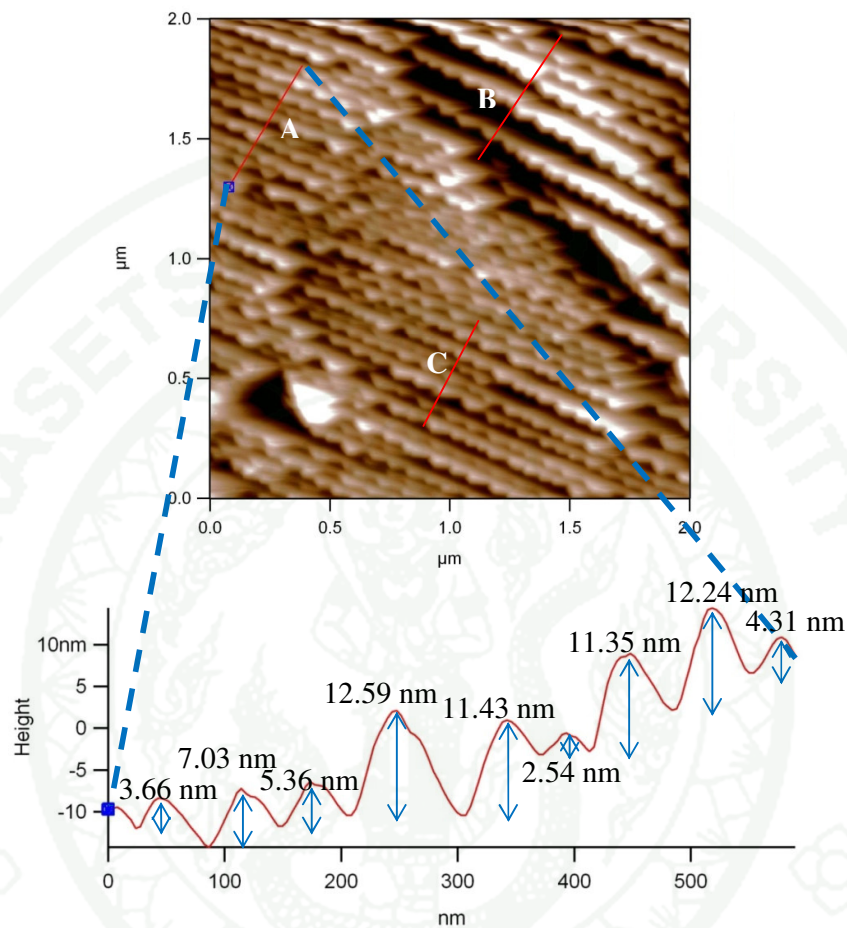


**Figure 104** Measurement of average step height of heated synthetic ruby (set 2) sample (RRb01c) on the miscut of prism  $[0\bar{1}10]$  face; note: the zigzag lines

**Table 34** The average step height measurement obtained from the A, B and C lines on Figure 104

Line	Step heights (nm)
A	2.54, 3.66, 4.31, 5.36, 7.03, 11.35, 11.43, 12.24, 12.59
B	5.76, 7.77, 19.28, 20.79, 33.64
C	3.52, 3.63, 3.75, 6.37, 11.63, 11.99, 13.65, 18.55
Average	10.49

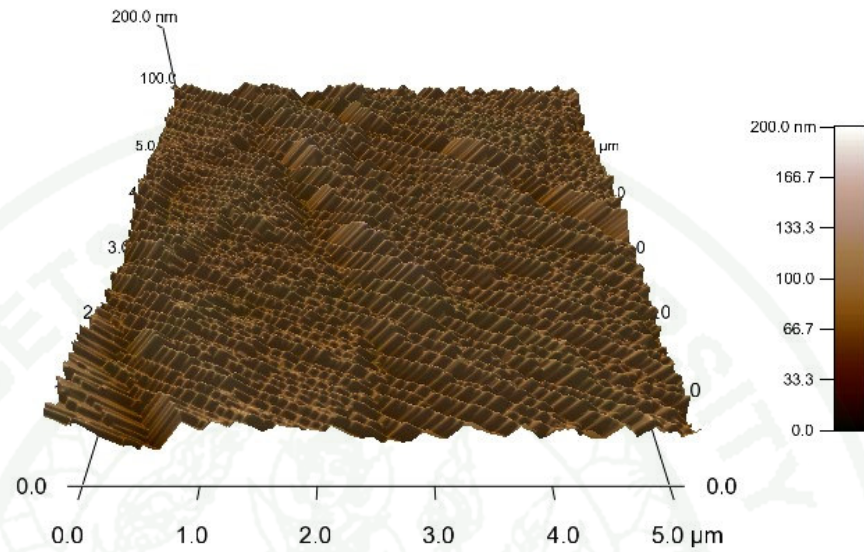


**Figure 105** 3D-Image ( $5.0 \times 5.0 \mu\text{m}^2$ ) of heated synthetic ruby (set 2) on the miscut of prism  $[0\bar{1}10]$  face of the sample RRb01c

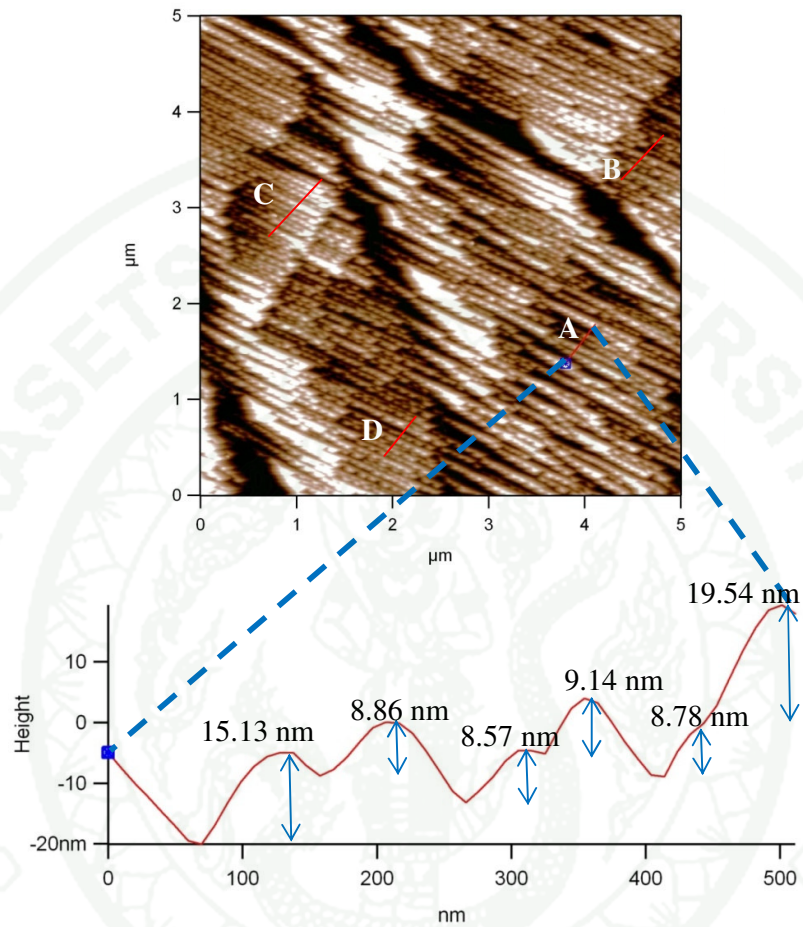


**Figure 106** Measurement of average step height of heated synthetic ruby (set 2) sample (RRb01c) on the miscut of prism  $[0\bar{1}10]$  face

1943

**Table 35** The average step height measurement obtained from the A, B, C and D lines on Figure 106

Line	Step heights (nm)
A	8.57, 8.78, 8.86, 9.14, 15.13, 19.54
B	5.07, 5.98, 6.77, 7.14, 7.14, 7.27, 8.36, 8.87
C	3.66, 3.88, 4.01, 4.87, 6.87, 7.75, 7.77, 7.96, 10.02
D	5.56, 6.57, 8.30, 11.10, 25.87
Average	8.60

### 3.15 RRb02a (unheated)

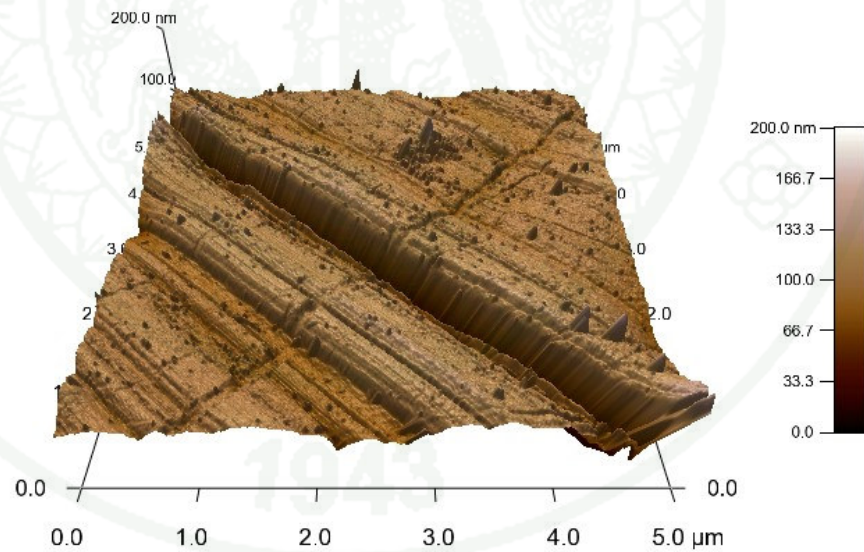


**Figure 107** 3D-Image ( $5.0 \times 5.0 \mu\text{m}^2$ ) of unheated synthetic ruby (set 2) on the miscut of prism  $[1 \bar{2} 10]$  face of the sample RRb02a; note: the scratch line

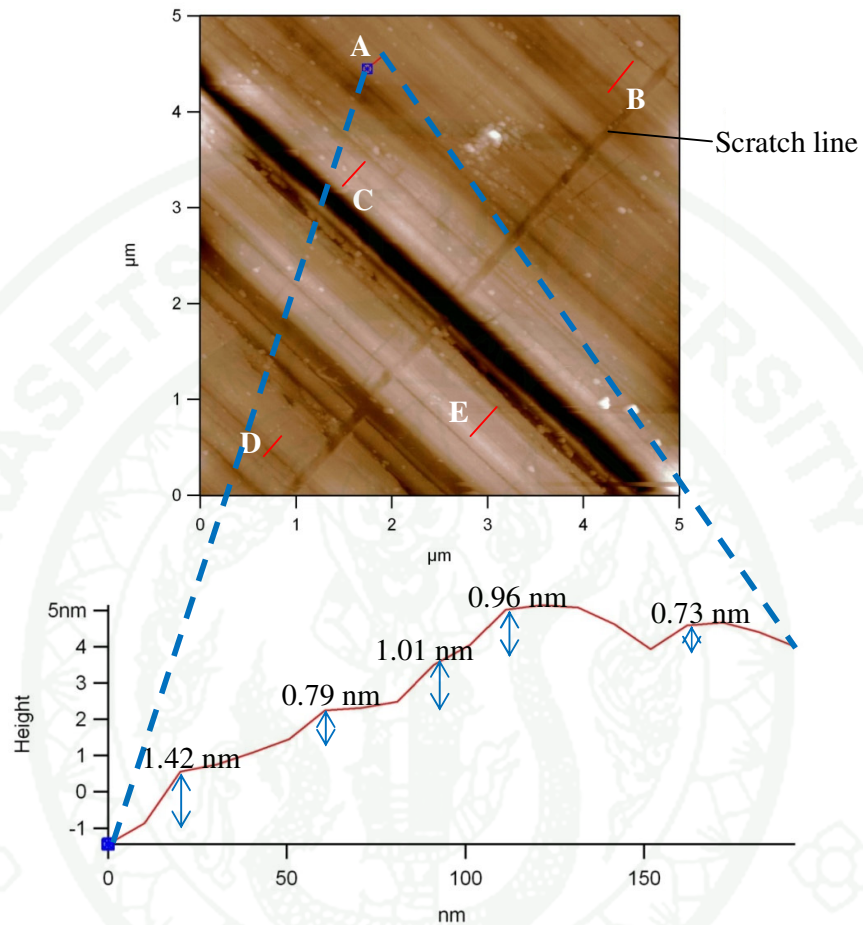


**Figure 108** Measurement of average step height of unheated synthetic ruby (set 2) sample (RRb02a) on the miscut of prism  $[1\bar{2}10]$  face; note: the scratch line

**Table 36** The average step height measurement obtained from the A, B, C, D and E lines on Figure 108.

Line	Step heights (nm)
A	0.73, 0.79, 0.96, 1.01, 1.42
B	2.41, 3.66, 9.23
C	2.32, 3.13, 8.15, 10.56
D	2.89, 5.50, 9.57
E	1.00, 1.00, 1.06, 2.45, 2.81, 4.55, 5.37
Average	3.66

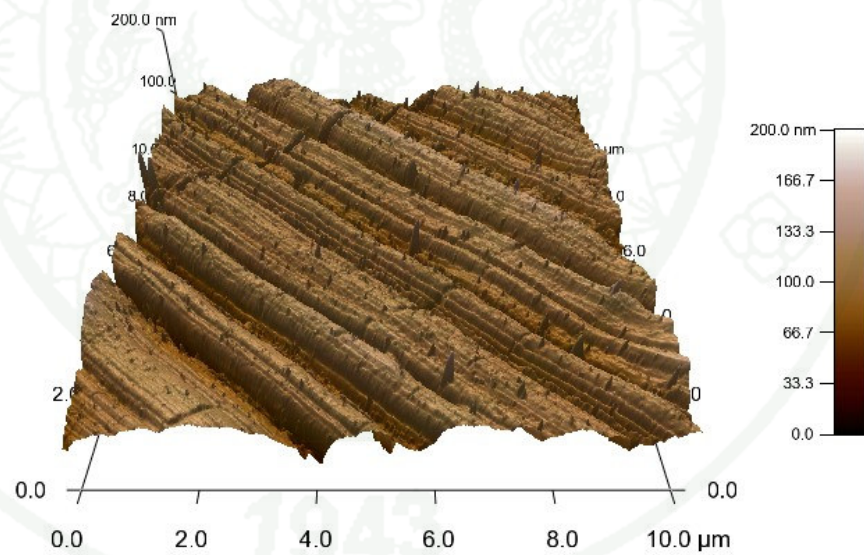


**Figure 109** 3D-Image ( $10.0 \times 10.0 \mu\text{m}^2$ ) of unheated synthetic ruby (set 2) on the miscut of prism  $[1\bar{2}10]$  face of the sample RRb02a

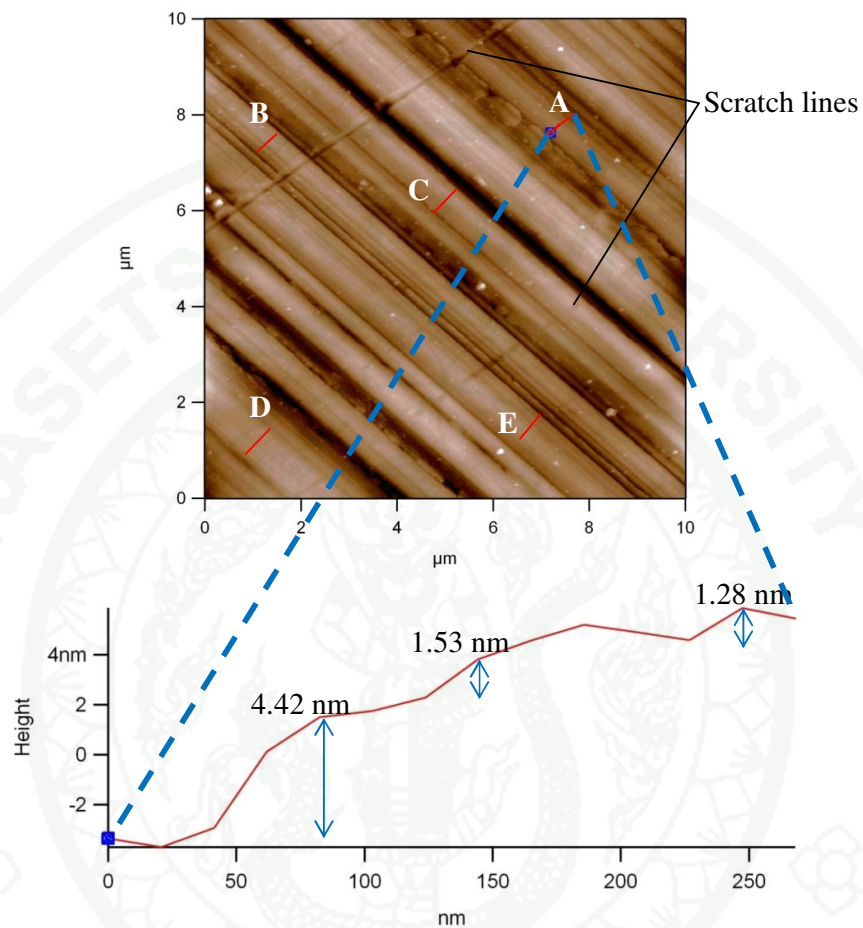


**Figure 110** Measurement of average step height of unheated synthetic ruby (set 2) sample (RRb02a) on the miscut of  $[1\bar{2}10]$  face; note: the scratch lines

**Table 37** The average step height measurement obtained from the A, B, C, D and E lines on Figure 110.

Line	Step heights (nm)
A	1.28, 1.53, 4.42
B	11.06, 11.15, 12.95
C	3.15, 7.34, 9.77, 9.99
D	0.74, 1.30, 1.75, 1.75, 3.66, 4.70, 9.06
E	3.59, 4.87, 6.22, 18.85
Average	5.51

### 3.16 RRb02c (heated)

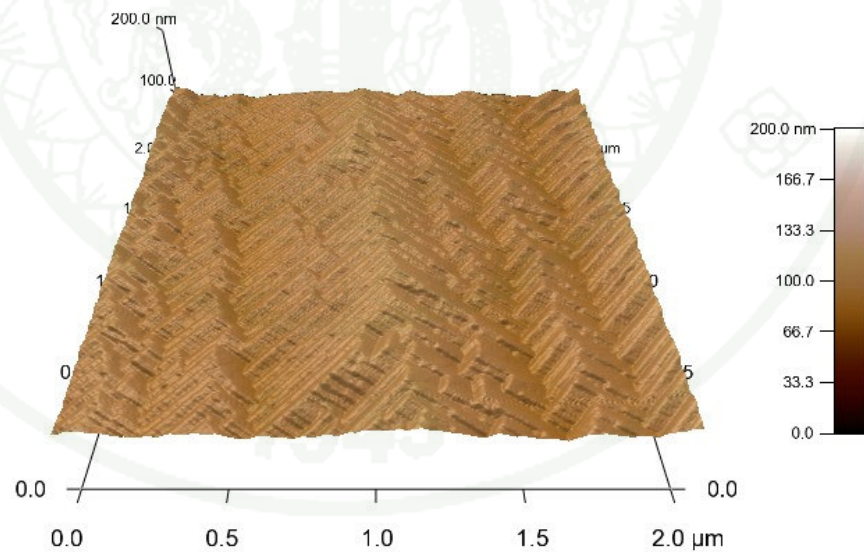


**Figure 111** 3D-Image ( $2.0 \times 2.0 \mu\text{m}^2$ ) of heated synthetic ruby (set 2) on the miscut of prism  $[1\bar{2}10]$  face of the sample RRb02c

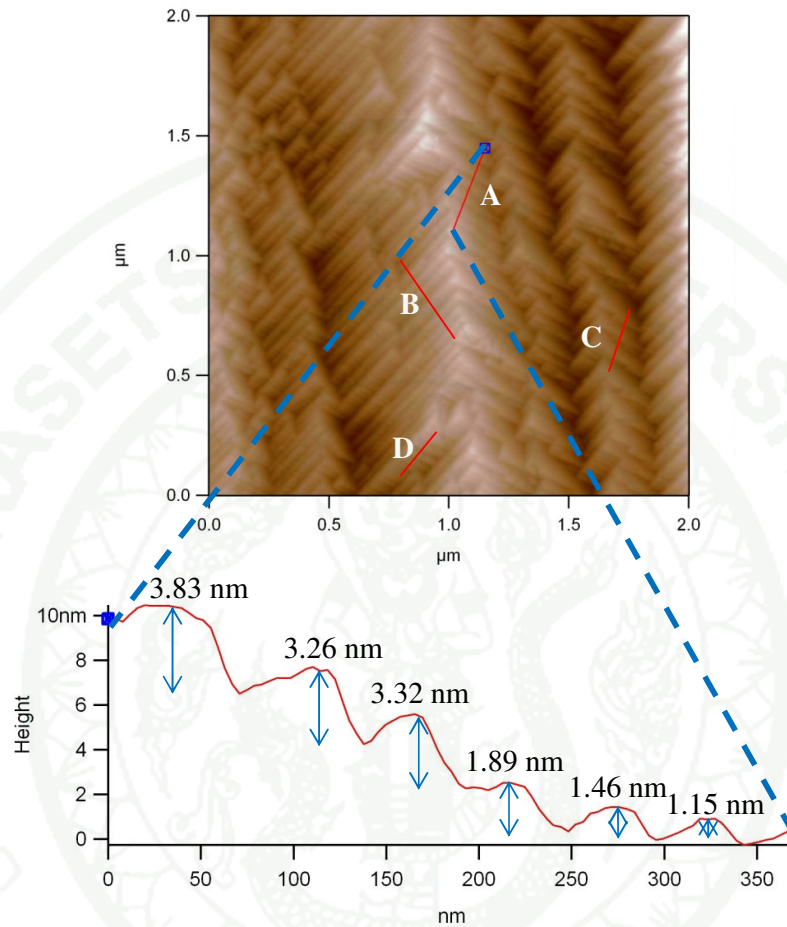


**Figure 112** Measurement of average step height of heated synthetic ruby (set 2) sample (RRb02c) on the miscut of prism  $[1 \bar{2}10]$  face

1943

**Table 38** The average step height measurement obtained from the A, B, C and D lines on Figure 112.

Line	Step heights (nm)
A	1.15, 1.46, 1.89, 3.26, 3.32, 3.83
B	1.42, 2.03, 2.08, 2.18, 2.32, 3.23, 4.12, 7.02
C	2.26, 3.58, 3.91
D	1.03, 1.08, 1.56, 2.60, 2.73, 3.01, 3.80
Average	2.70

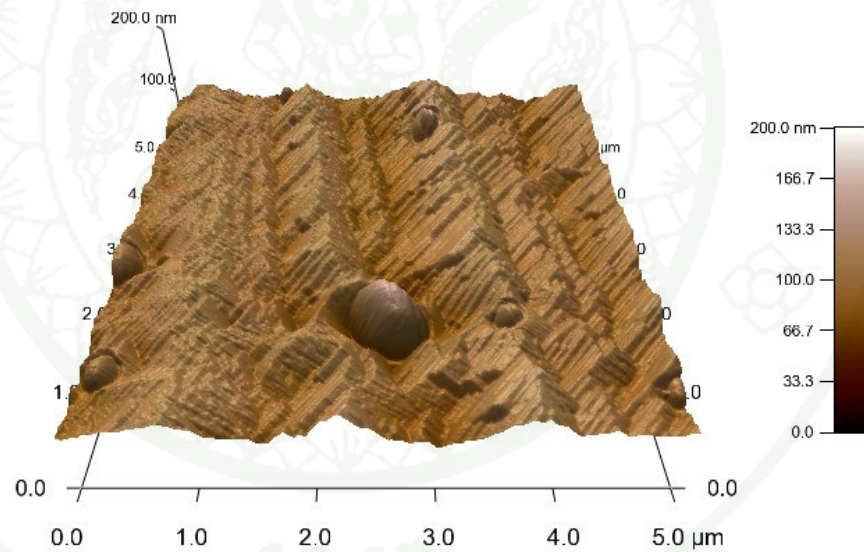


**Figure 113** 3D-Image ( $2.0 \times 2.0 \mu\text{m}^2$ ) of heated synthetic ruby (set 2) on the miscut of prism  $[1\bar{2}10]$  face of the sample RRb02c; note: the impurities

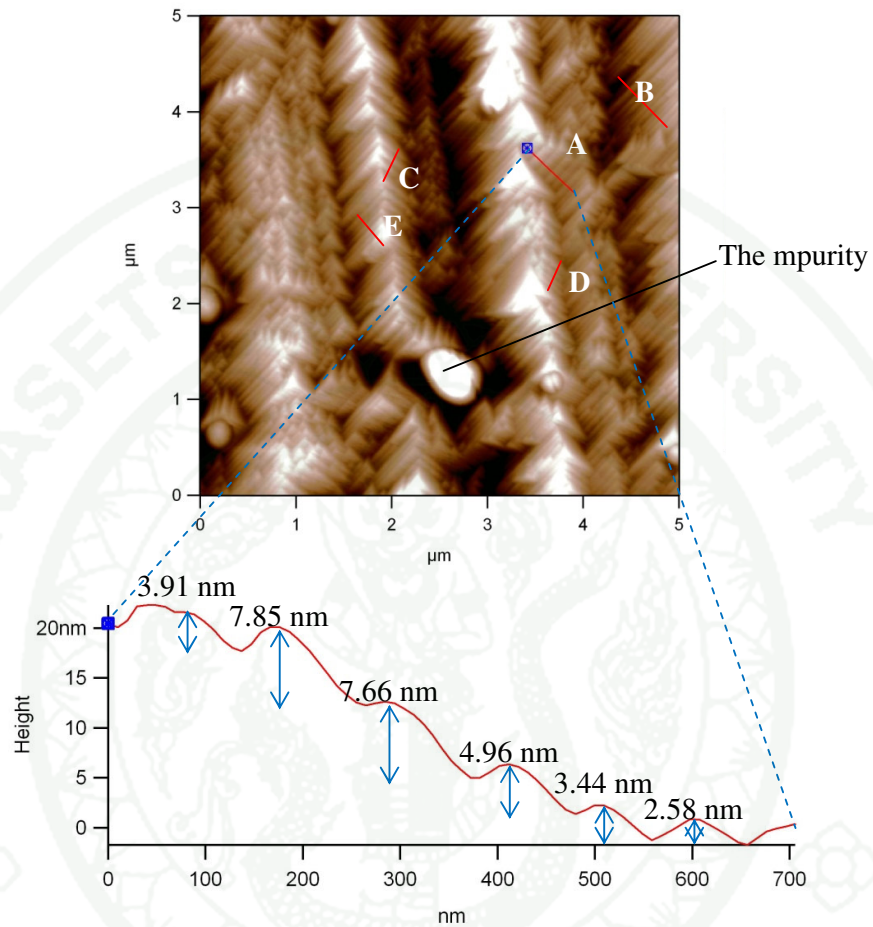


**Figure 114** Measurement of average step height of heated synthetic ruby (set 2) sample (RRb02c) on the miscut of prism  $[1\bar{2}10]$  face; note: the impurities

**Table 39** The average step height measurement obtained from the A, B, C, D and E lines on Figure 114.

Line	Step heights (nm)
A	2.58, 3.44, 3.91, 4.96, 7.66, 7.85
B	2.90, 2.96, 3.60, 5.61
C	1.07, 2.66, 2.75, 2.82, 3.25, 4.30
D	2.03, 5.11, 5.80
E	1.68, 2.07, 2.53, 2.81, 2.87, 3.16, 4.11, 6.75, 8.42
Average	3.92

### 3.17 RR04a (unheated)

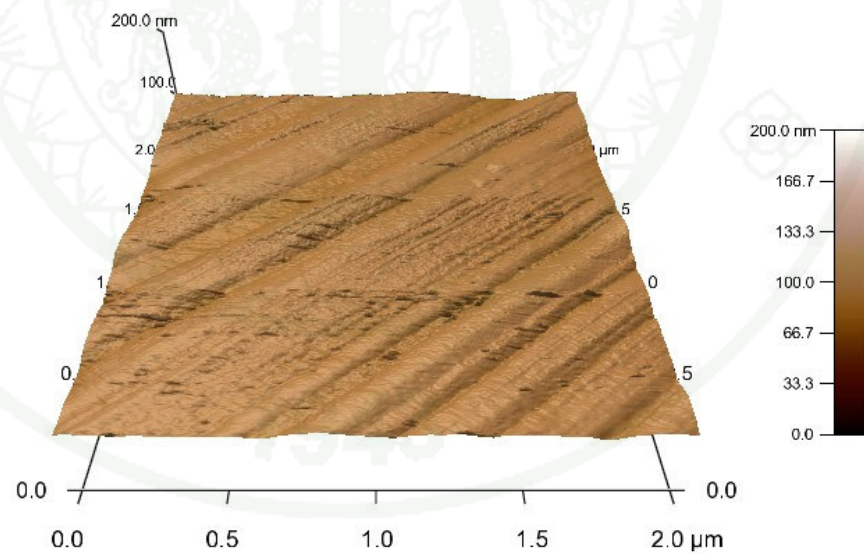


**Figure 115** 3D-Image ( $2.0 \times 2.0 \mu\text{m}^2$ ) of unheated synthetic ruby (set 2) on the miscut of prism  $[\bar{1}\bar{1}20]$  face of the sample RRb04a

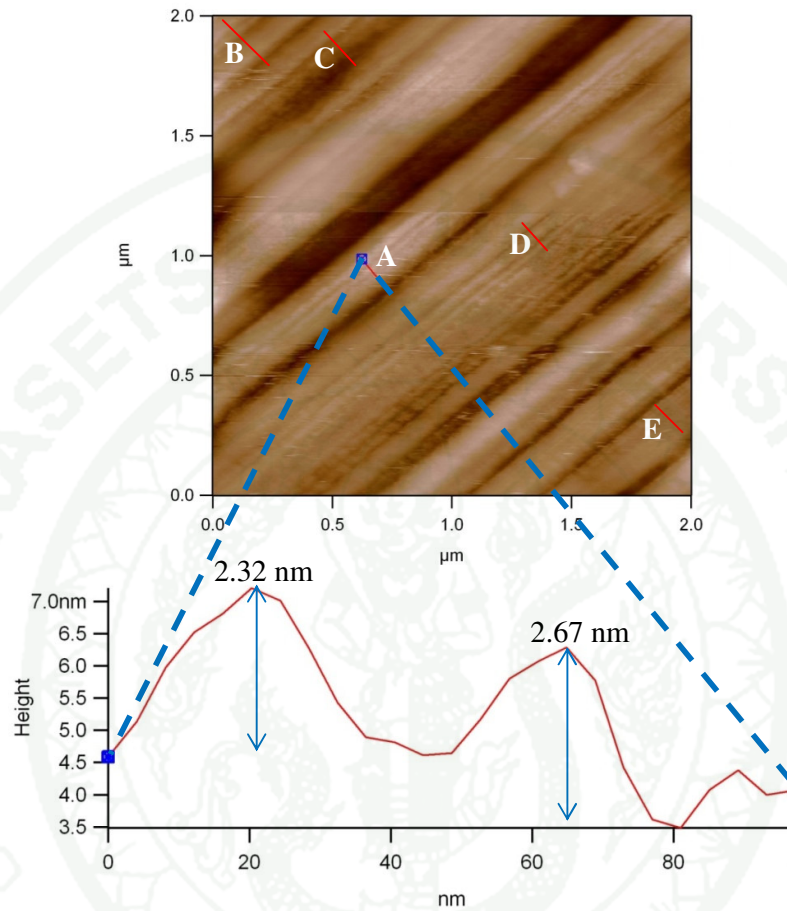


**Figure 116** Measurement of average step height of unheated synthetic ruby (set 2) on the miscut of prism  $[\bar{1}\bar{1}20]$  face (RRb04a)

1943

**Table 40** The average step height measurement obtained from the A, B, C, D and E lines on Figure 116.

Line	Step heights (nm)
A	2.32, 2.67
B	1.82, 2.07, 5.09
C	0.22, 0.34, 0.42, 0.50, 0.72, 0.78, 0.86, 0.96
D	1.62, 1.87, 2.79, 3.44
E	0.91, 0.97, 1.88, 3.35
Average	1.70

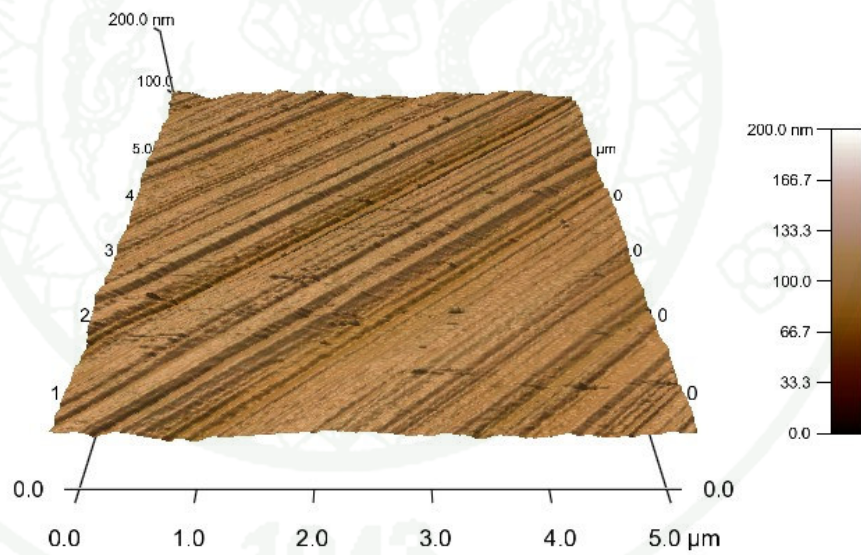


**Figure 117** 3D-Image ( $5.0 \times 5.0 \mu\text{m}^2$ ) of unheated synthetic ruby (set 2) on the miscut of prism  $[\bar{1}\bar{1}20]$  face of the sample RRb04a

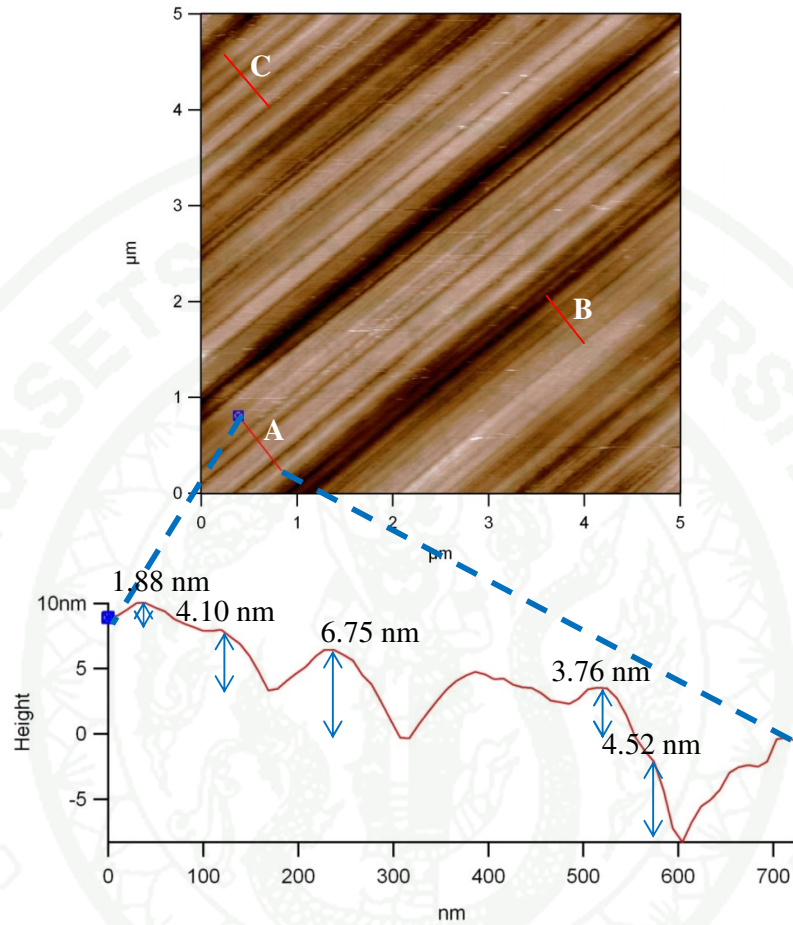


**Figure 118** Measurement of average step height of unheated synthetic ruby (set 2) sample (RRb04a) on the miscut of prism  $[\bar{1}\bar{1}20]$  face

**Table 41** The average step height measurement obtained from the A, B and C lines on Figure 118

Line	Step heights (nm)
A	1.88, 3.76, 4.10, 4.52, 6.75
B	1.01, 2.32, 2.54, 3.80, 4.03, 7.75
C	1.62, 3.52, 5.03, 5.11, 7.46
Average	4.07

## 3.18 RRb04c (heated)

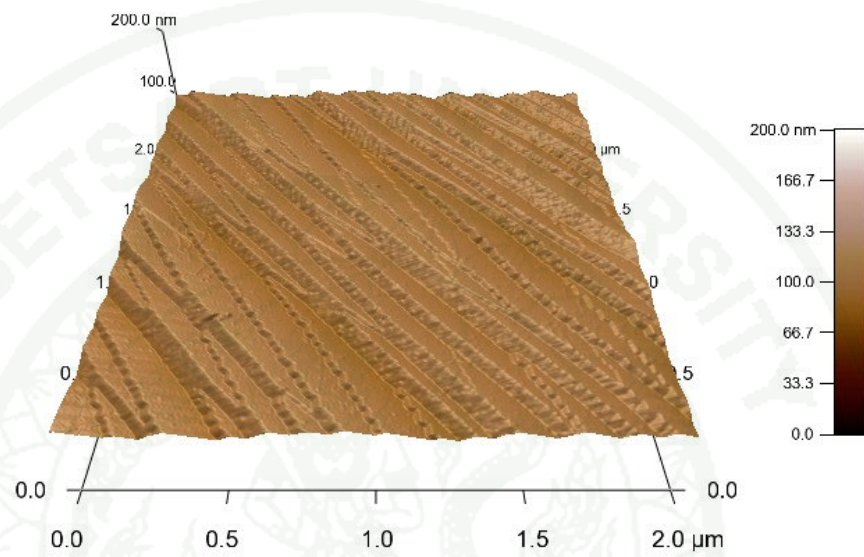


**Figure 119** 3D-Image ( $2.0 \times 2.0 \mu\text{m}^2$ ) of heated synthetic ruby (set 2) on the miscut of prism  $[\bar{1}\bar{1}20]$  face of the sample RRb04c; note: the zigzag line

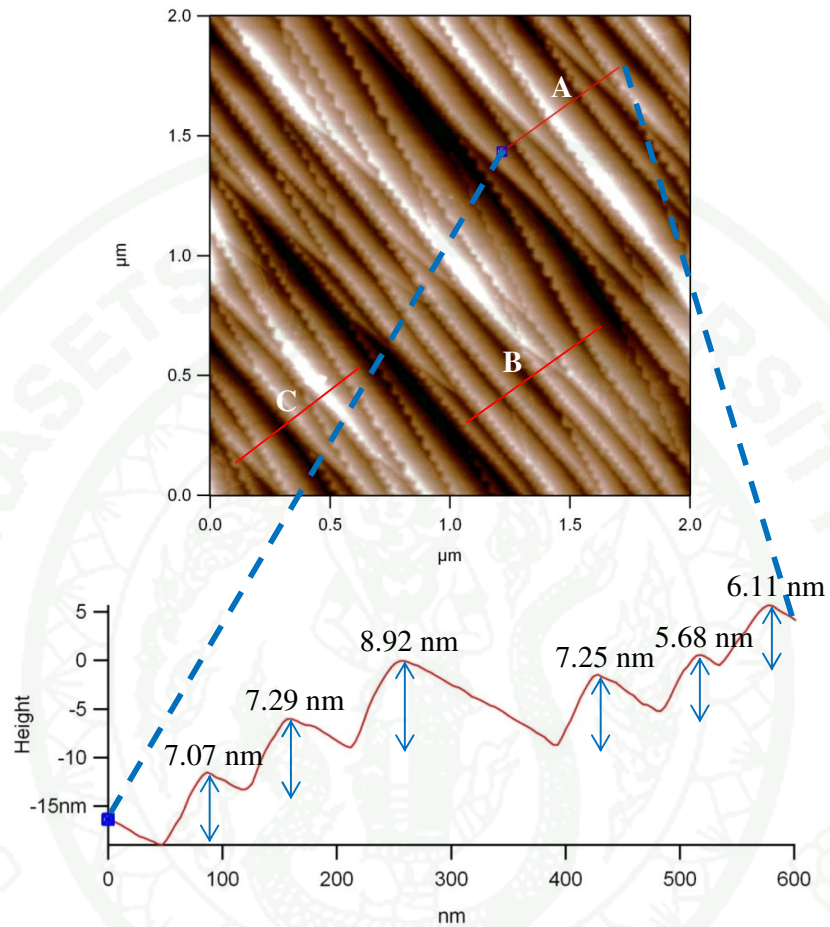


**Figure 120** Measurement of average step height of heated synthetic ruby (set 2) sample (RRb04c) on the miscut of prism  $[\bar{1}\bar{1}20]$  face; note: the zigzag lines

**Table 42** The average step height measurement obtained from the A-C lines on Figure 120

Line	Step heights (nm)
A	5.68, 6.11, 7.07, 7.25, 7.29, 8.92
B	2.46, 3.43, 6.63, 8.37, 10.72, 12.96
C	3.10, 4.31, 4.86, 6.19, 9.28, 14.84
Average	7.19

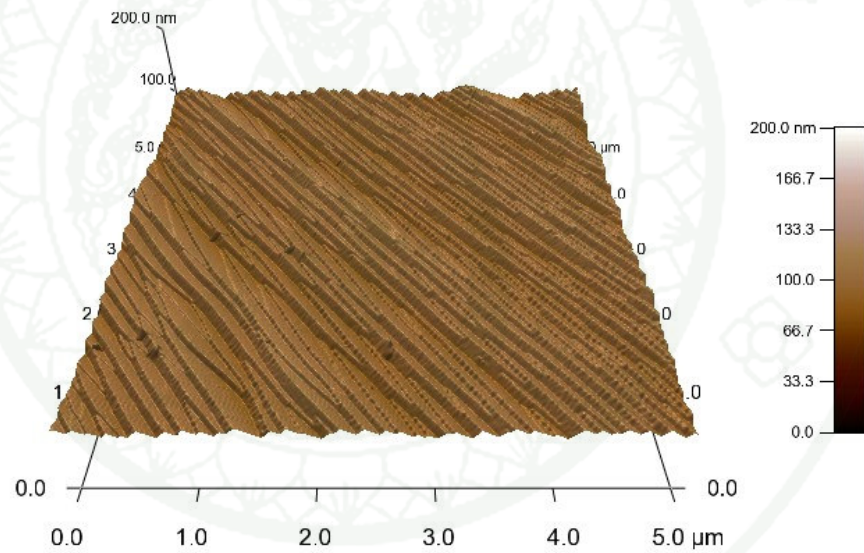


**Figure 121** 3D-Image ( $5.0 \times 5.0 \mu\text{m}^2$ ) of heated synthetic ruby (set 2) on the miscut of prism  $[\bar{1}\bar{1}20]$  face of the sample RRb04c; note: the zigzag lines

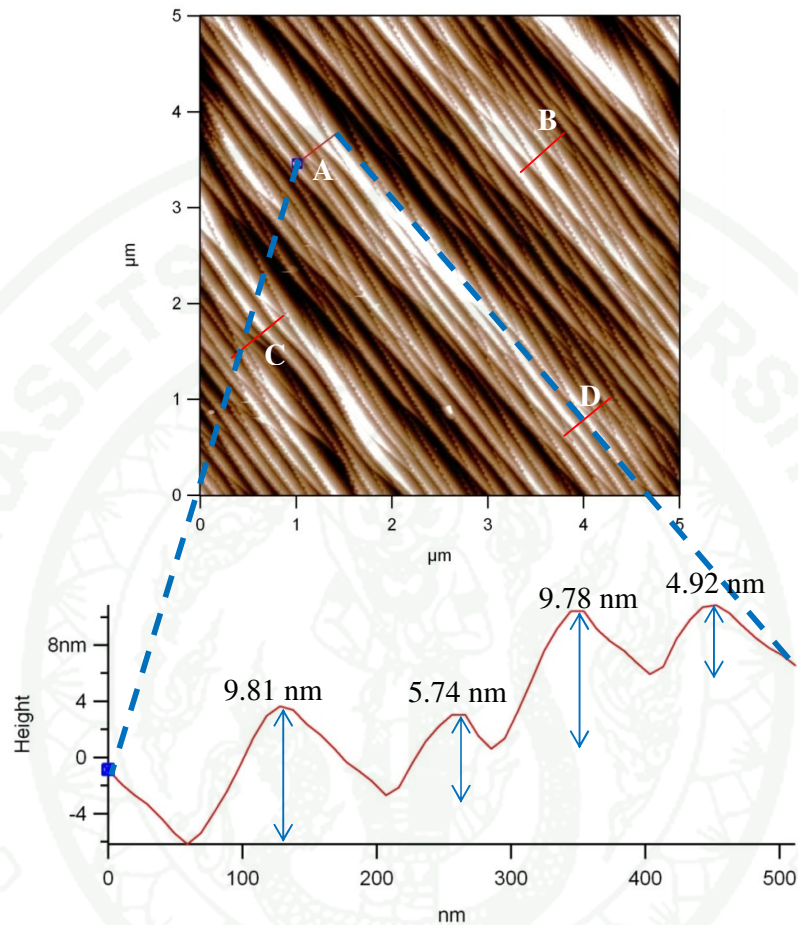


**Figure 122** Measurement of average step height of heated synthetic ruby (set 2) sample (RRb04c) on the miscut of prism  $[\bar{1}\bar{1}20]$  face; note: the zigzag lines

**Table 43** The average step height measurement obtained from the A, B, C and D lines on Figure 122.

Line	Step heights (nm)
A	4.92, 5.74, 9.78, 9.81
B	0.60, 2.06, 3.83, 5.69, 6.19
C	3.84, 4.93, 9.58, 10.60, 12.73
D	1.26, 1.40, 1.94, 4.54, 5.31, 7.99, 9.12
Average	5.80

### 3.19 RRb05a (unheated)

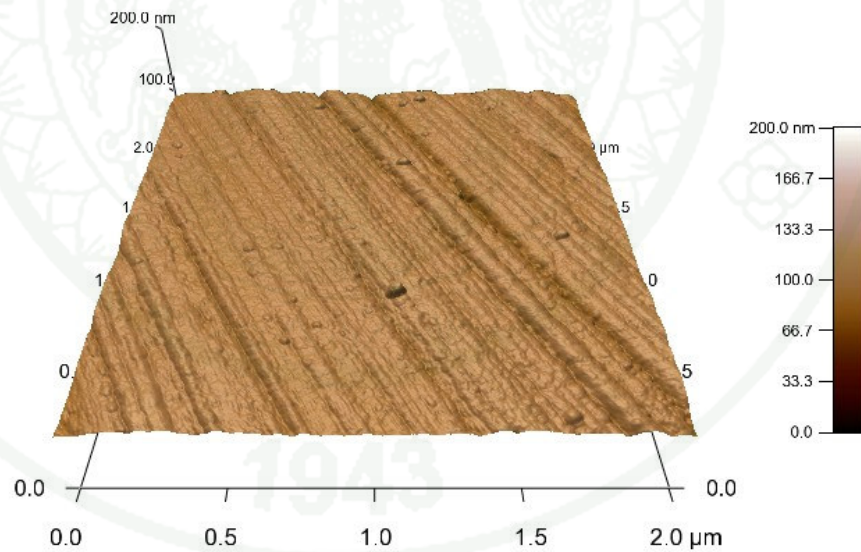


**Figure 123** 3D-Image ( $2.0 \times 2.0 \mu\text{m}^2$ ) of unheated synthetic ruby (set 2) on the miscut of pinacoid [0001] face of the sample RRb05a

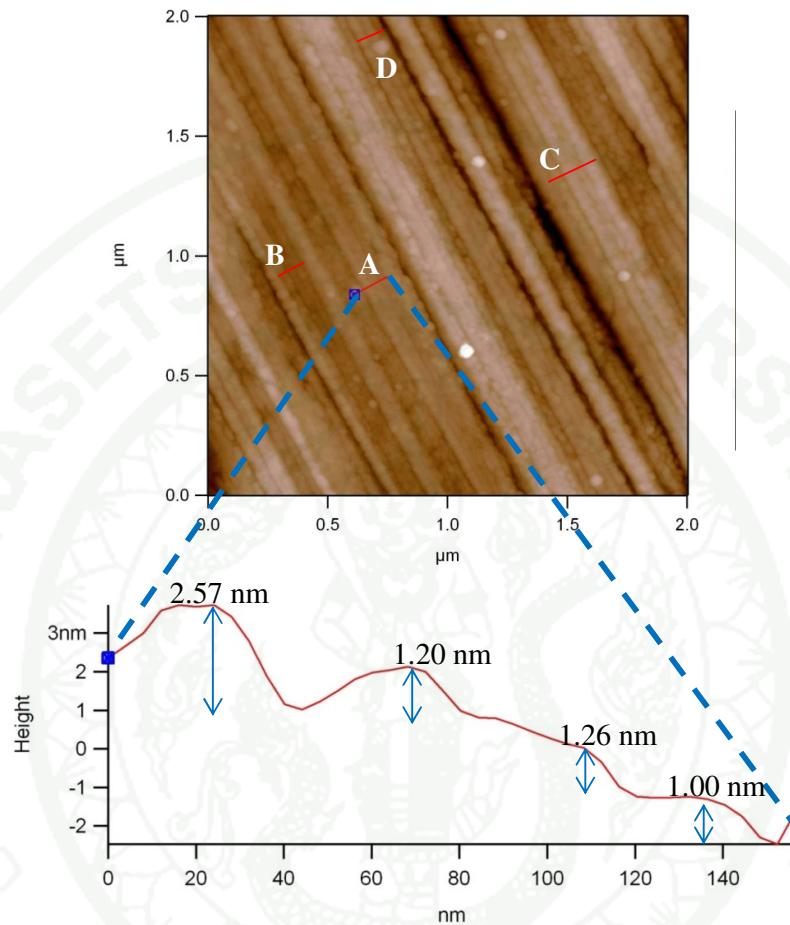


**Figure 124** Measurement of average step height of unheated synthetic ruby (set 2) sample (RRb05a) on the miscut of pinacoid [0001] face

**Table 44** The average step height measurement obtained from the A, B, C and D lines on Figure 124

Line	Step heights (nm)
A	1.00, 1.20, 1.26, 2.57
B	0.16, 0.28, 0.53, 0.91, 2.32
C	2.15, 3.38, 4.42
D	0.60, 1.19, 1.98, 2.92
Average	1.68

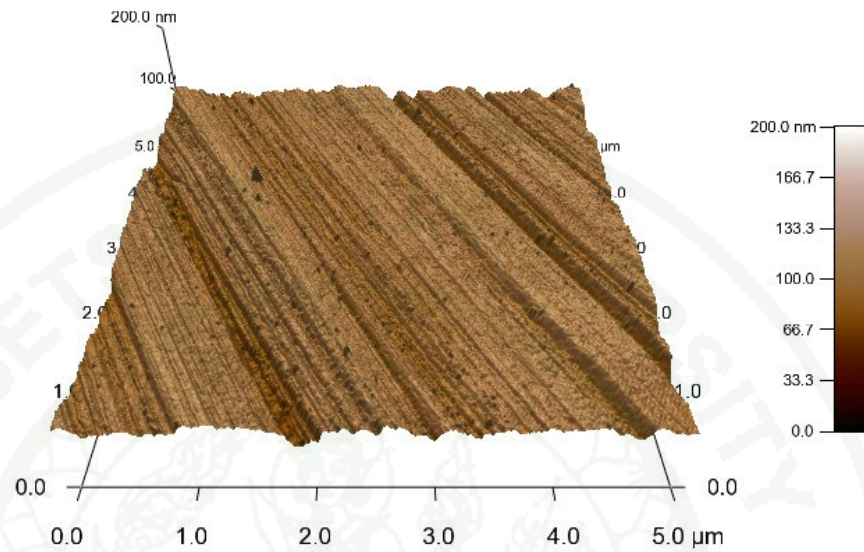


**Figure 125** 3D-Image ( $5.0 \times 5.0 \mu\text{m}^2$ ) of unheated synthetic ruby (set 2) on the miscut of pinacoid [0001] face of the sample RRb05a

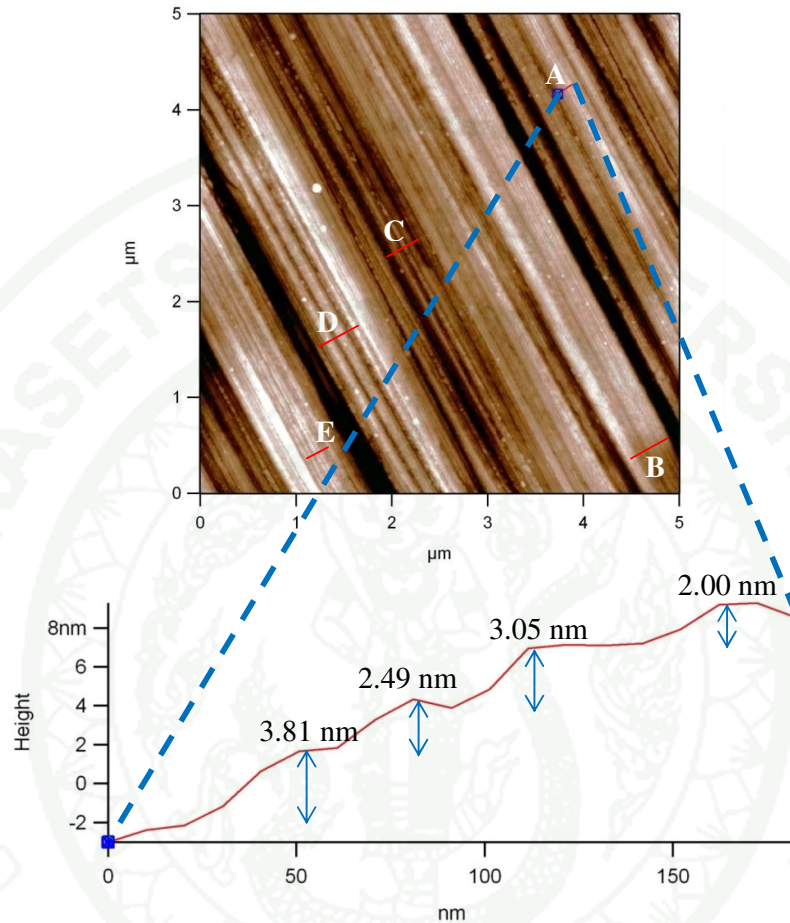


**Figure 126** Measurement of average step height of unheated synthetic ruby (set 2) sample (RRb05a) on the miscut of pinacoid [0001] face

**Table 45** The average step height from the A, B, C, D and E lines on Figure 126

Line	Step heights (nm)
A	2.00, 2.49, 3.05, 3.81
B	1.84, 2.22, 3.86, 4.14, 8.10
C	1.83, 3.25, 9.54, 10.06
D	3.16, 3.23, 4.09, 4.61, 4.81, 4.81, 8.88, 10.35
E	1.75, 2.46, 3.67, 6.21
Average	4.56

## 3.20 RRb05e (heated)

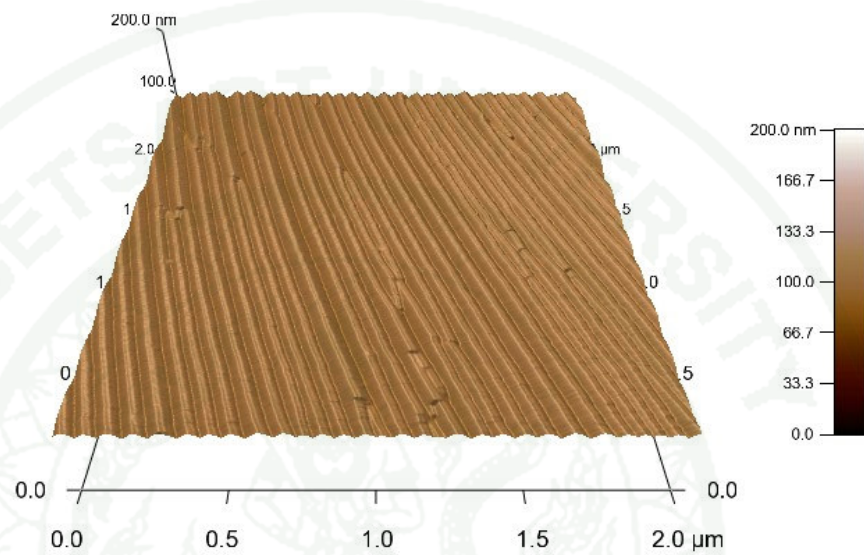


**Figure 127** 3D-Image ( $2.0 \times 2.0 \mu\text{m}^2$ ) of heated synthetic ruby (set 2) on the miscut of pinacoid [0001] face of the sample RRb05e; note: this pinacoid face shows the junction point that also found by Cuccureddu *et al.*, 2010.

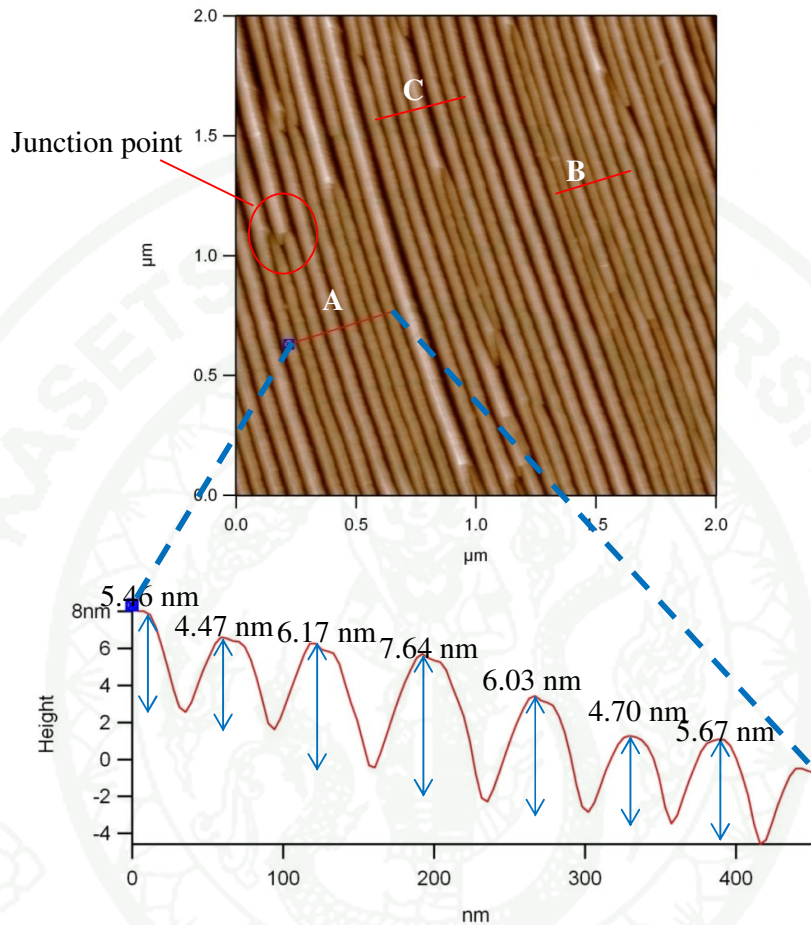


**Figure 128** Measurement of average step height of heated synthetic ruby (set 2) sample (RRb05e) on the miscut of pinacoid [0001] face; note: the junction point

**Table 46** The average step height measurement obtained from the A, B and C lines on Figure 128

Line	Step heights (nm)
A	4.47, 4.70, 5.46, 5.67, 6.03, 6.17, 7.64
B	2.35, 2.70, 3.92, 5.37, 5.58, 6.09
C	5.29, 5.47, 5.78, 6.37, 7.14, 10.44
Average	5.61

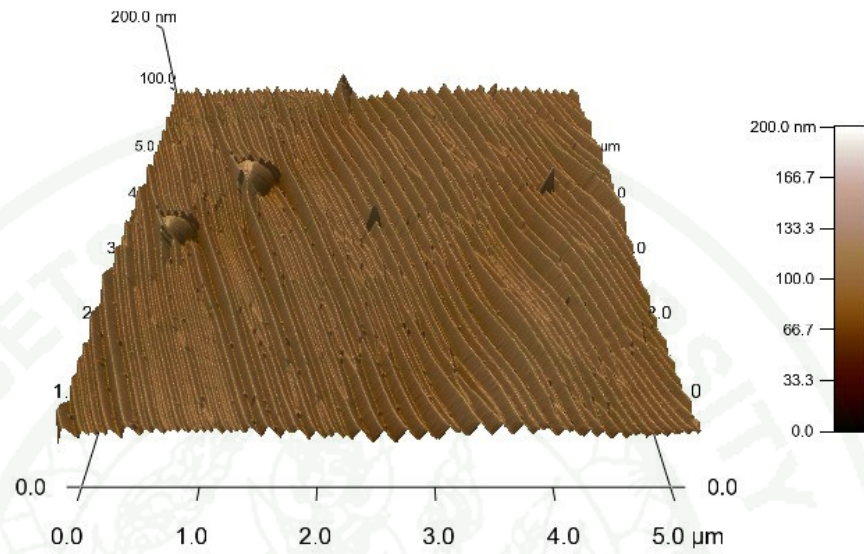


**Figure 129** 3D-Image ( $5.0 \times 5.0 \mu\text{m}^2$ ) of heated synthetic ruby (set 2) on the miscut of pinacoid [0001] face of the sample RRb05e

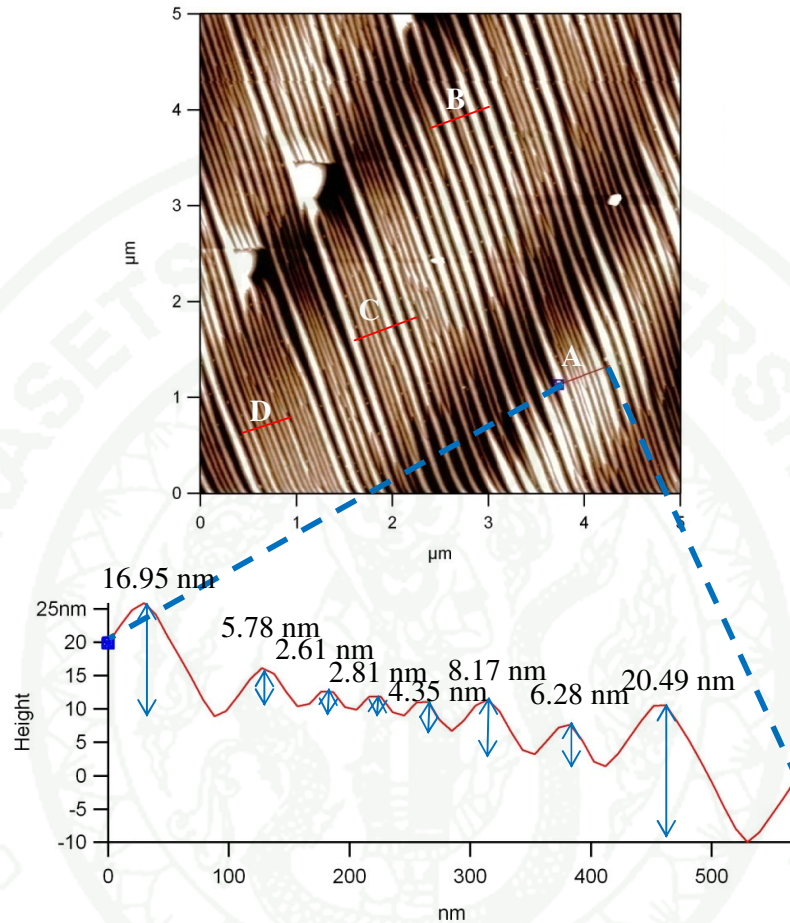


**Figure 130** Measurement of average step height of heated synthetic ruby (set 2) on the miscut of pinacoid [0001] face of the sample RRb05e

**Table 47** The average step height from the A-D lines on Figure 130

Line	Step heights (nm)
A	2.61, 2.81, 4.35, 5.78, 6.28, 8.17, 16.95, 20.49
B	1.80, 14.08, 17.69, 18.35, 21.14
C	6.61, 6.61, 7.39, 10.47, 11.39, 12.41, 19.41
D	3.28, 5.38, 7.24, 7.29, 7.44, 8.43, 10.11
Average	9.78

## Discussion

### 1. Sample materials

From the results of physical and spectroscopic properties, and chemical analyses, the two boules of synthetic corundum that were cut and polished into 5 orientations each showing the same refractive index (RI) values of 1.762 and 1.770. The pink sapphire and ruby sample show the average specific gravity (SG) values of 3.95 and 3.96, respectively as shown in table 3 and table 4. This could reveal the two boules were produced from the same synthetic process and having almost the same homogeneity. When considering absorption spectra (UV-Vis, FTIR) coupled with trace element analyses (LA-ICPMS), the results are in good agreement, i.e., the differences in Cr concentrations giving the different UV-Vis absorptions, and –Ti-OH vibrations are clearly shown in the FTIR.

### 2. Spectroscopic results

#### 2.1 The UV-Vis-NIR spectra of synthetic corundum samples

In this study, the synthetic pink sapphire and ruby reveal the UV-Vis absorptions of  $\text{Cr}^{3+}$  at 405 and 555 nm, and there is the additional tiny photoluminescence (PL) peak of Cr at 695 nm (Aizawa *et al.*, 2009) shown only in the ruby sample spectra. The absorbance in the UV-Vis range involves the electron transition from  $T_{2g}$  to  $E_g$  in octahedral field. At the energy level, the electrons transition to  ${}^4T_2$  and  ${}^4T_1$  energy levels correspond to the photon energies at 2.23 and 3 eV, respectively, as shown in Tanabe-Sugano diagram in Figure 5, and the yellow-red and violet absorptions occur at about 555 and 405 nm, respectively. The synthetic corundum samples absorb at the violet more than the yellow-red region, resulting in the higher intensity at 405 nm than the 555 nm, and the transmittance of red is more than blue component. The synthetic ruby set shows the stronger  $\text{Cr}^{3+}$  absorption than

those of the pink sapphire because the ruby sample contains higher amount of trivalent chromium than those in the pink set.

Before applying the path length correction, the absorption spectrum of each sample seems to be inhomogeneous (Figure 48), when correct the absorptions with the sample path length, the spectra look more identical (Figure 49). This is proven that the samples of the same boule would have the same homogeneity.

Kittiauchawal *et al.* (2000) reported that the hexagonal parameters  $a$  and  $c$  of the corundum after heating have been changed, which corresponds to this study, that the 405 nm absorptions on the  $c$ -face of the annealed pink sapphire and ruby samples show higher intensities for about 3 and 1.5 times, respectively, than those of he before annealing (Figure 46). In contrast, also at 405 nm, the after annealing pink sapphire and ruby absorb at the prism face less than those before annealing about 1.5 and 1.2 times, respectively (Figure 47).

## 2.2 The infrared spectrum of the synthetic ruby samples

In these synthetic ruby samples, the absorption peaks related with  $-OH$  stretching vibration of corundum structure occur at  $3309, 3237 \text{ cm}^{-1}$  (Beran and Rossman, 2006; Eigenmann and Gunthard, 1971, 1972; Wathanakul *et al.*, 2006).

Smith (1995) reported that hydrogen atoms are generally gathering with the corundum structure as charge compensation with different transition metal ions. The absorption peak intensities and positions are affected with  $-OH$  bonding, which bonded with the trace elements such as Ti, Fe, etc.

Volynet *et al.* (1972, 1974) has indicated that hydrogen atoms bound to various trace transitional metal ion, occupying interstitial sites between two oxygen atoms (-OM-) and the absorption peaks of -OH at 3309 and 3237  $\text{cm}^{-1}$  correspond to Ti-OH and V-OH vibrations, respectively which are the same absorption peaks in this study.

Aromdee (1992) reported that the atomic mass of metal ions affects the absorption of the substrate. The higher atomic mass causes the lower frequency of the absorption, consistent with the absorption peaks of -OH at 3181  $\text{cm}^{-1}$  that is the metal-OH which has higher atomic mass than V-OH.

The absorption peak at 2926  $\text{cm}^{-1}$  is possibly affected by contamination of the sample as there might be some organic oil film coated on the surface (Sakkaravej, 2004). The synthetic ruby samples undergone heating at high temperature (1650 °C), show no absorption peaks of such at 3309, 3237 and 3184  $\text{cm}^{-1}$  because the heat breaks the OH bonding with those transition metal ions. The unheated samples show the absorption peaks at 3309 and 3237  $\text{cm}^{-1}$  because Ti and V might be added in the production as present in the trace element results analysed by LA-ICPMS (Table 7). The absorption peaks at 3184  $\text{cm}^{-1}$  may be caused by a metal-OH bonding, which can be a metal ion with higher atomic mass than the vanadium according to Aromdee, 1992.

### **3. Surface study and factors that would affect the surface images**

#### **3.1 Atomic Force Microscope (AFM)**

AFM is the sensitive equipment to moisture and the vibration of surrounding. When there is too much moisture around AFM, the tip may not place at the surface sample, but the water molecules. The images of this case would be the artifact. Besides, the vibration of surrounding can affect AFM operation and the tip. The vibration around AFM affects the movement of the sample while measuring and impact the detector that interprets the wrong surface image. In addition, the vibration

can damage the sharpness of the tiny tip that directly affects to the measurement of the surface.

### 3.2 Sample orientations

The orientation is the important factor that would result the different surface images as shown in this study. The pictures of the miscut on c-plane of the heated synthetic pink sapphire sample (set 1) resemble the c-plane experiment of Cuccureddu *et al.*, 2010 (Figure 131). The pattern of step in nano-scale and the misalignments of atomic steps in the red circles as shown in Figure 131 are also characteristics of c-plane. These mismatched steps look like the junction points, and are the areas that the step/s combines with the other step/s to be another higher number steps after heating. The picture on a prism face of the heated synthetic pink sapphire samples (set 1) resembles the sample image of Curiotto and Chatain, 2009 (Figure 132) that showed the zigzag lines, which are the characteristic of prism face. Though the synthetic ruby samples (set 2) were cut following the synthetic pink sapphire boule, but there would be some degrees of miscut of those of the synthetic pink sapphire. The miscut of c-plane of the synthetic ruby samples (set2) resembles the c-plane experiment of Cuccureddu *et al.*, 2010 (Figure 131). The prism face of the heated synthetic ruby samples (set 2) resembles the sample image of Curiotto and Chatain, 2009 (Figure 132).

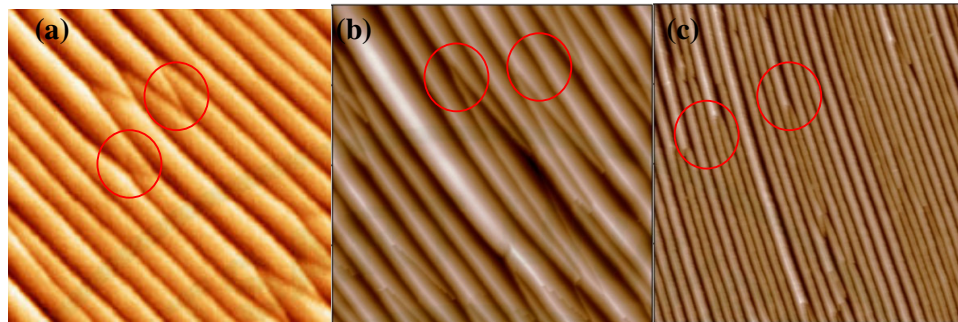


**Figure 131** The c-plane image in nano-scale provided by Cuccureddu *et al.*, 2010 (a), compared to the c-plane images of a synthetic pink sapphire sample (b) and, that of a synthetic ruby sample (c) in this study, showing the weaving structure of the mismatched atomic steps.

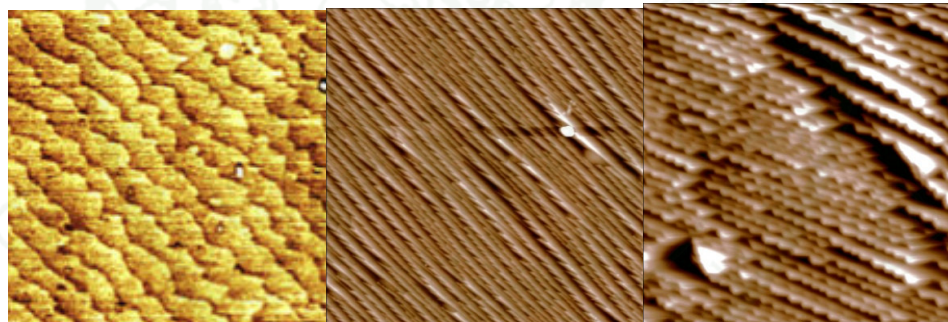


**Figure 132** The prism-face image in nano-scale of Curiotto and Chatain, 2009 (a), showing the ropy structure like the prism-face images of a synthetic pink sapphire sample (b) and, that of a synthetic ruby sample (c).

Theoretically, the different atomic orientation would affect the varieties of step height; the monostep of the basal pinacoid should be about one oxygen layer height that is about 0.21 nm as Pham Van *et al.*, 1998 (Figure 133). The oxygen layer height in different orientations does not equal, for example, the oxygen layer height of  $[1\bar{1}00]$  is approximately 0.13 nm (Figure 134), and the oxygen height of  $[0\bar{1}10]$  is about 0.15 nm (Figure 135). This theoretical atomic model provides this study the approximate figures of the minimum atomic step height or monostep that at the different faces can be the different values.

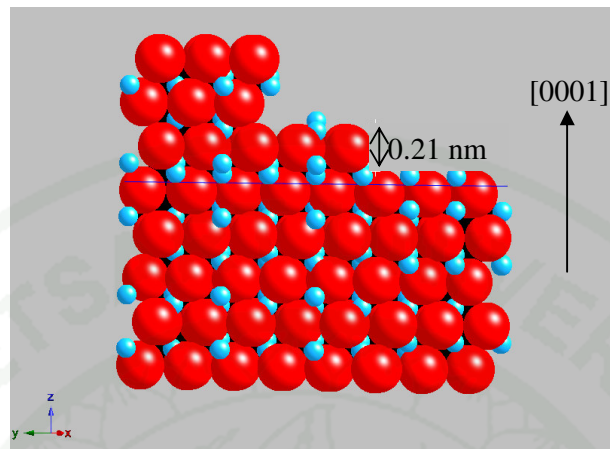


**Figure 133** The oxygen height at a side view of  $[0001]$ , which is about 0.21 nm.  
(model illustrated by Crystal Maker program software)

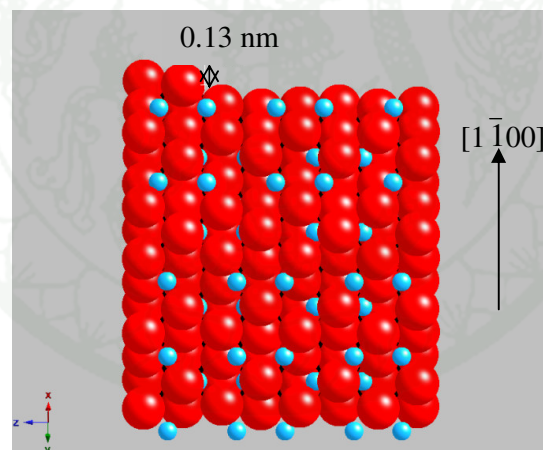


**Figure 134** The oxygen height at a side view of  $[1\bar{1}00]$ , which is about 0.13 nm.  
(model illustrated by Crystal Maker program software)

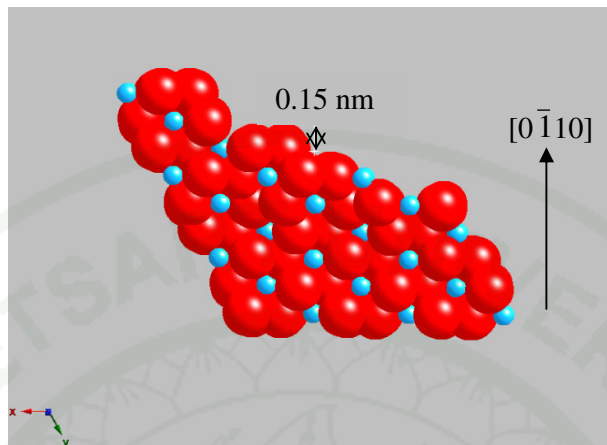


**Figure 135** The oxygen height at a side view of  $[0\bar{1}10]$ , which is about 0.15 nm. (model illustrated by Crystal Maker program software)

### 3.3 Surface polishing quality

The polishing is the procedure to take the smooth surface. The monostep will obviously and often be recorded when operating on the highly well polished gemstone quality such as the alumina substrate samples from the experiments of materials scientists. Normally, the substrates could have been ordered or purchased from a manufacture that produces the sapphire substrate at a mirror shine polishing quality (Simeonov and Lederman, 2009). The sample surface in this study presents many multiplesteps caused by the polishing quality that is lower than that of the substrate produced for the materials science study.

### 3.4 AFM images

The step height measurement depends on the AFM images; if the image has many impurities, the measurement will be difficult and may take the wrong step height values and artifacts. Besides, the artifact which occurs while AFM is operating, affects the quality of the image. The step height measurement cannot perform in the artifact area as shown in Figure 73.

#### 4. Integrated approach using spectroscopic properties and AFM results

The UV-Vis-NIR spectra of the heated sample at the basal pinacoid face and the other prism faces have higher and lower intensities, than the unheated one, respectively, that corresponding to Kittiauchawal *et al.* (2005) who reported the changes of the hexagonal lattice parameters ( $a$ ,  $c$  and  $c/a$ ) after heating the ruby samples (see also the corundum structure and axes in Figure 136). The results implied that after annealing the ruby structure change to the better stability. This reason supports the AFM results that after annealing; the pattern of the surfaces is more ordered, the step edges are clearer and sharper (Pham Van *et al.*, 1998; Cuccureddu *et al.*, 2010; Lhuaamporn *et al.*, 2010) than those of the unannealed samples, and the average step heights tend to be increased (Table 48), which is in consistent with Simeonov and Lederman, 2009. In this study, the average step heights on the basal pinacoid and prism faces of annealed samples are about 13 and 8 nm, respectively. The step height values on the miscut pinacoid [0001] are more obvious than those of on the other prism faces (Table 48). These results indicate that the surface is more ordered, and there are combinations of two steps to be the higher multiplesteps during the thermal treatment or annealing.

The results of AFM and UV-Vis-NIR spectra can distinguish the heated from the unheated synthetic samples. This can also be supported by IR spectra that the unheated samples show  $\text{-metal-OH}$  stretchings, where they can normally be eliminated after heating in oxidizing environment, i.e. in the electric furnace. These metal ions can be accordingly traced by the LA-ICPMS analyses.

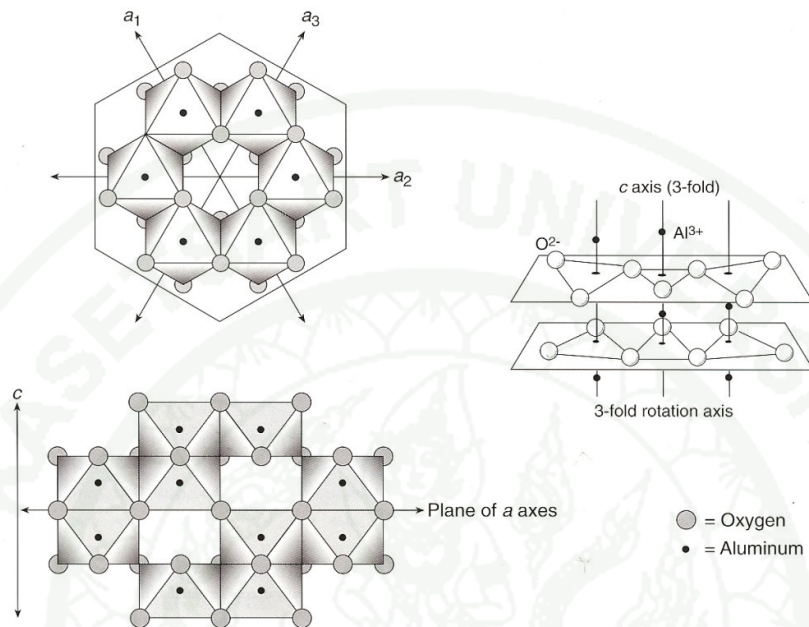


**Figure 136** Three different views of the structure of corundum; the top shows the structure looking down the  $c$  axis, below is a view perpendicular to the  $c$  axis and right is a perspective view.

**Source:** Hughes (1997)

**Table 48** The average step height of the samples at five orientations

Orientation	Pink sapphire (set 1)		Ruby (set 2)	
	Sample	Height (nm)	Sample	Height (nm)
$[1\bar{1}00]$	RR01a (unheated)	4.25	RRb01a (unheated)	2.82
	RR01d (heated)	5.56	RRb01d (heated)	3.39
$[0\bar{1}10]$	RR01b (unheated)	4.52	RRb01b (unheated)	3.53
	RR01c (heated)	12.19	RRb01c (heated)	11.52
$[1\bar{2}10]$	RR02a (unheated)	2.95	RRb02a (unheated)	4.56
	RR02c (heated)	5.67	RRb02c (heated)	12.2

**Table 48** (Continued)

Orientation	Pink sapphire (set 1)		Ruby (set 2)	
	Sample	Height (nm)	Sample	Height (nm)
$[\bar{1}\bar{1}20]$	RR04a (unheated)	4.65	RRb04a (unheated)	4.26
	RR04c (heated)	5.14	RRb04c (heated)	5.14
[0001]	RR05a (unheated)	5.37	RRb05a (unheated)	3.98
	RR05e (heated)	18.10	RRb05e (heated)	8.10

## CONCLUSION AND RECOMMENDATION

### Conclusion

From the experimental results and discussion of this study, the conclusion can be made as the followings:

The UV-Vis-NIR absorption peaks of the trivalent chromium of the synthetic pink sapphire and ruby samples are at 405, 555 nm, and the absorption peak at 695 nm is shown only in the synthetic ruby samples. The absorption peak at 405 nm on the basal pinacoid; the after annealing pink sapphire and ruby samples present higher intensity for about 3 and 1.5 times, respectively, but on the after annealing on the other prism show lower intensity for about 1.5 and 1.2 times, respectively, than the before annealing (Table 5). The calculation of the absorbance to the same path length; the samples tend to have the homogeneity.

The FTIR absorption spectra of the synthetic pink sapphire and ruby samples show the pattern of CO<sub>2</sub> at 2345 cm<sup>-1</sup>, and the C-H stretching at 2926 cm<sup>-1</sup>, which may indicate contamination from the organic oil film coated on the surface. The absorption spectra of metal-OH stretchings such as Ti-OH and V-OH, show in the unannealed samples, only. The unannealed samples show the absorption peak of Ti-OH and V-OH stretching at 3309 and 3237, respectively (Volynet *et al.*, 1972, 1974). These results are in consistent to the analyses detected by LA-ICPMS (Table 6). It's possible that beside Al<sub>2</sub>O<sub>3</sub> and the colouring element like Cr, there might be addition of some other metal elements added to the synthetic process.

Atomic Force Microscope (AFM) is the advanced technique for the surface measurement; its uses could be applied for thin film materials. The surface image visibility at high polishing quality depends on the sharpness of the tip while measuring the sample. The AFM technique can distinguish the annealed synthetic corundum from the unannealed one by applying the differences of the step pattern and the step edge of the samples. The steps of each annealed sample surface is better

ordered leading to the step pattern to be obviously changed; also the step edge of annealed sample is sharper than that of the unannealed one, because there are the ordered steps after annealing. The average step height of the heated samples at the c-face is about 13 nm, which is more than that on the prism faces, that is about 8 nm. The multiple steps occur in the unannealed samples, and, hence, vice versa for the monostep.



### **Recommendation**

Based on this research results, the recommendations and applications can be suggested as the followings:

1. The surfaces study in micro-nano scale should be studied and experimented in natural gemstones, in order to be proven, whether or not the features can be used to indicate the heating evidence.
2. The tests of surface quality should be carried out, e.g., on same samples but different cutters, superb vs good polishing qualities, different cutting processes, etc.
3. The polishing samples should be studied by AFM technique in order to examine the influence of surface repolishing after annealing.
4. More AFM applications should be studied, e.g. measuring samples in different environments ( $N_2$  perching, scanning in water, etc) in order to obtain the effective capability of the instrument.
5. More applications for the gem treatments can be studied, i.e., Be-diffusion, irradiation, coating, etc.

## LITERATURE CITED

- Aizawa, H., K. Ito, S. Takahashi, S. Komuro, Y. Miyazaki and T. Katsumata. 2009. Fabrication of Ruby thin film for temperature indicator application, pp. 3293-3296. *In International Joint Conference 2009*. 18-21 August 2009, Fukuoka International Congress Center. Japan.
- Aromdee, C. 1992. **Infrared Spectroscopy**. Faculty of Pharmaceutical. Khon Kaen University, Khon Kaen., Thailand.
- Bard, J.P. 1986. **Microtextures of Igneous and Metamorphic Rocks**. D. Reidel Publishing, Holland.
- Beran, A. and G.R. Rossman. 2006. OH in naturally occurring corundum. **European Journal of Mineralogy**. 18(4): 441-447.
- Birdi, K.S. 2003. **Scanning Probe Microscopes: Applications in Science and Technology**. CRC Press, Florida.
- Bowen, W.R. and N. Hilal. 2009. **Atomic Force Microscopy in Process Engineering**. Butterworth-Heinemann, USA.
- Cuccureddu, F., S. Murphy, I.V. Shvets, M. Porcu, H.W. Zandbergen, N.S. Sidorov and S.I. Bozhko. 2010. Surface orphology of c-plane sapphire produced by high temperature anneal. **Journal of Surface Science**. 604: 1294-1299.
- Curiotto, S. and D. Chatain. 2009. Surface morphology and composition of c-, a- and m-sapphire surfaces. **Journal of Surface Science**. 603: 2688-2697.
- Eigenmann, K. and Hs. H. Gunthard. 1971. Hydrogen Incorporation in Doped  $\alpha$ -Al<sub>2</sub>O<sub>3</sub> by High Temperature Redox Reactions. **Chemical Physics Letters**. 12(1): 12-15.

- Eigenmann, K. and Hs. H. Gunthard. 1972. Valence State Reactions and Biparticle Formation of Fe and Ti doped Sapphire. **Chemical Physics Letters**. 13(1): 58-61.
- Hammond, C. 1998. **The Basics of Crystallography and Diffraction**. Oxford University Press Inc, New York.
- Heffelfinger, J.R. and C.B. Carter. 1997. Mechanisms of surface faceting and coarsening. **Journal of Surface Science**. 389: 188-200.
- Heffelfinger, J.R., M.W. Bench and C.B. Carter. 1997. Steps and the structure of the (0001) alumina surface. **Journal of Surface Science**. 370: L168-L172.
- Hughes, D. 2012. **Verneuil Process**. Available Source: <http://www.wikipedia.org>, January 12, 2012.
- Hughes R.W. 1997. **Ruby and Sapphire**. RWH Publishing, USA.
- Kittiauchawal, T., S. Limsuwan and P. Winotai. 2005. Effects of Heat Treatment on Physical Properties of Natural Ruby, pp. 460-466. *In Proceedings of the 43<sup>th</sup> of Kasetsart University*. 1-4 February 2005, Kasetsart University. Bangkok, Thailand.
- Kunz, G.F. 1913. **The curious Lore of Precious Stones**. J.B. Lippinco Publishing, Dover.
- Kurnosikov, O. L. Pham Van and J. Cousty. 2000. About anisotropy of atomic-scale height step on (0001) sapphire surface. **Journal of Surface Science**. 459: 256-264.

- Lhuaamporn, T., S. Pongkrapan and P. Wathanakul. 2010. Micro-nano Scaled Surface Features of Synthetic Ruby at Different Orientations before and after Annealing, pp. 179-181. *In Proceedings of Provenance and Properties of Gems and Geo-Materials*. 17-24 October 2010, Hanoi University. Hanoi, Vietnam.
- Lourdudoss, S. 2008. **Advanced Semiconductor Materials**. Available Source: <http://www.imit.kth.se>, November 30, 2010.
- Markiewicz, P. 2011. **The Atomic Force Microscope**. Available Source: <http://www.weizmann.ac.il>, December 20, 2011.
- Nassau, K. 1886. **Gems Made by Man**. Gemological Institute of America, USA.
- Nassau, K. 1994. **Gemstone Enhancement Science and State of the Art**. Redwood Books, Wiltshire.
- Nassau, K. 2001. **The Physics and Chemistry of Color: the Fifteen Causes of Colour**. John Wiley and Son, New York.
- Pham Van, L., O. Kurnosikov and J. Cousty. 1998. Evolution of steps on vicinal (0001) surfaces of alumina. **Journal of Surface Science**. 411: 263-271.
- Sakkaravej, S. 2004. **Thermal Enhancement of Some Blue Sapphires from Madagascar**. M.S. Thesis, Chulalongkorn University.
- Simeonov, K., D. Lederman. 2009. Surface structure of  $(11\bar{2}0)$   $\text{Al}_2\text{O}_3$  single crystals after high temperature annealing. **Journal of Surface Science**. 603: 232-236.
- Smith, C.P. 1995. A Contribution to Understanding the Infrared Spectra of Rubies from Mong Hsu, Myanmar. **Journal of Gemmology**. 24(5): 321-335.

Smith, L. 2002. **A tutorial on Principal Components Analysis**. Cornell University, USA.

Volynets, F.K., V.G. Vorobev and E.A. Sidorova. 1972. Infrared Absorption Bands in Corundum Crystals. **Journal of Applied Spectroscopy**. 10: 665-667.

Volynets, F.K., E.A. Sidrova and N.A. Stsepuro. 1974. OH-groups in corundum crystals which were grown with the Verneuil technique. **Journal of Applied Spectroscopy**. 17: 1088-1091.

Wathanakul P., B. Sriprasert, P. Lomthong, T. Leelawathanasuk, S. Singbamroong, T. Pavaro, C. Somboon and S. Sakkaravej. 2006. **Gemstone Databases for Origin Determination Report**. The Gem and Jewelry Institute of Thailand.

Webexhibits Organization. 2012. **Why are Ruby Red**. Available Source: <http://www.webexhibits.org/causesofcolor/6AA>, January 10, 2012.

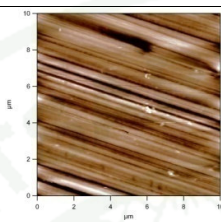
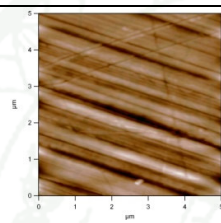
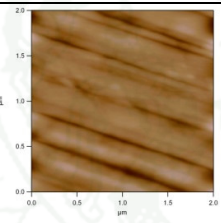
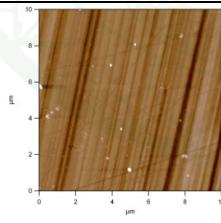
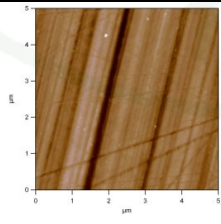
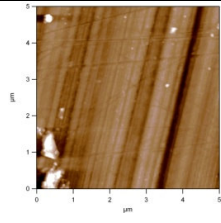
Yoshimoto M., T. Maeda, T. Ohnishi, H. Koinuma and O. Ishiyama 1995. Atomic-scale formation of ultrasmooth surfaces on sapphire substrates for high-quality thin-film fabrication. **Journal of Applied Physics Letters**. 67: 2615-2617.

1943

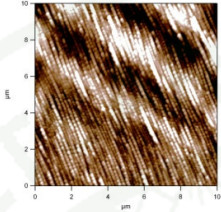
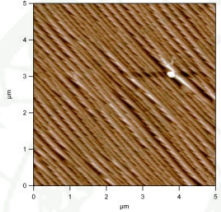
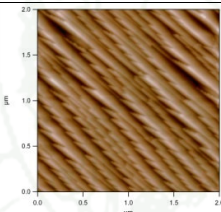
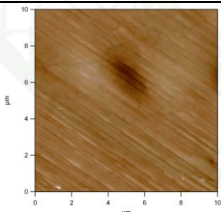
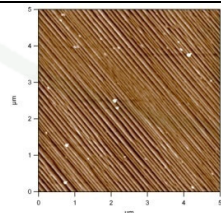
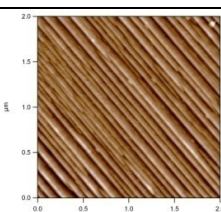


**APPENDIX**

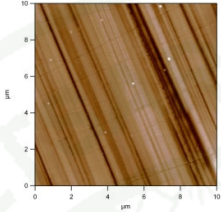
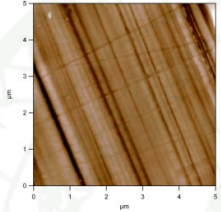
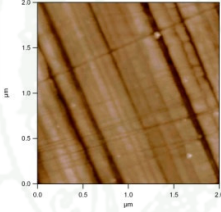
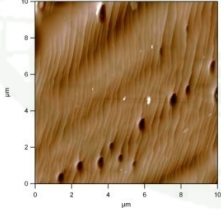
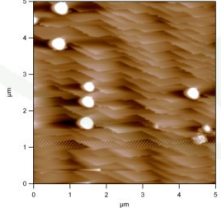
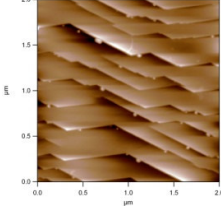
**Appendix Table 1** The average step height measurement of the samples

Sample	Image	Step height (nm)
RR01a (10×10 μm <sup>2</sup> ) [1 $\bar{1}$ 00] unheated		1.99, 4.16, 3.98, 5.67, 8.87, 1.01, 3.18, 3.33, 2.24, 5.78, 2.92, 3.15, 4.22, 6.34
RR01a (5×5 μm <sup>2</sup> ) [1 $\bar{1}$ 00] unheated		4.76, 2.09, 1.03, 2.12, 1.58, 2.53, 5.08, 2.88, 3.38, 0.89, 3.84, 5.54, 6.48, 5.58, 4.79, 7.35, 3.00, 6.61, 2.26, 4.57, 4.08, 4.24, 2.40, 0.76, 9.52, 1.87, 2.85, 6.18, 7.22
RR01a (2×2 μm <sup>2</sup> ) [1 $\bar{1}$ 00] unheated		5.08, 9.73, 2.88, 3.38, 0.89, 3.84, 5.54, 6.48, 5.58, 4.79
RR01b (10×10 μm <sup>2</sup> ) [0 $\bar{1}$ 10] unheated		4.12, 5.07, 6.71, 3.05, 5.42, 3.35, 4.75, 7.24, 6.27, 3.24, 8.33, 2.77, 6.09, 4.06, 1.67, 1.28, 6.35,
RR01b (5×5 μm <sup>2</sup> ) [0 $\bar{1}$ 10] unheated		2.89, 1.73, 9.09, 7.16, 3.44, 5.37, 4.40, 2.10, 4.14, 3.31, 6.30, 6.20, 5.17, 4.54, 1.76, 1.22
RR01b (5×5 μm <sup>2</sup> ) [0 $\bar{1}$ 10] unheated		2.33, 1.62, 1.52, 7.97, 9.13, 2.35, 3.95, 2.34, 5.70, 6.28, 4.33, 1.99, 1.92, 6.34, 5.37, 3.18, 3.60, 2.02, 3.31, 6.52, 2.82, 3.64, 6.19

Appendix Table 1 (Continued)

Sample	Image	Step height (nm)
RR01c (10×10 μm <sup>2</sup> ) [0 $\bar{1}$ 10] heated		6.42, 8.54, 8.57, 11.35, 8.15, 7.22, 4.30, 4.98, 3.77, 3.93, 3.97, 3.92, 3.30
RR01c (5×5 μm <sup>2</sup> ) [0 $\bar{1}$ 10] heated		8.45, 21.38, 12.37, 14.95, 14.37, 15.73, 26.84, 18.35, 24.19, 16.28, 8.12, 11.05, 22.97, 6.76, 14.09, 12.75, 12.02, 10.05, 8.22, 10.92, 15.722, 23.88, 26.83, 17.31, 15.66, 4.76, 27.43, 20.04
RR01c (2×2 μm <sup>2</sup> ) [0 $\bar{1}$ 10] heated		11.34, 10.83, 5.60, 22.82, 14.68, 26.30, 22.27, 34.80, 25.30, 8.67, 10.83, 6.61, 21.84, 30.15, 27.43
RR01d (10×10 μm <sup>2</sup> ) [1 $\bar{1}$ 00] heated		2.08, 3.17, 2.48, 2.32, 3.07, 2.32, 2.25, 1.86, 1.91, 2.44, 2.34, 2.55, 3.76, 3.81, 2.26, 8.50, 5.53, 6.12, 8.49, 6.79, 3.96, 4.13, 7.10, 9.25, 9.3, 6.95, 5.24, 6.65, 7.80
RR01d (5×5 μm <sup>2</sup> ) [1 $\bar{1}$ 00] heated		2.89, 1.73, 9.09, 7.16, 3.44, 5.37, 4.40, 2.10, 4.14, 3.31, 6.30, 6.20, 5.17, 4.54, 1.76, 1.22, 9.26, 8.62, 7.04, 8.34, 6.90, 6.06, 8.12, 9.41, 8.84, 6.79, 8.21, 8.49, 7.82, 7.67, 7.87, 6.07, 8.85, 8.04, 5.54, 6.12
RR01d (2×2 μm <sup>2</sup> ) [1 $\bar{1}$ 00] heated		6.39, 8.36, 3.71, 7.06, 6.89, 6.18, 1.01, 8.62, 1.27, 6.94, 5.86, 5.44, 11.30

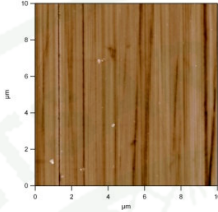
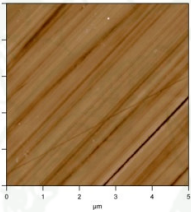
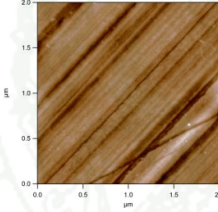
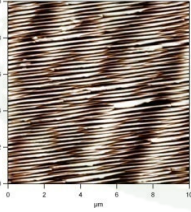
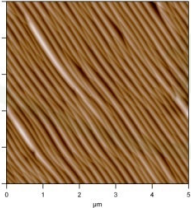
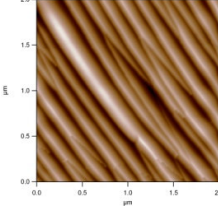
**Appendix Table 1** (Continued)

Sample	Image	Step height (nm)
RR02a (10×10 μm <sup>2</sup> ) [1 $\bar{2}$ 10] unheated		2.40, 7.56, 1.06, 1.43, 3.25, 1.43, 1.28, 4.11, 1.87, 2.81, 4.94, 1.33, 2.21, 2.93, 2.11, 1.37, 2.06, 3.31, 2.09, 7.01
RR02a (5×5 μm <sup>2</sup> ) [1 $\bar{2}$ 10] unheated		3.55, 3.52, 3.28, 4.71, 2.58, 2.57, 2.11, 1.33, 2.97, 5.72, 1.44
RR02a (2×2 μm <sup>2</sup> ) [1 $\bar{2}$ 10] unheated		1.16, 0.68, 0.83, 2.01, 0.84, 1.81, 1.30, 2.88, 1.76, 0.75, 3.99, 2.59, 2.84, 0.84, 1.29
RR02c (10×10 μm <sup>2</sup> ) [1 $\bar{2}$ 10] heated		5.47, 6.90, 4.95, 5.01, 8.59, 4.70, 5.10, 4.17, 8.78, 4.82, 8.04, 6.61, 6.39, 6.84, 5.28, 8.44, 4.09, 11.07, 8.22, 9.22, 6.23, 10.74
RR02c (5×5 μm <sup>2</sup> ) [1 $\bar{2}$ 10] heated		5.76, 1.54, 3.25, 4.11, 3.12, 4.12, 3.99, 4.34, 5.47, 2.56, 2.64, 3.53, 4.53, 2.15, 3.02, 4.03, 4.14, 8.65, 8.92, 6.81, 5.29, 3.17, 5.08, 5.64, 1.17, 8.87, 4.64, 4.65, 5.44
RR02c (2×2 μm <sup>2</sup> ) [1 $\bar{2}$ 10] heated		6.37, 3.15, 11.81, 4.22, 3.84, 3.58, 8.18, 5.04, 3.48, 6.50, 4.89, 3.51, 6.51, 1.96, 3.97, 3.94

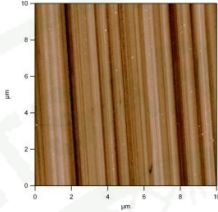
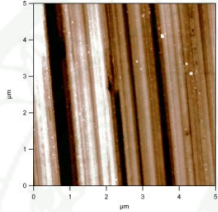
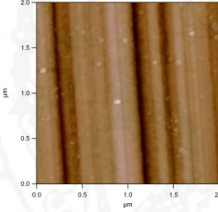
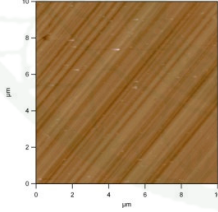
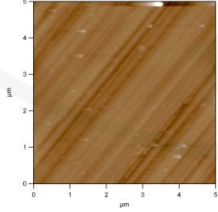
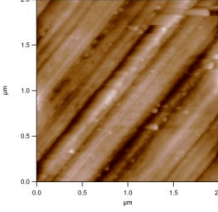
**Appendix Table 1** (Continued)

Sample	Image	Step height (nm)
RR04a (10×10 μm <sup>2</sup> ) [1̄ 1̄ 20] unheated		7.15, 8.38, 3.57, 8.26, 3.53, 3.20, 10.32, 10.37, 9.20, 2.33, 2.39, 3.29, 3.78, 3.43, 2.40, 8.66, 8.25, 2.29
RR04a (5×5 μm <sup>2</sup> ) [1̄ 1̄ 20] unheated		1.79, 1.05, 4.02, 3.9, 1.10, 0.85, 1.96, 2.28, 2.03, 1.17, 1.16, 2.31, 5.15, 2.81, 0.87, 1.52, 2.08, 0.99, 1.40, 4.05
RR04a (2×2 μm <sup>2</sup> ) [1̄ 1̄ 20] unheated		1.65, 6.28, 3.67, 2.44, 2.91, 4.77, 3.94, 8.83, 4.57, 3.25, 2.33
RR04c (10×10 μm <sup>2</sup> ) [1̄ 1̄ 20] heated		2.84, 3.02, 1.06, 6.02, 0.77, 0.66, 6.41, 12.34, 13.65, 10.06, 1.06, 0.72, 12.61, 0.90, 0.84
RR04c (5×5 μm <sup>2</sup> ) [1̄ 1̄ 20] heated		9.77, 10.59, 2.22, 18.83, 1.53, 2.70
RR04c (2×2 μm <sup>2</sup> ) [1̄ 1̄ 20] heated		12.27, 2.87, 1.25, 1.45, 1.47, 1.20, 1.17

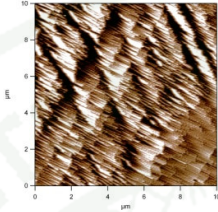
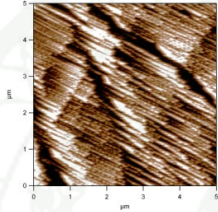
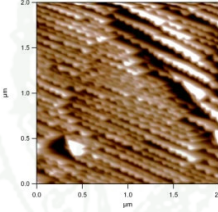
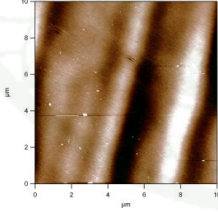
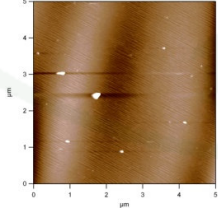
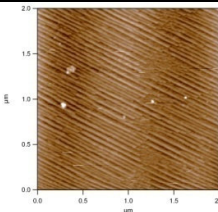
**Appendix Table 1** (Continued)

Sample	Image	Step height (nm)
RR05a (10×10 μm <sup>2</sup> ) [0001] unheated		9.83, 4.20, 2.33, 1.51, 4.28, 6.45, 2.66, 1.41, 5.96, 1.67, 8.31, 3.15, 1.16, 8.34, 2.84, 3.40, 4.32, 4.01, 5.20
RR05a (5×5 μm <sup>2</sup> ) [0001] unheated		8.40, 8.05, 6.22, 6.91, 7.98, 3.35, 2.52, 7.78, 8.16, 3.18, 2.22, 1.47, 1.49, 1.03, 0.81, 2.22, 1.12, 1.17, 1.68, 3.59, 13.92, 10.91
RR05a (2×2 μm <sup>2</sup> ) [0001] unheated		0.92, 0.20, 1.10, 0.85, 0.57, 1.23, 0.91, 0.98, 0.84, 0.99, 0.84
RR05e (10×10 μm <sup>2</sup> ) [0001] heated		3.49, 16.46, 17.49, 21.12, 15.44, 20.03, 13.50, 15.01, 10.43, 13.33, 19.80, 18.22
RR05e (5×5 μm <sup>2</sup> ) [0001] heated		22.09, 26.84, 29.18, 26.44, 12.43, 6.27, 22.55, 12.65, 33.95, 24.70, 30.75, 16.04, 32.30, 33.04, 26.69, 13.92, 10.91, 18.46, 177.05, 18.98, 19.41, 20.85
RR05e (2×2 μm <sup>2</sup> ) [0001] heated		19.13, 23.30, 20.18, 10.99, 10.80, 20.84, 12.56, 9.49, 23.52, 20.19, 24.85, 25.38, 22.49, 18.22, 19.42

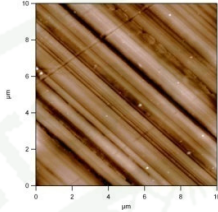
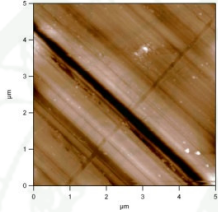
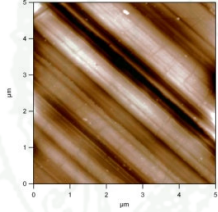
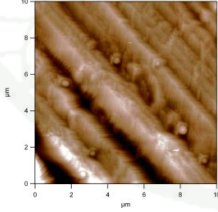
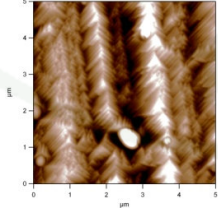
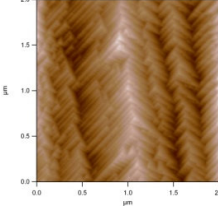
Appendix Table 1 (Continued)

Sample	Image	Step height (nm)
RRb01a (10×10 μm <sup>2</sup> ) [1 $\bar{1}$ 00] unheated		2.66, 2.10, 7.97, 2.13, 2.42, 7.47, 1.75, 6.12, 2.64, 4.21, 5.52
RRb01a (5×5 μm <sup>2</sup> ) [1 $\bar{1}$ 00] unheated		1.64, 3.82, 2.81, 4.42, 3.25, 4.32, 2.89, 1.17, 3.37, 3.81
RR0b01a (2×2 μm <sup>2</sup> ) [1 $\bar{1}$ 00] unheated		1.27, 1.75, 1.17, 1.54, 1.17, 4.38, 1.18, 2.92, 2.35, 2.19, 2.68, 3.57, 1.7, 3.75, 4.43
RRb01b (10×10 μm <sup>2</sup> ) [0 $\bar{1}$ 10] unheated		4.12, 2.49, 0.66, 3.34, 3.89, 0.75, 1.95, 5.32, 2.30, 1.02, 1.12, 4.57, 2.77
RRb01b (5×5 μm <sup>2</sup> ) [0 $\bar{1}$ 10] unheated		1.33, 3.47, 1.67, 5.20, 4.44, 5.94, 5.21, 1.81, 1.36, 1.51, 1.54, 4.22
RRb01b (2×2 μm <sup>2</sup> ) [0 $\bar{1}$ 10] unheated		2.69, 1.17, 1.63, 1.11, 1.46, 5.37, 1.57, 2.62, 0.42, 0.61, 5.28

**Appendix Table 1** (Continued)

Sample	Image	Step height (nm)
RRb01c (10×10 μm <sup>2</sup> ) [0 $\bar{1}$ 10] heated		19.52, 8.32, 2.19, 26.30, 2.55, 28.40, 4.7110.13, 12.64, 8.06, 13.49, 8.89, 6.92, 7.14, 3.89, 15.09, 11.91, 11.87, 19.64
RRb01c (5×5 μm <sup>2</sup> ) [0 $\bar{1}$ 10] heated		19.54, 8.78, 9.13, 8.56, 8.86, 15.13, 6.12, 6.13, 19.55, 9.93, 6.57, 11.01, 8.30, 5.56, 8.36, 25.86, 7.12, 7.26, 6.87, 7.96, 7.75, 10.02
RRb01c (2×2 μm <sup>2</sup> ) [0 $\bar{1}$ 10] heated		7.77, 5.76, 19.28, 20.78, 4.31, 12.24, 11.34, 2.53, 11.42, 12.58, 5.35, 7.03, 3.66
RRb01d (10×10 μm <sup>2</sup> ) [1 $\bar{1}$ 00] heated		1.42, 1.34, 1.75, 0.73, 1.86, 1.65, 1.99, 1.15, 1.67, 0.95, 1.63, 1.55, 1.33,
RRb01d (5×5 μm <sup>2</sup> ) [1 $\bar{1}$ 00] heated		2.09, 2.66, 1.74, 2.51, 3.53, 2.63, 2.53, 1.17, 2.16, 3.18, 3.29, 2.31, 3.22, 2.74, 3.79, 4.34, 3.13, 2.64, 3.42, 4.28, 3.64, 2.95, 2.48, 2.16, 2.17, 1.91, 3.45, 3.64, 2.23, 2.72
RRb01d (2×2 μm <sup>2</sup> ) [1 $\bar{1}$ 00] heated		4.03, 4.64, 4.30, 2.79, 1.65, 2.08, 3.26, 2.85, 2.18, 3.32

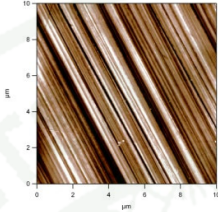
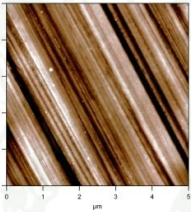
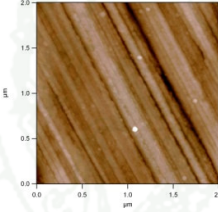
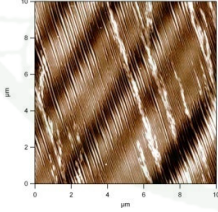
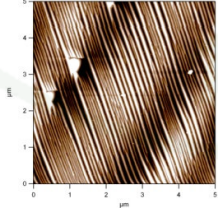
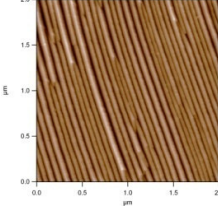
**Appendix Table 1** (Continued)

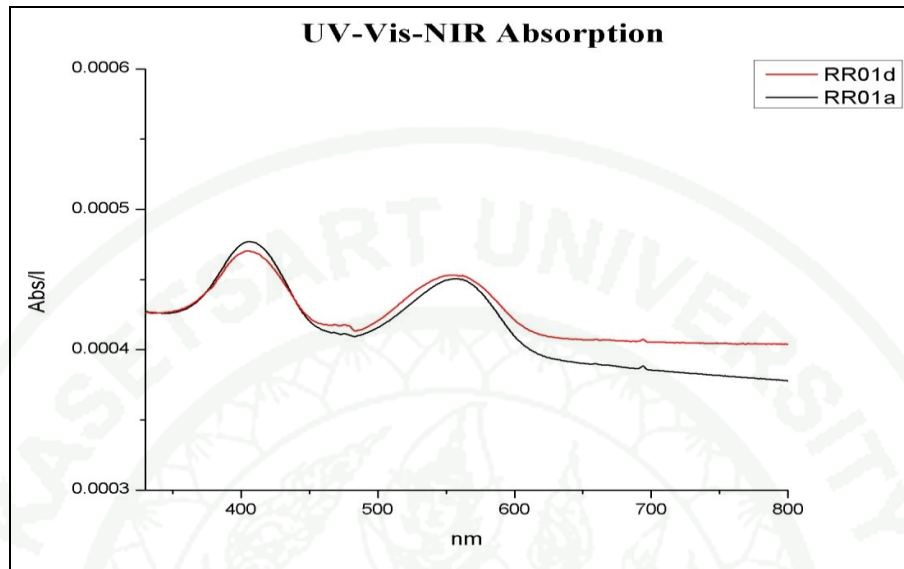
Sample	Image	Step height (nm)
RRb02a (10×10 μm <sup>2</sup> ) [0 $\bar{1}$ 10] unheated		1.28, 1.52, 4.42, 6.22, 4.86, 3.59, 3.15, 1.30, 1.75, 3.67, 0.74, 1.75, 4.70, 9.06
RRb02a (5×5 μm <sup>2</sup> ) [0 $\bar{1}$ 10] unheated		2.89, 5.5, 2.46, 7.31, 1.01, 1.42, 0.79, 5.81, 3.29, 7.67, 3.15, 1.48, 2.82, 2.58, 3.25
RRb02a (5×5 μm <sup>2</sup> ) [0 $\bar{1}$ 10] unheated		9.77, 3.15, 7.34, 1.30, 3.67, 1.75, 7.40, 4.70, 3.13, 1.05, 2.50
RRb02c (10×10 μm <sup>2</sup> ) [1 $\bar{1}$ 00] heated		1.42, 1.34, 1.75, 0.73, 1.86, 1.65, 1.99, 1.15, 1.67, 0.95, 1.63, 1.55, 1.33
RRb02c (5×5 μm <sup>2</sup> ) [1 $\bar{1}$ 00] heated		15.03, 21.11, 31.57, 32.20, 33.80, 28.04, 7.29, 8.41
RRb02c (2×2 μm <sup>2</sup> ) [1 $\bar{1}$ 00] heated		3.15, 2.82, 3.25, 2.58, 2.73, 1.39, 9.19, 3.09

Appendix Table 1 (Continued)

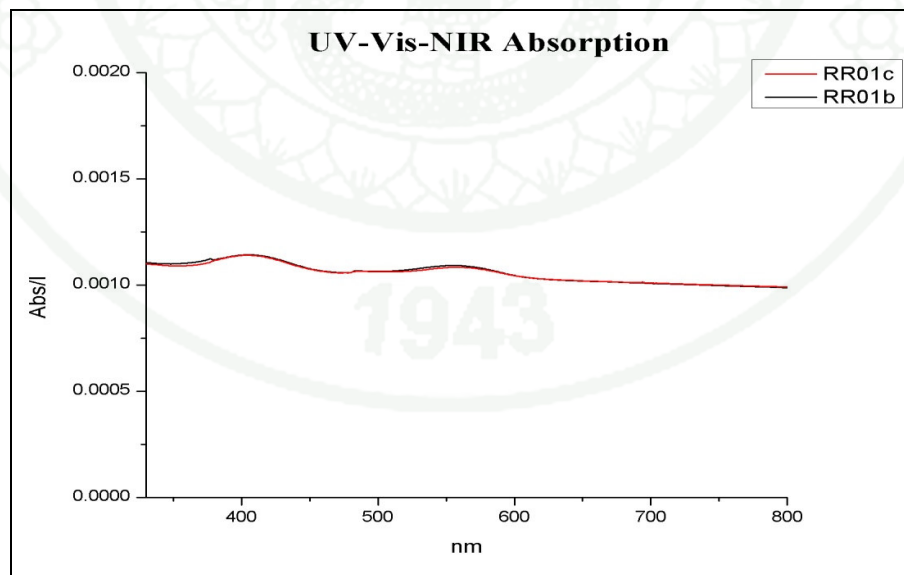
Sample	Image	Step height (nm)
RRb04a (10×10 μm <sup>2</sup> ) [1̄ 1̄ 20] unheated		7.15, 9.18, 1.69, 3.87, 1.12, 2.15, 1.13
RRb04a (5×5 μm <sup>2</sup> ) [1̄ 1̄ 20] unheated		3.53, 5.11, 1.62, 5.03, 7.46, 4.10, 6.75, 11.75, 3.80, 1.01, 2.53, 4.03, 2.32, 7.75
RRb04a (2×2 μm <sup>2</sup> ) [1̄ 1̄ 20] unheated		4.31, 3.09, 4.85, 6.18, 5.09, 2.07, 1.82, 2.32, 2.67
RRb04c (10×10 μm <sup>2</sup> ) [1̄ 1̄ 20] heated		2.85, 3.03, 1.06, 6.03, 0.77, 6.41, 12.34, 10.07, 1.01, 0.72, 12.61, 0.90
RRb04c (5×5 μm <sup>2</sup> ) [1̄ 1̄ 20] heated		9.77, 10.59, 2.23, 10.60, 12.73, 6.93, 3.83, 9.57, 5.30, 1.26, 4.54, 1.39, 9.12, 7.99, 1.94
RRb04c (2×2 μm <sup>2</sup> ) [1̄ 1̄ 20] heated		1.20, 1.16, 8.08, 0.81, 2.20, 1.54, 1.33, 2.70

Appendix Table 1 (Continued)

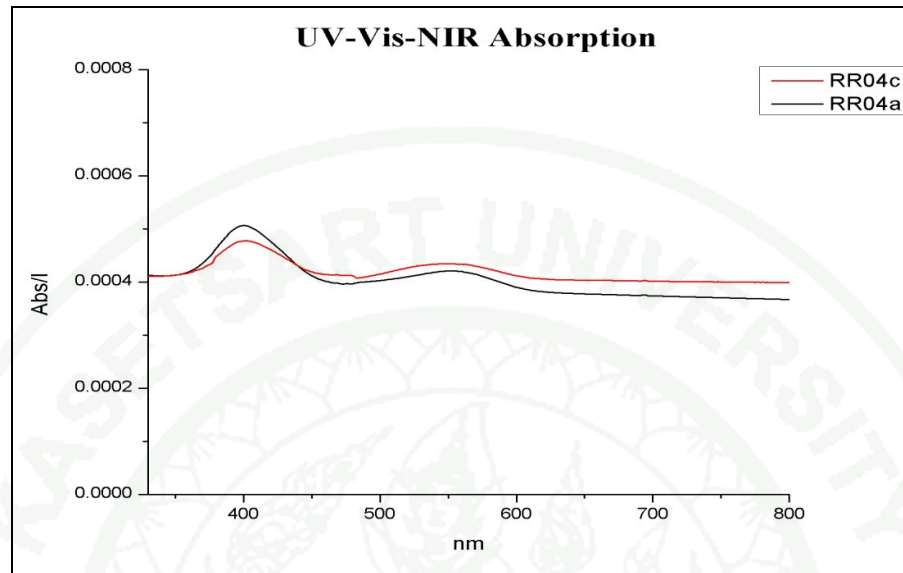
Sample	Image	Step height (nm)
RRb05a (10×10 μm <sup>2</sup> ) [0001] unheated		2.22, 3.00, 7.94, 4.39, 2.17, 1.94, 7.95, 4.47, 9.40
RRb05a (5×5 μm <sup>2</sup> ) [0001] unheated		1.75, 6.21, 3.67, 2.48, 2.00, 3.05, 2.49, 3.81, 8.10, 4.14, 1.84, 3.86, 2.22, 3.25, 9.54, 1.84, 3.16, 4.61, 4.09, 8.87, 3.23, 4.83, 4.82
RRb05a (2×2 μm <sup>2</sup> ) [0001] unheated		3.38, 4.42, 2.15, 2.32, 0.90, 0.53, 0.16, 0.28, 2.57, 1.19, 1.26, 1.01, 1.98, 1.19, 2.92
RRb05e (10×10 μm <sup>2</sup> ) [0001] heated		6.48, 6.93, 8.10, 7.03, 3.42, 7.00, 7.81, 4.15, 2.77, 3.63, 2.77, 3.48, 4.02
RRb05e (5×5 μm <sup>2</sup> ) [0001] heated		14.08, 5.77, 4.35, 8.17, 6.28, 5.38, 7.24, 7.44, 7.29, 8.43, 10.11, 12.41, 11.38, 7.39, 6.61, 6.61, 10.47
RRb05e (2×2 μm <sup>2</sup> ) [0001] heated		3.92, 6.09, 5.58, 5.37, 13.66, 15.34, 5.46, 4.47, 6.16, 7.63, 6.02, 4.69, 5.67



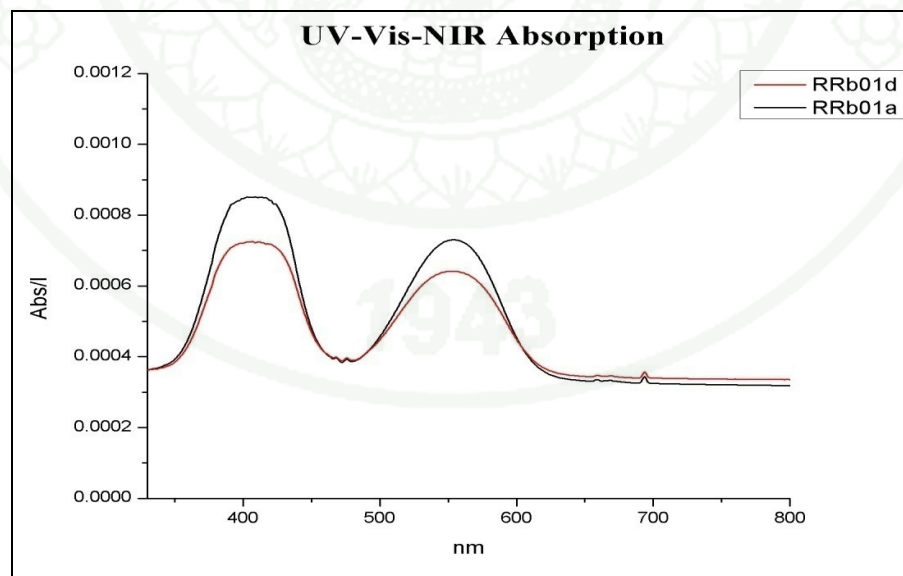
**Appendix Figure 1** UV-Vis-NIR absorption spectrum at the miscut prism  $[1\bar{1}00]$  face of heated sample (RR01d) has lower absorption than the unheated one (RR01a).



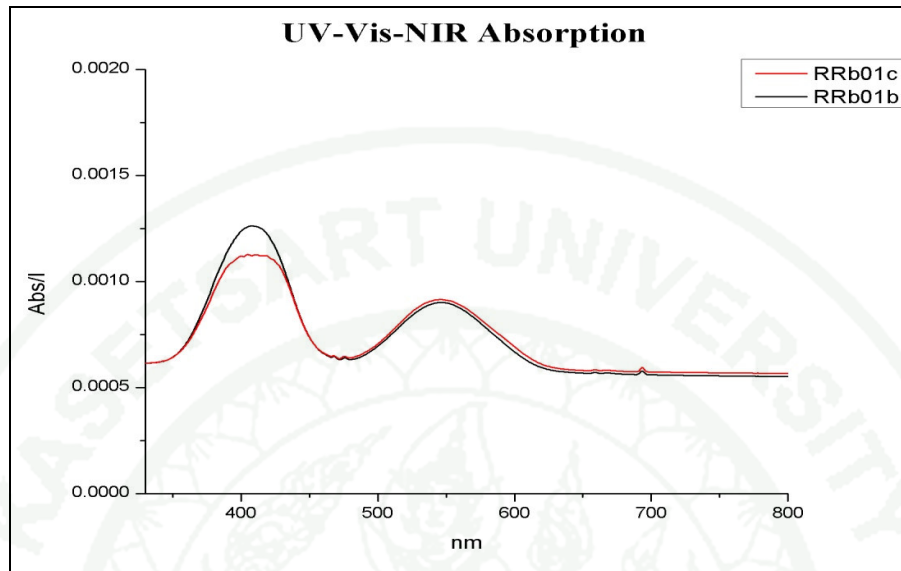
**Appendix Figure 2** UV-Vis-NIR absorption spectrum at the miscut prism  $[0\bar{1}10]$  face of heated sample (RR01c) has lower absorption than the unheated one (RR01b).



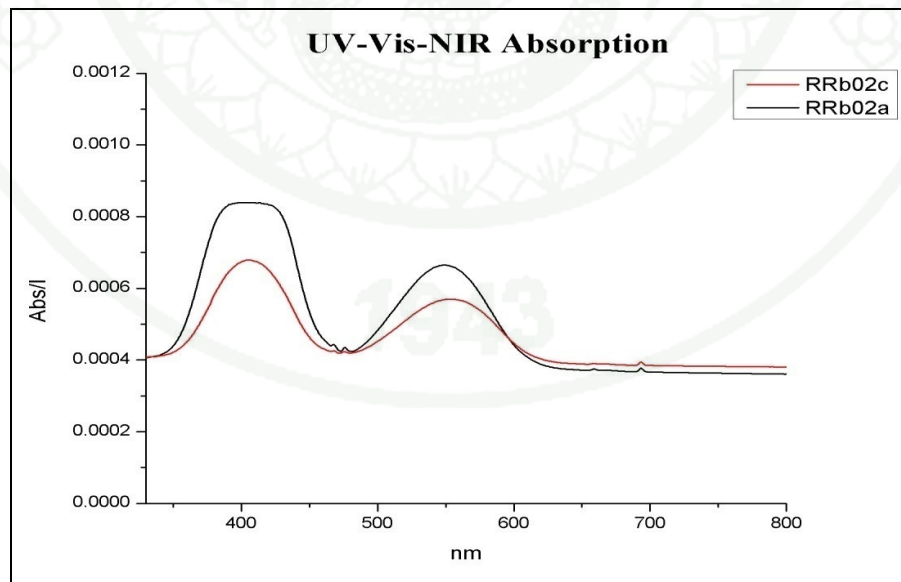
**Appendix Figure 3** UV-Vis-NIR absorption spectrum at the miscut prism  $[\bar{1}\bar{1}00]$  face of heated sample (RR04c) has lower absorption than the unheated one (RR04a).



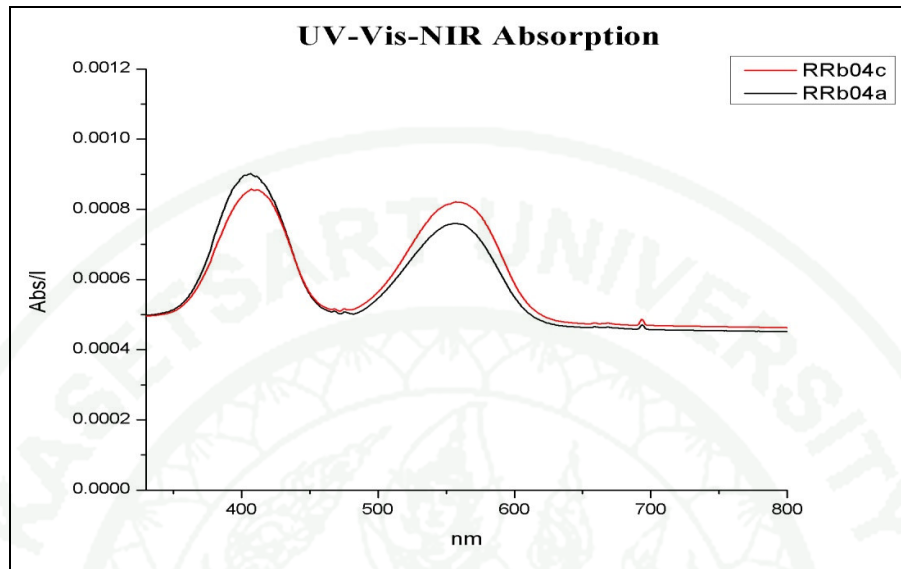
**Appendix Figure 4** UV-Vis-NIR absorption spectrum at the miscut prism  $[1\bar{1}00]$  face of heated sample (RRb01d) has lower absorption than the unheated one (RRb01a).



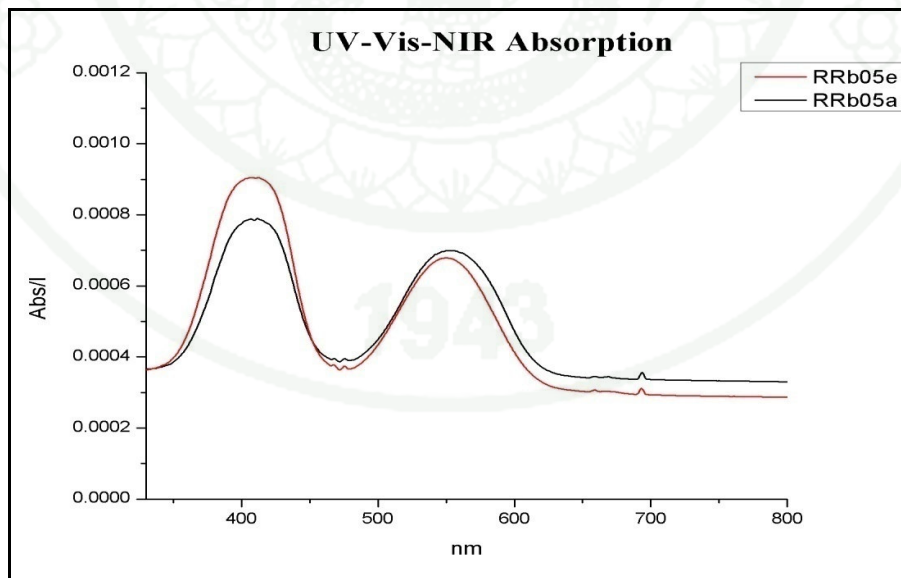
**Appendix Figure 5** UV-Vis-NIR absorption spectrum at the miscut prism  $[1\bar{1}00]$  face of heated sample (RRb01c) has lower absorption than the unheated one (RRb01b).



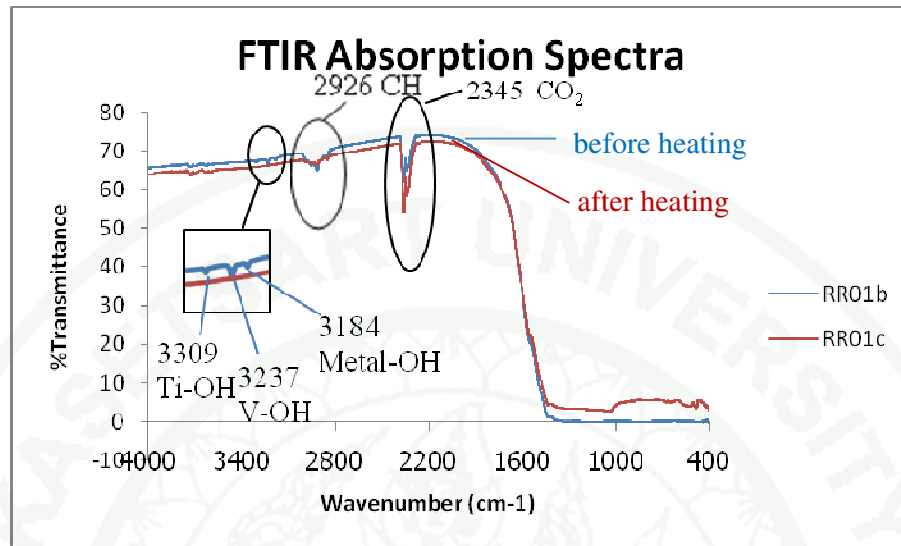
**Appendix Figure 6** UV-Vis-NIR absorption spectrum at the miscut prism  $[1\bar{2}10]$  face of heated sample (RRb02c) has lower absorption than the unheated one (RRb02a).



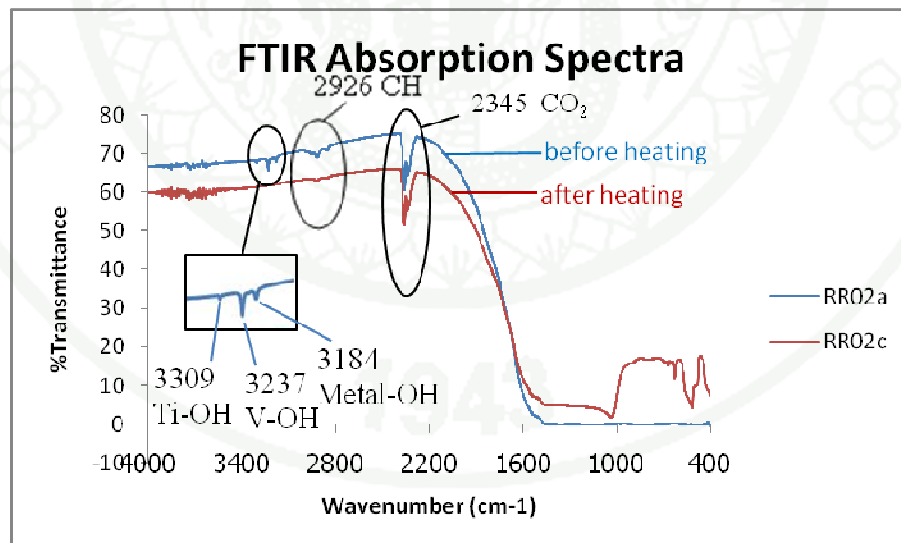
**Appendix Figure 7** UV-Vis-NIR absorption spectrum at the miscut prism  $[\bar{1}\bar{1}00]$  face of heated sample (RRb04c) has lower absorption than the unheated one (RRb04a).



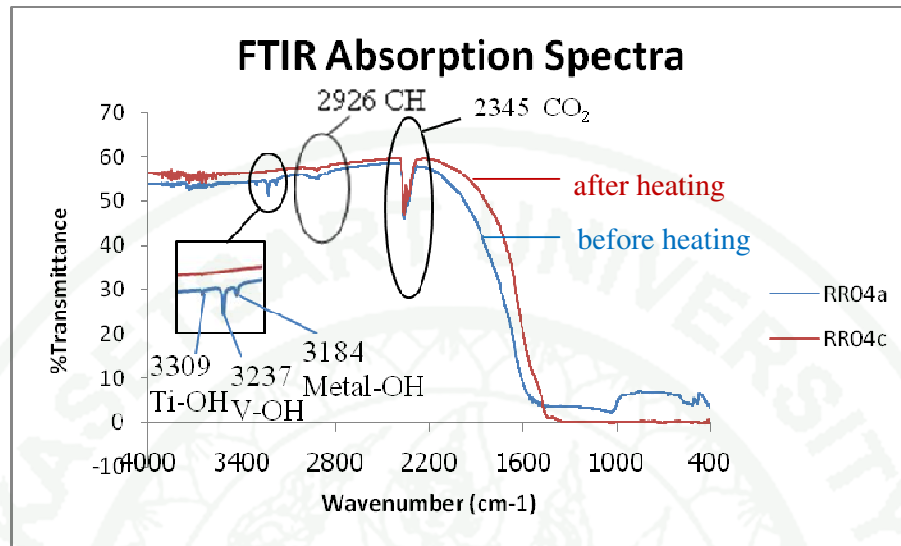
**Appendix Figure 8** UV-Vis-NIR absorption spectrum at the miscut prism  $[\bar{1}\bar{1}00]$  face of heated sample (RRb05e) has higher absorption than the unheated one (RRb05a).



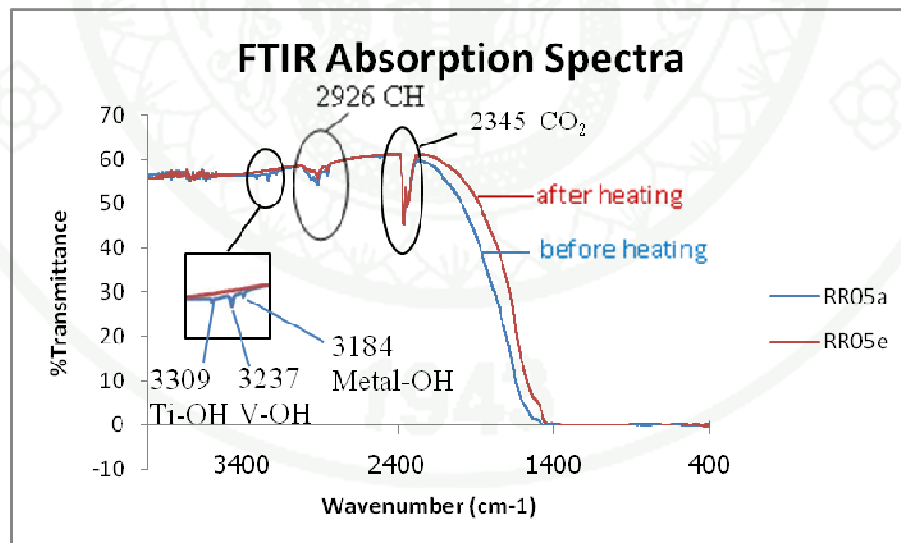
**Appendix Figure 9** FTIR spectra of synthetic pink sapphire samples set 1, through the miscus prism  $[0\bar{1}10]$  face of the samples (RR01b, RR01c).



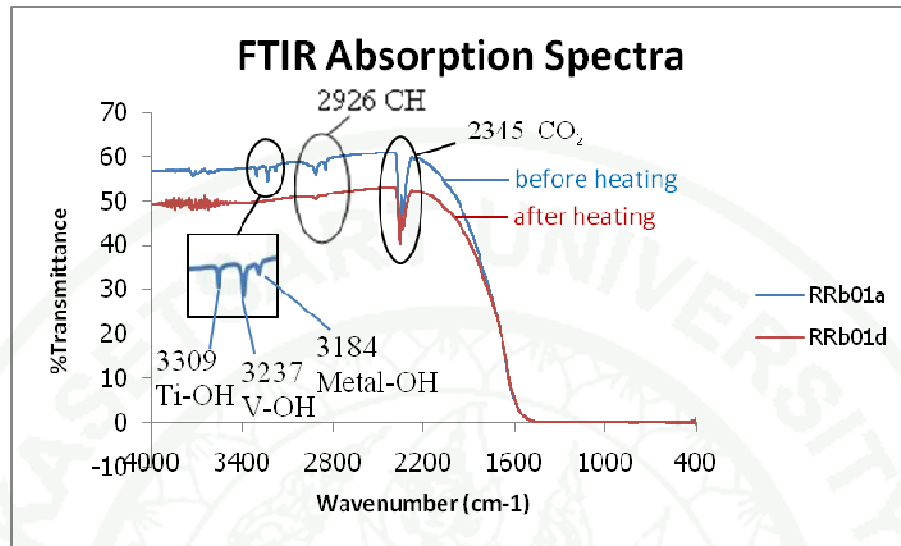
**Appendix Figure 10** FTIR spectra of synthetic pink sapphire samples set 1, through the miscus prism  $[1\bar{2}10]$  face of the samples (RR02a, RR02c).



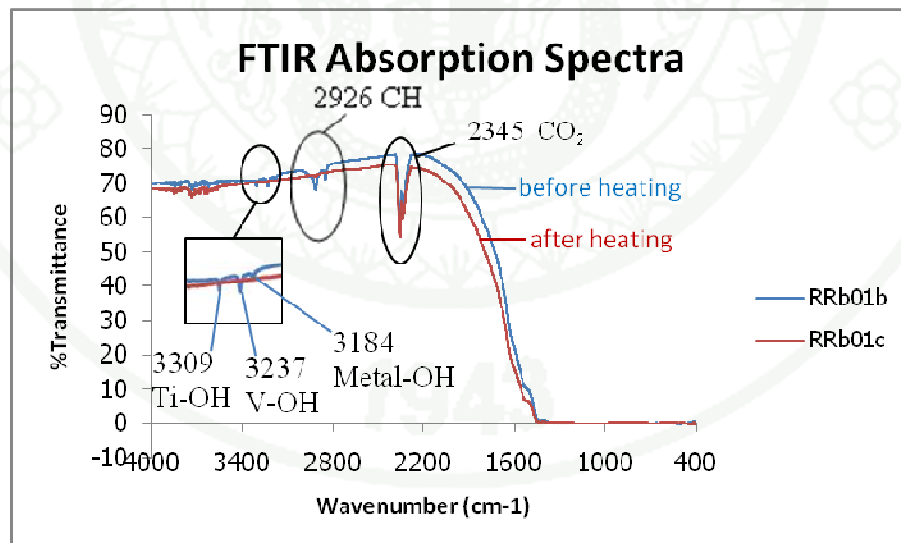
**Appendix Figure 11** FTIR spectra of synthetic pink sapphire samples set 1, through the miscus prism  $[\bar{1}\bar{1}20]$  face of the samples (RR04a, RR04c).



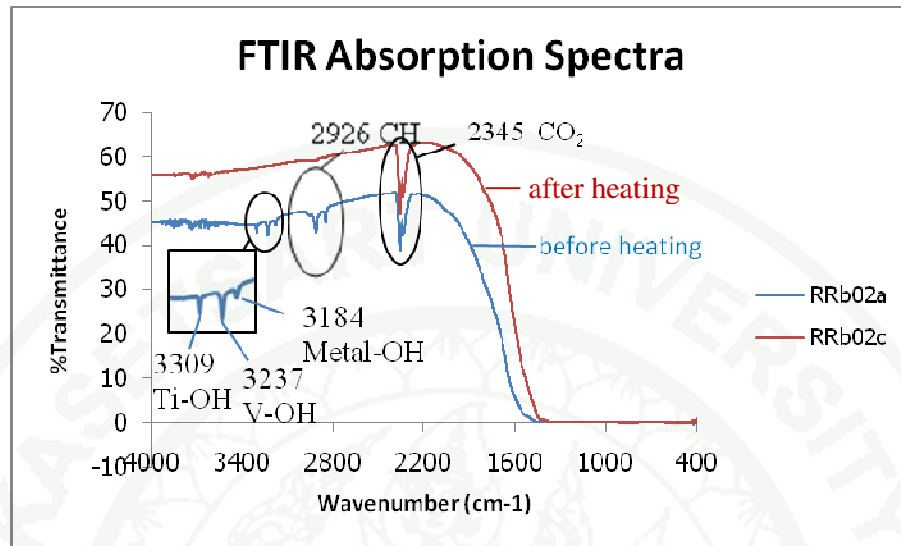
**Appendix Figure 12** FTIR spectra of synthetic pink sapphire samples set 1, through the miscus pinacoid  $[0\bar{1}10]$  face of the samples (RR05a, RR05e).



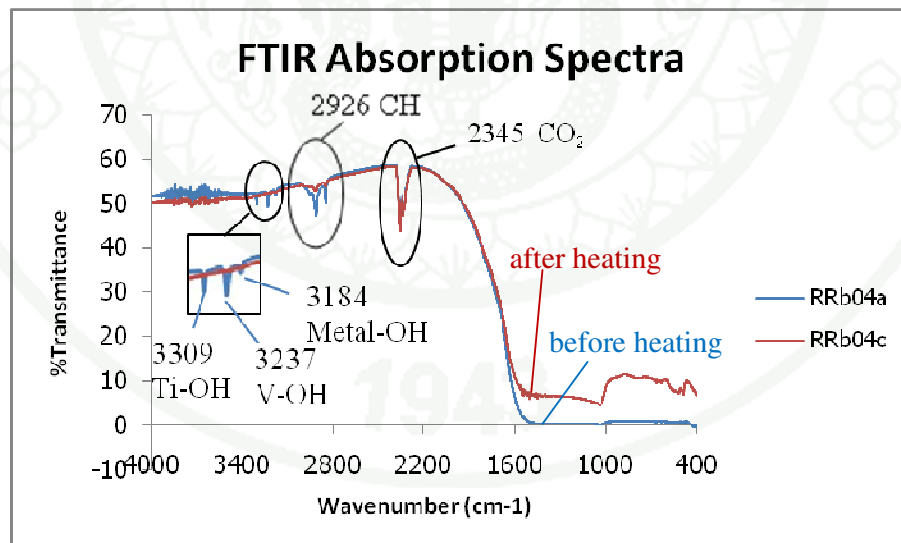
**Appendix Figure 13** FTIR spectra of synthetic ruby samples set 2, through the miscus prism  $[1\bar{1}00]$  face of the samples (RRb01a, RRb01d).



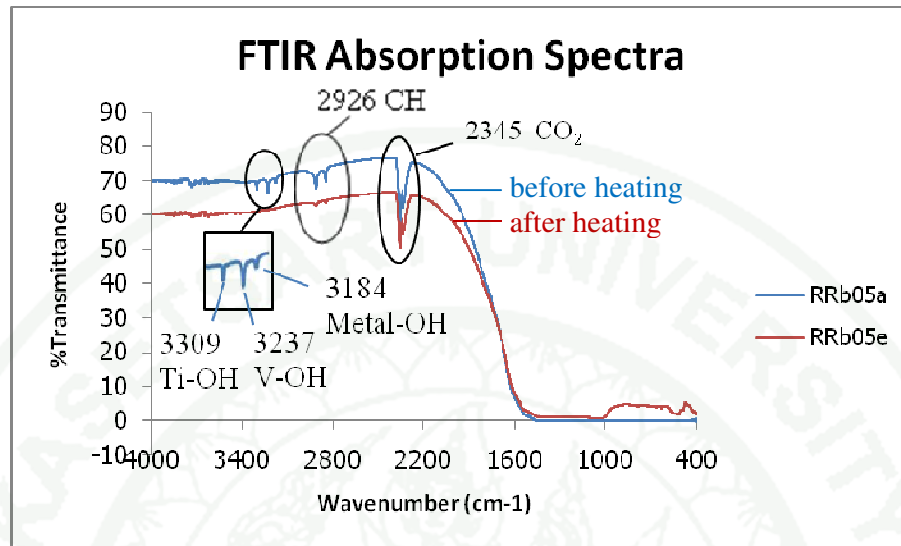
**Appendix Figure 14** FTIR spectra of synthetic ruby samples set 2, through the miscus prism  $[0\bar{1}10]$  face of the samples (RRb01b, RRb01c).



**Appendix Figure 15** FTIR spectra of synthetic ruby samples set 2, through the miscus prism  $[1\bar{1}210]$  face of the samples (RRb02a, RRb02c).



**Appendix Figure 16** FTIR spectra of synthetic ruby samples set 2, through the miscus prism  $[\bar{1}\bar{1}20]$  face of the samples (RRb04a, RRb04c).



**Appendix Figure 17** FTIR spectra of synthetic ruby samples set 2, through the miscus pinacoid [0001] face of the samples (RRb05a, RRb05e).

## CURRICULUM VITAE

**NAME** : Mr. Thanapong Lhuaamporn

**BIRTH DATE** : September 17, 1986

**BIRTH PLACE** : Bangkok, Thailand

<b>EDUCATION</b>	<b>: <u>YEAR</u></b>	<b><u>INSTITUTE</u></b>	<b><u>DEGREE/DIPLOMA</u></b>
	2008	Kasetsart Univer.	B.S. (Industrial Chemistry)

**POSITION/TITLE** :

**WORK PLACE** : The Gem and Mineral Sciences Special Research Unit, Department of Earth Science, Faculty of Science, Kasetsart University

**SCHOLARSHIP/AWARDS** : The Gem and Mineral Sciences Special Research Unit

